Exotic superconducting mechanisms in Fe and CeCu2Si2 under pressure

Holmes, Alexander Thomas

Université de Genève
Département de physique
de la matière condensée

Faculté des Sciences
Professeur J.-M. Triscone
Docteur D. Jaccard

Exotic Superconducting Mechanisms in Fe and $CeCu_2Si_2$ under Pressure

Thèse

présentée à la Faculté des sciences de l'Université de Genève
pour obtenir le grade de docteur ès sciences, mention physique

par

Alexander Thomas Holmes

de

Brighton (Royaume Uni)

Thèse N° 3539

Genève
Atelier de reproduction de la Section de physique
2004

La Faculté des sciences, sur le préavis de Messieurs J.-M. TRISCONE, professeur ordinaire et directeur de thèse (Département de physique de la matière condensée), D. JACCARD, docteur et co-directeur de thèse (Département de physique de la matière condensée), K. MIYAKE, professeur (Osaka University - Graduate School of Engineering Science - Department of Physical Science – Division of Materials Physics - Osaka, Japon) et S.R. JULIAN, docteur (University of Cambridge - Cavendish Laboratory - Low Temperature Physics - Cambridge, Grande-Bretagne), autorise l'impression de la présente thèse, sans exprimer d'opinion sur les propositions qui y sont énoncées.

Genève, le 20 juillet 2004

Thèse - 3539 -

P. Spierer

Le Doyen, Pierre SPIERER

Contents

Résumé

Introduction

Cette thèse présente l'étude de deux supraconducteurs. Il s'agit du fer pur dans sa phase ε, un métal de transition $3d$ observée à haute pression, et du $CeCu_2Si_2$, un composé intermétallique dont les propriétés sont dominées par les électrons $4f$. La supraconductivité dans le phase ε du fer a été découverte très récemment, et le $CeCu_2Si_2$ a été l'objet de nombreuses études depuis plus d'une vingtaine d'années. Pourtant, ces deux systèmes ne sont pas totalement dissemblables.

Le magnétisme joue un rôle très important dans les propriétés du fer et du $CeCu_2Si_2$, mais d'une façon assez différente dans les deux cas. Le fer montre un magnétisme itinérant à pression ambiante, alors que le $CeCu_2Si_2$ possède des moments localisés avec des corrélations antiferromagnétiques. Dans les deux cas, l'ordre magnétique et la supraconductivité sont trouvés très proches l'un de l'autre. Ceci est surprenant, étant donné que ces comportements sont normalement antagonistes.

Ce n'est pas seulement le magnétisme qui est important dans ses systèmes. Dans le cas du fer, la supraconductivité se trouve proche d'une transition structurale *et* magnétique, et dans le $CeCu_2Si_2$, nous pensons que la supraconductivité est reliée en partie avec une transition de valence.

La problématique

Ces remarques introduisent la question à laquelle nous essayerons de répondre : quel est le mécanisme de supraconductivité dans le fer ε et le $CeCu_2Si_2$? La proximité du magnétisme et de la supraconductivité n'est qu'une raison parmi d'autres de penser que ce n'est pas un mécanisme BCS conventionnel.

Il se trouve que les propriétés à très basse température du fer et du $CeCu_2Si_2$ sont dominées par la concurrence entre différents états fondamentaux. La pression est un outil puissant pour sonder, d'une façon propre et continue, les effets de cette compétition entre états.

La pression permet de varier les propriétés électroniques d'un matériau, qui dépendent fortement du volume. Le couplage entre les électrons de conduction et ceux localisés près des noyaux atomiques est modifié, de même que la densité d'état des électrons de conduction. Le résultat de ces changements peut être qu'une nouvelle structure cristalline ou configuration électronique devient l'état de plus basse énergie.

Il semble que cette concurrence entre différents états fondamentaux presque dégénérés est à l'origine de la supraconductivité dans le fer et le $CeCu_2Si_2$. Près d'une transition de phase, il existe plusieurs configurations du système avec une énergie équivalente. Les électrons de conduction sont diffusés par des fluctuations entre ces états, et ces fluctuations sont à l'origine de multiples effets hors du commun, entre autre la supraconductivité et les comportements dit fermion lourd.

Dans le cas du Fe-ε, discuté au chapitre 4, la supraconductivité, découverte en 2001 par Shimizu et al. se trouve proche d'une transition de premier ordre, séparant deux configurations structurales et magnétiques différentes. Dans le $CeCu_2Si_2$, présenté au chapitre 5, la supraconductivité est renforcée sous pression, et ce travail de thèse démontre que ce phénomène est relié à une transition de valence.

Si les fluctuations entre états fondamentaux dégénérés sont à l'origine de la supraconductivité et des propriétés non-conventionnelles de l'état normal, il doit y avoir des corrélations entre les deux. Nous pouvons ainsi étudier le mécanisme de supraconductivité en mesurant les propriétés de l'état normal, à l'aide de sondes telles que la résistivité électrique ou la calorimétrie alternative, avec la température et la pression comme paramètres de contrôle.

Concepts théoriques

Dans le chapitre 2, après avoir brièvement introduit le mécanisme de supraconductivité dans les systèmes traditionnels, les deux explications principales pour le couplage non-conventionnel sont décrites. Il s'agit de l'échange de fluctuations critiques quantiques, soit de nature magnétique, soit de valence. Ces dernières apparaissent dans le $CeCu_2Si_2$, et sont liées à un deuxième point critique quantique caractérisé par un changement abrupt du nombre d'électrons f dans le cérium.

La supraconductivité induite par fluctuations de valence est un nouveau mécanisme proposé récemment (Miyake et al. [1999]), basé sur des observations indiquant que le $CeCu_2Si_2$ et son homologue isoélectronique $CeCu_2Ge_2$ subissent un changement rapide de valence autour de la pression qui correspond au maximum de la température critique T_c.

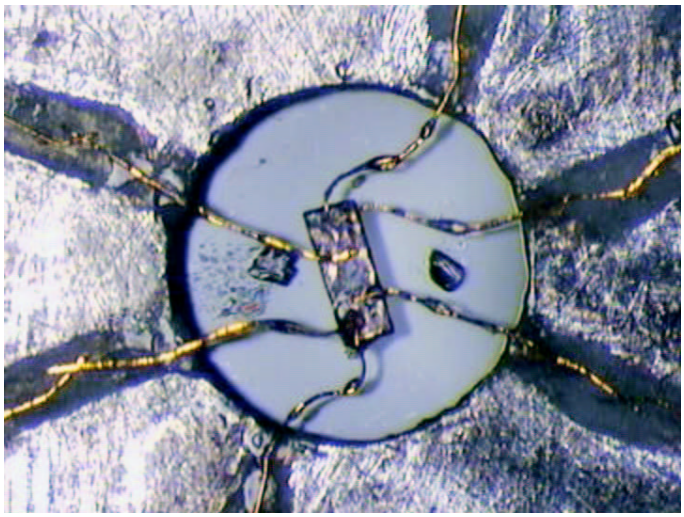

Figure 1: Cellule hélium avant pressurisation, avec un diamètre initial de 600 μm. L'échantillon de $CeCu_2Si_2$ été coupé et poli à des dimensions $230 \times 80 \times 20$ μm^3. Les contacts électriques sont formés par soudure par point, et deux thermocouples Au/AuFe sont soudés aux deux bouts de l'échantillon. Les fils de diamètre 5 μm sont isolés du joint par un mélange Al_2O_3/epoxy, contenu dans des fentes de profondeur 12-15 μm. Deux éclats de rubis permettent la détermination de la pression par fluorescence. (Construit en collaboration avec D. Jaccard.)

Techniques expérimentales

Nous avons utilisé deux méthodes de production de haute pression :

Technique Bridgman. Celle-ci comprend deux enclumes opposées, à support massif, destinées à bloquer une force uniaxiale. Entre les enclumes se trouve la cellule de pression elle-même, composée d'un joint annulaire compressible contenant un milieu transmetteur de la pression (un solide mou) enrobant l'échantillon. Les fils de mesure sont introduits à travers des fentes dans le joint.

Enclumes diamants/milieu transmetteur hélium. Cette technique permet d'avoir les meilleurs conditions de pression hydrostatique à basse température. La cellule est formée d'un joint métallique qui piège le milieu de transmission contenant l'échantillon. Le joint doit se déformer d'une manière plastique pour absorber la compressibilité de l'hélium, toute en assurant la fiabilité et l'isolation des contacts électriques.

Le montage de la cellule hélium avec six fils dont deux thermocouples soudés à l'échantillon de $CeCu_2Si_2$ (voir fig. 1), a permis des mesures simultanées de résistivité et de calorimétrie alternative sur un même échantillon jusqu'à des pressions et des températures jamais atteintes auparavant.

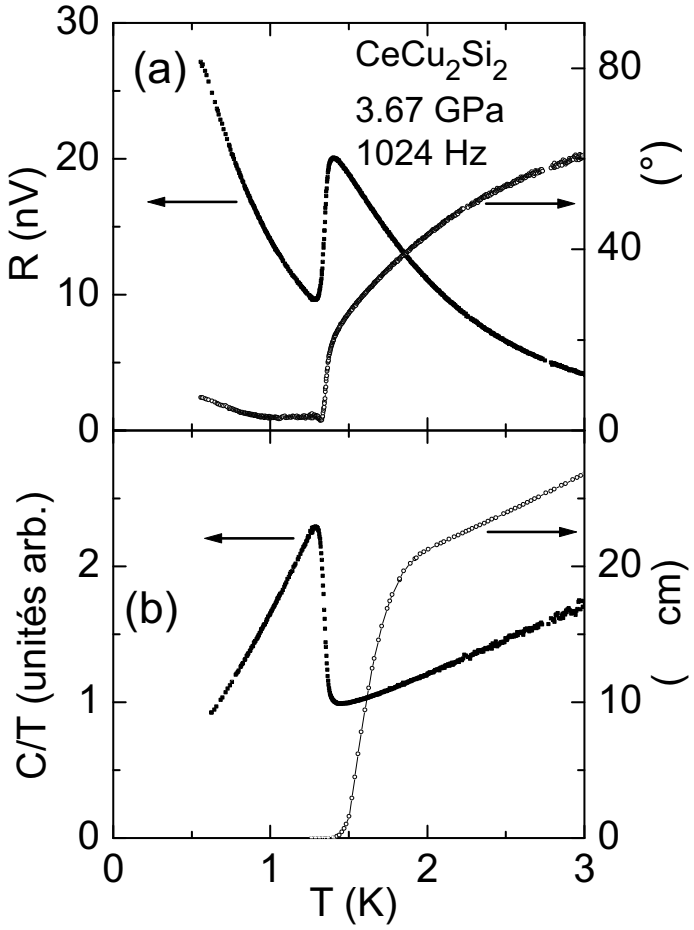

Figure 2: Transition supraconductrice du $CeCu_2Si_2$ vue en résistivité et calorimétrie alternative dans un milieu de pression hélium. La partie (a) montre le signal brut d'amplitude et de phase du thermocouple, et la partie (b) montre le signal traité pour déterminer C_P, en comparaison avec la transition résistive.

Cette dernière technique consiste à chauffer l'échantillon d'une façon périodique, et à mesurer les oscillations de température qui en résultent. Si la fréquence est suffisamment haute, l'échantillon est effectivement découplé de son voisinage, ce qui permet des mesures de très haute sensibilité dans des conditions qui sont loin d'être adiabatiques. Même quand les conditions de mesure sont moins favorables, par exemple quand il y a un fort couplage thermique avec le milieu de pression, un modèle simple permet d'extraire une valeur permettant de suivre à une très bonne approximation la chaleur spécifique de l'échantillon. Un exemple est donné dans la fig. 2, où la transition supraconductrice du $CeCu_2Si_2$ est clairement visible dans le signal calorimétrique et dans la résistivité.

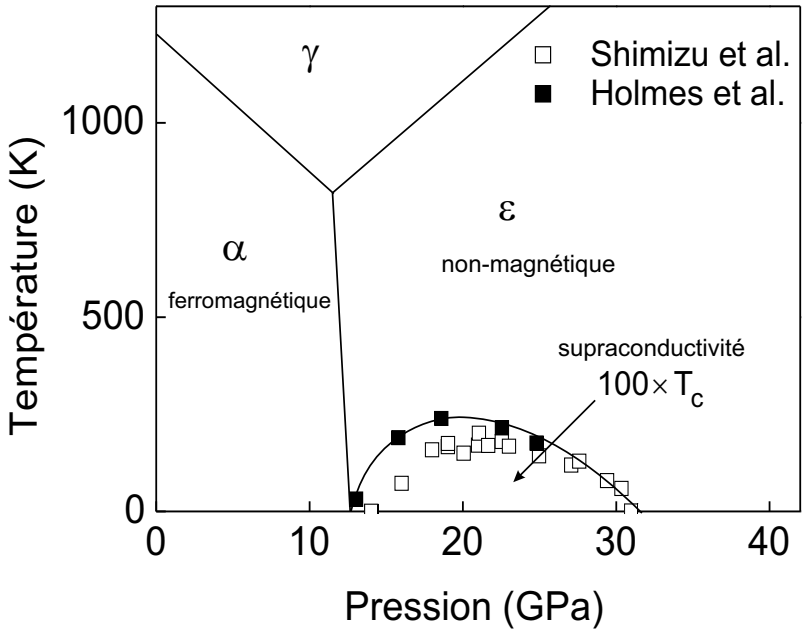

Figure 3: Diagramme de phase du fer, montrant la région supraconductrice dans la phase ε. Les carrés blancs représentent les valeurs de T_c obtenues par Shimizu et al. [2001], et les symboles noirs sont les résultats présentés dans cette thèse. On peut noter l'émergence de la phase supraconductrice directement à la transition α-ε.

Fer

Dans le chapitre 4, nous examinons le cas du fer, un métal de transition dont les propriétés sont dominées par ses électrons $3d$. La supraconductivité et une déviation au comportement du liquide de Fermi ont été trouvées près d'une transition de phase, où la concurrence entre différents états fondamentaux donne lieu à des mécanismes exotiques de diffusion.

La supraconductivité se trouve près de la frontière avec la phase cubique centrée α, qui est la phase ferromagnétique trouvée sous conditions ambiantes. En appliquant la pression, le fer se transforme dans la phase hexagonale compacte ε autour de 13 GPa, et les premières traces de supraconductivité sont observables juste après cette transition. Dans cette phase, qui ne montre pas de traces expérimentales d'ordre magnétique, plusieurs calculs numériques ont prédits un état fondamental antiferromagnétique, dont les fluctuations sont responsables de l'interaction supraconductrice.

Nous avons étudié, sous pression quasi-hydrostatique, plusieurs échantillons de fer de très haute pureté. Le désordre structural peut être induit pendant la préparation des échantillons, et réduit par méthode de recuit à 1000°C pendant 24 heures sous haut vide ($< 10^{-7}$ torr). Ces variations de méthode de préparation ont un grand effet sur

la résistivité résiduelle ρ_0 de l'échantillon. Ceci est une bonne sonde expérimentale de la supraconductivité non-conventionelle, parce que l'état supraconducteur est extrêmement sensible au désordre, et peut être détruit si le libre parcours moyen ℓ devient inférieur à la longueur de cohérence ξ.

Nous avons confirmé les résultats initiaux de Shimizu, et le diagramme de phase résultant est montré en fig. 3. Les résultats que nous présentons démontrent la sensibilité de l'état supraconducteur au désordre, et établissent le lien entre les propriétés de l'état normal et T_c. Le comportement très anormal de la résistivité ρ au-dessus de T_c dans la phase ε a été établi, avec des lois de puissance $\rho = \rho_0 + AT^{5/3}$ sur une grande gamme de pression et de température. Ces observations tendent à prouver que le mécanisme de supraconductivité est non-conventionnel, et que la symétrie des paires de Cooper est probablement de type triplet, induite par des fluctuations ferromagnétiques, en contradiction avec les prédictions théoriques. Cette conclusion reste encore à confirmer, notamment à cause de la nature premier ordre et martensitique de la transition α-ε.

$CeCu_2Si_2$

L'idée de concurrence entre états fondamentaux est très importante dans le cas des fermions lourds. Il s'agit en majorité de composés intermétalliques de terres rares, avec des propriétés dominées par leurs électrons f. Le $CeCu_2Si_2$ appartient à une classe importante de fermions lourds, les composés du cérium, et c'est d'ailleurs le premier composé de cette classe à avoir été découvert supraconducteur (Steglich et al. [1979]). Dans le chapitre 5, nous discutons les preuves qui mènent à la conclusion que la supraconductivité à haute pression dans ce composé est due aux fluctuations de valence.

Nous avons fait des mesures simultanées de résistivité et de calorimétrie alternative sur un monocristal de $CeCu_2Si_2$ sous des conditions de pression idéales. Ces mesures ont démontré une série d'anomalies autour de la pression où T_c atteint sa valeur maximale. Nous pouvons faire le lien avec la théorie de fluctuations de valence, discutée dans le chapitre 2. Ceci permet d'expliquer non seulement la supraconductivité, mais d'autres anomalies, comme le maximum de résistivité résiduelle, et l'anomalie dans la constante de Sommerfeld.

Suite à ces mesures sur un seul échantillon dans les meilleures conditions de mesure, nous avons fait une étude systématique de la variation des propriétés à haute pression de plusieurs échantillons d'origines et de préparations différentes. L'influence de la direction du courant par rapport aux axes cristallographiques et l'effet de la contrainte uniaxiale ont été étudiés.

La figure 4 montre la série d'anomalies qui coïncide avec le maximum de T_c sous pression, et un changement de régime d'un comportement fortement corrélé à un

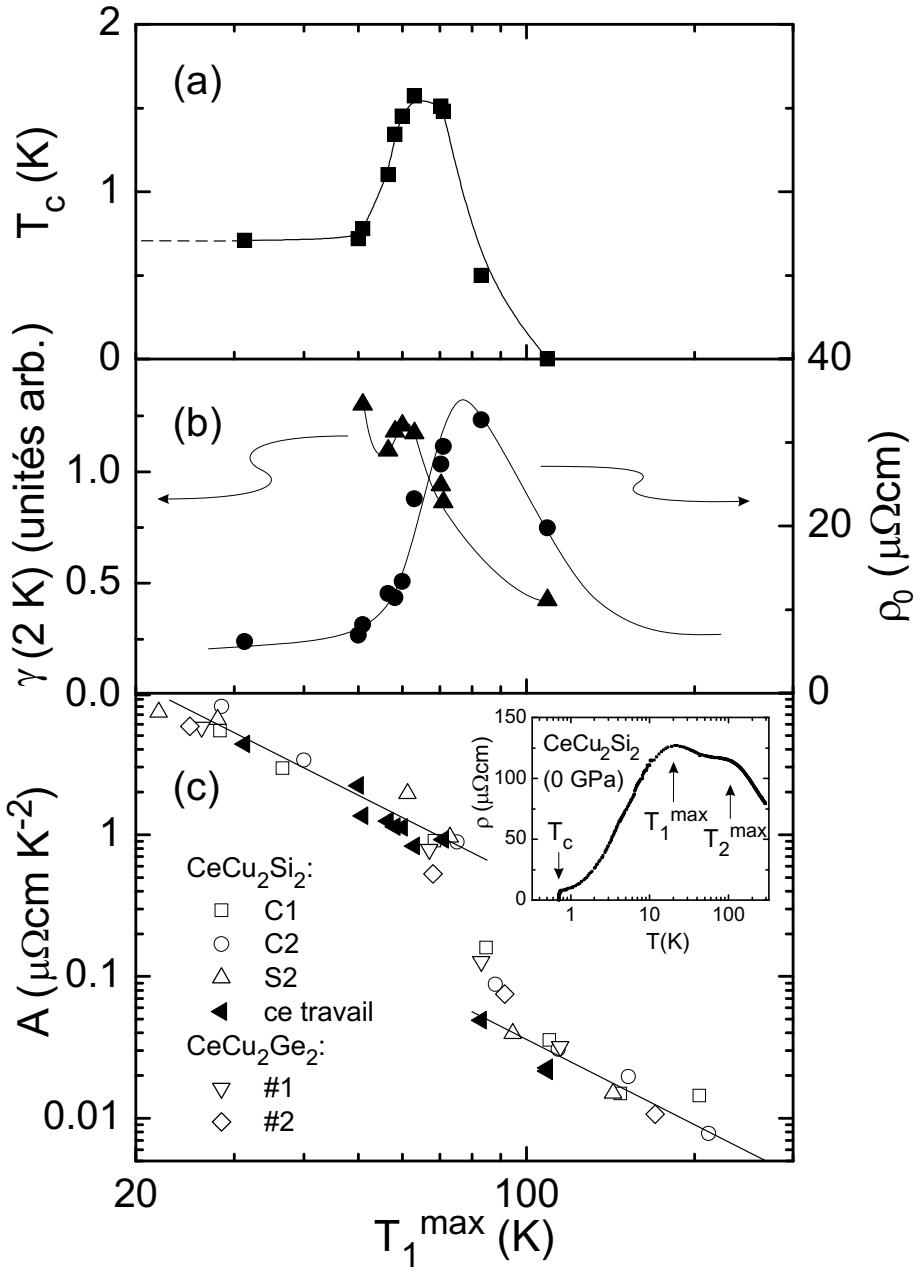

Figure 4: $T_1^{\max}$ (défini dans l'encadré) est une mesure de l'énergie caractéristique du système. Le graphique (c) de $\log(A)$ en fonction de $\log(T_1^{\max})$ montre les deux régions où la loi attendue $A \propto (T_1^{\max})^{-2}$ est suivie. La transition de valence correspond à la rupture de cette loi d'échelle. Ceci coïncide avec d'autres anomalies, notamment (a) de la température de transition supraconductrice, et (b) de la résistivité résiduelle ρ_0 et le coefficient électronique de la chaleur spécifique γ. La pression augmente vers la droite de la figure.

comportement faiblement corrélé. Ce dernier est indiqué par la relation entre le coefficient $A \propto \rho/T^2$ de la résistivité et la position du premier maximum de résistance, $T_1^{\max}$. Ce changement de régime indique que l'occupation du niveau f baisse d'une façon abrupte à ce point.

La figure 5 montre le nouveau diagramme de phase du system $CeCu_2(Si/Ge)_2$ basé sur le travail présenté ici. La nouveauté principale est l'existence d'une deuxième pression critique P_v, où des fluctuations de valence dominent les propriétés du système. Autour de $P_v \simeq 4.5$ GPa, la supraconductivité est induite par échange de fluctuations de valence. La résistivité de la phase normale est linéaire en température, et la résistivité résiduelle est fortement augmentée à ce point par rapport à sa valeur à pression ambiante.

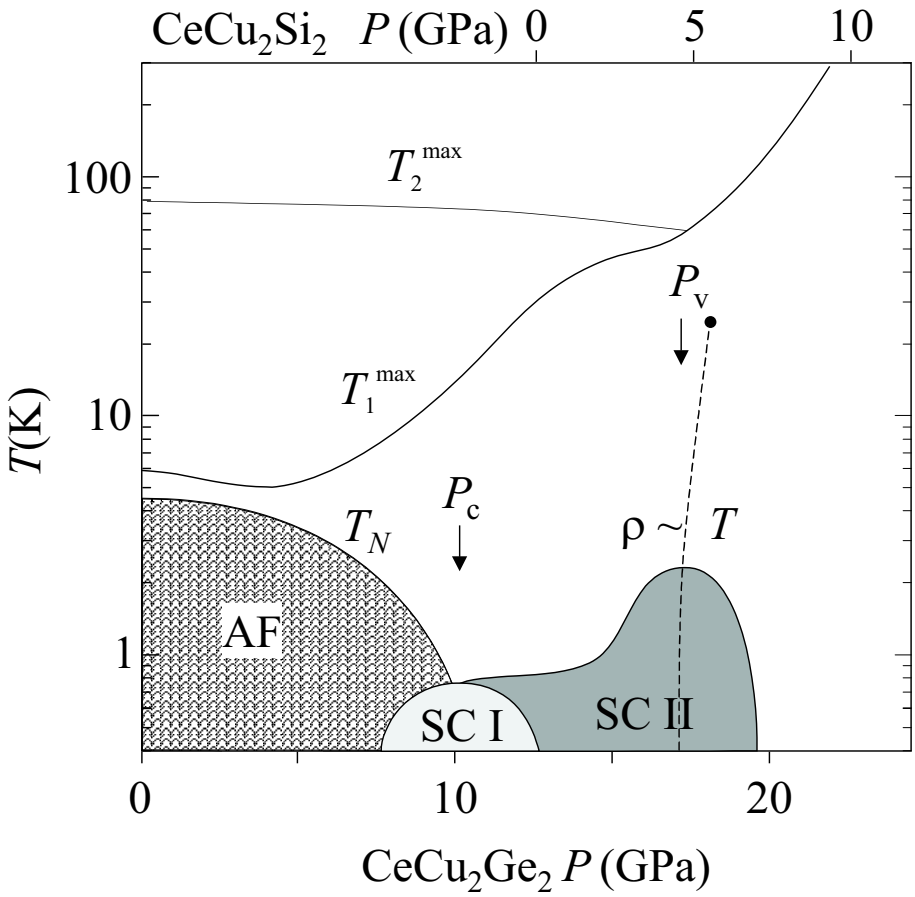

Figure 5: Diagramme de phase schématique du système $CeCu_2(Si/Ge)_2$, montrant les deux pressions critiques P_c et P_v. A P_c, pression à laquelle la température d'ordre antiferromagnétique $T_N \to 0$, des fluctuations antiferromagnétiques sont responsables de la supraconductivité dans la région *SC I* ; autour de P_v, dans la région *SC II*, le mécanisme d'appariement des électrons dépend de l'échange de fluctuations de valence, et la résistivité est linéaire en température. Les maxima de résistivité, aux températures T_1^{max} et T_2^{max}, se réunissent à la pression P_v. La ligne en trait-tirés représente une transition de premier ordre présumée à la transition de valence, avec un point critique entre 10 K et 300 K.

Conclusions

D'après les résultats expérimentaux et théoriques présentés dans les chapitres 2, 4, et 5, nous sommes parvenus aux conclusions suivantes :

- La supraconductivité dans le fer-ε est vraisemblablement d'origine non-conventionelle, avec un mécanisme d'appariement des électrons dû à l'échange de fluctuation de spin. Il semble que les paires de Cooper sont dans l'état spin-triplet, et sont formées grâce à des fluctuations ferromagnétiques. Ceci est en contradiction avec la plupart des travaux théoriques, qui prédisent un état fondamental antiferromagnétique.

- Le $CeCu_2Si_2$ montre un nouveau type de point critique quantique, à une pression P_v autour de 4.5 GPa, où les propriétés électroniques sont dominées par des fluctuations de valence.

- La supraconductivité à haute pression dans le $CeCu_2Si_2$ est liée à une transition de valence à P_v, avec un mécanisme d'appariement des électrons basé sur l'échange de fluctuations de valence.

- Les propriétés de $CeCu_2Si_2$ autour de P_v sont extrêmement sensibles à l'anisotropie dans les conditions de pression, et aux minuscules variations de la pureté des échantillons.

- Le modèle proposé par K. Miyake, et discuté dans le chapitre 2, prédit un grand nombre des propriétés observées dans le $CeCu_2Si_2$ autour de P_v, y compris la supraconductivité.

- Ce mécanisme peut être compris en tant qu'interaction extrêmement localisée, basée sur l'écrantage des ions Ce^{4+} isolés.

Chapter 1

General Introduction

1.1 ε-Iron and $CeCu_2Si_2$

This thesis is about two superconductors: iron and $CeCu_2Si_2$. The former was discovered to be superconducting at high pressure in its ε-phase very recently, while the properties of $CeCu_2Si_2$ have been studied closely for over twenty years. Iron is an element, and $CeCu_2Si_2$ a complex intermetallic compound, so what do they have in common?

Most obviously, magnetism plays an important role in iron and $CeCu_2Si_2$, though in very different ways. Iron is an itinerant ferromagnet in ambient conditions, and $CeCu_2Si_2$ has localised moments which order antiferromagnetically. In both cases magnetic order and superconductivity, two usually antagonistic properties, are found in close proximity.

1.2 The question

This introduces the question posed in this thesis: what is the superconducting mechanism in ε-iron and $CeCu_2Si_2$? There are many reasons to think that it is not a conventional BCS-type mechanism in either system, the proximity of magnetism and superconductivity being just one.

To answer this, pressure is an extremely useful tool. Pressure enables us to continuously vary the electronic properties of a material, which are highly sensitive to volume. It changes the coupling between conduction electrons and those localised in the ionic core, and it varies the density of states of itinerant electrons. In doing so, a different crystal structure or electronic configuration may become the new lowest energy state.

It appears to be this competition between different, nearly degenerate, ground states which drives the superconductivity of both ε-iron and $CeCu_2Si_2$. Close to a phase boundary, there are many possible configurations of equal energy, which can result in large-amplitude fluctuations of some ordering parameter of the system. These fluctuations can scatter electrons and are responsible for a large number of unconventional properties, from superconductivity to heavy fermion behaviour.

Superconductivity in iron lies close to a first order phase boundary between different structural, and magnetic, configurations. In $CeCu_2Si_2$, superconductivity is enhanced under pressure, and the evidence presented in this thesis is intended to demonstrate that this is related to a first-order, or nearly so, valence transition.

If fluctuations between degenerate ground states are responsible for both unconventional superconducting and normal state properties, there will be correlations between the two. We can therefore make conjectures about the superconducing mechanism using our knowledge of the normal state, obtained from resistivity and specific heat measurements.

1.3 The answer?

In the case of iron, according to the evidence presented in chapter four, the most likely pairing mechanism is that mediated by magnetic fluctuations. The nature of these fluctuations is still unclear, as is the relationship, if any, with the α-ε structural transition. However we can conclude that there is a strong possibility of ε-Fe being a ferromagnetically mediated spin-triplet superconductor.

$CeCu_2Si_2$ is even more interesting. While it is widely accepted that the superconductivity at ambient pressure is mediated by antiferromagnetic spin fluctuations, the evidence presented in chapter five strongly suggests that a new mechanism is responsible for the pairing at high pressure. The attractive interaction is based on the exchange of valence fluctuations, the theory of which is discussed in detail in chapter two. While this may turn out to be nothing more than a scientific curiosity, we believe that this phenomenon is not confined to $CeCu_2Si_2$.

Chapter three contains the experimental methods used to obtain the results presented in chapters four and five, including a novel statistical method based on Bayesian analysis, which proves useful in the fitting of non-Fermi liquid laws to the resistivity.

Chapter 2

Theoretical concepts

Ever since Landau developed his Fermi-liquid theory of metals, the quasiparticle description of charge carriers in solids has been immensely successful. Even in materials with strongly interacting electrons, this picture has proved useful, with the interactions absorbed into strongly renormalised effective masses and quasiparticle lifetimes.

In most normal metals, the principle interactions present in the system, relevant to the electronic properties, are between the conduction electrons and the ionic lattice, where departures from perfect periodicity leads to scattering of the charge-carrying quasiparticles and hence to electrical resistance.

Bardeen, Cooper and Schrieffer (BCS) [1957] showed that polarisation of the lattice can provide an attractive interaction between two electrons, leading to the formation of a bosonic paired state known as a Cooper pair. These condense to form the collective ground state at the origin of superconductivity.

Cooper [1956] had shown that any attractive interaction between quasiparticles can cause the Fermi-liquid to be unstable to a superconducting ground state, and it is more exotic interactions, of a mostly electronic origin, which concern us in this thesis.

The same interactions that are responsible for superconductivity are visible in the scattering of normal state quasiparticles, so resistivity is a useful tool for exploring these.

In this chapter I will briefly summarise the behaviour expected in systems governed by phonons, and by magnetic fluctuations. The former case is extremely well understood, and the latter has been studied extensively elsewhere. Finally I will describe in some detail the recent theory of valence fluctuations, which we believe is at the origin of a new mechanism of superconductivity in heavy fermions, particularly the $CeCu_2(Si/Ge)_2$ system.

2.1 Phonon scattering and BCS superconductivity

The electrical resistivity ρ in most metals at high temperatures is dominated by electron-phonon scattering. A simple model (see for example Ashcroft and Mermin [1976]) predicts that the ρ should depend on T in the following way:

$$\rho \sim \begin{cases} T & (T \gg \Theta_D) \\ T^5 & (T \ll \Theta_D) \end{cases}, \tag{2.1}$$

where Θ_D is the Debye temperature, which is a measure of the phonon energy scale. The linear high temperature behaviour is determined largely by the number of excited phonon modes, while faster dependence at low temperature is due to the fact that low-$\mathbf{q}$ scattering at small angles is less efficient.

BCS showed that the critical temperature T_c of phonon-mediated superconductivity was given in the simplest case by

$$k_B T_c = 1.14\hbar\omega_c e^{-1/N(E_F)V}, \tag{2.2}$$

where ω_c is a cutoff frequency of the order of the Debye temperature Θ_D, $N(E_F)$ is the density of states of the conduction electrons at the Fermi energy, and V is a constant potential representing the attractive interaction between electrons.

2.2 Magnetism, quantum critical points, and magnetically mediated superconductivity

2.2.1 Kondo effect and RKKY interaction

The Kondo effect describes the interaction between a magnetic impurity (with a spin $\mathbf{S}$) embedded in a metal. If the conduction electron have spin $\mathbf{s}$, the interaction is given by the Hamiltonian

$$H = -J\mathbf{S} \cdot \mathbf{s}. \tag{2.3}$$

If the coupling constant J is negative, screening of the impurity spin by the conduction electrons is favoured and a Kondo singlet with a binding energy $k_B T_K$ is formed at low temperature. The Kondo energy $k_B T_K$ is given by

$$k_B T_K \sim \frac{1}{N(E_F)} e^{-\frac{1}{JN(E_F)}}. \tag{2.4}$$

For an impurity system, this leads to an increase in resistance at low temperature due to resonant scattering from the magnetic impurities. Heavy fermion compounds

consist of a lattice of magnetic atoms, and below a temperature $T^* \sim T_K$ a coherent state develops and the resistance drops rapidly below this. As $T \to 0$, Fermi-liquid behaviour is recovered with resistivity $\rho = \rho_0 + AT^2$, with a very large A coefficient, reflecting the enhanced effective mass in the so-called heavy-fermion system.

The Kondo effect supresses magnetic ordering in an f-electron system; however, there is a competing effect, known as the Ruderman-Kittel-Kasuya-Yosida (RKKY) interaction. The latter describes the way the f electrons interact with each other via the conduction electrons, and it tends to favour a magnetically ordered ground state. The energy associated with the RKKY interaction is

$$k_B T_{RKKY} \sim J^2 N(E_F). \tag{2.5}$$

The coupling constant J can be adjusted by pressure, chemical substitution, or magnetic field. At one particular value, J_c, the Kondo and RKKY interactions are equal and opposite, and the magnetically ordered and non-magnetic ground states are degenerate. This is known as a quantum critical point (QCP).

At a QCP, the magnetic ordering temperature (e.g. the Néel temperature T_N for an antiferromagnet) is driven to zero. At the resulting $T = 0$ second order phase transition the correlation length for magnetic fluctuations diverges, resulting in low energy, large amplitude fluctuations in magnetisation.

These fluctuations interact with the conduction electrons, leading to so-called non Fermi-liquid behaviour, where unusual power laws in the resistivity and other properties such as susceptibility and specific heat are found.

The resistivity close to a magnetic QCP will usually follow a power law $\rho(T) = \rho_0 + AT^n$, with a range of validity which depends on how close the system is to the QCP. The exponent n is predicted to be 3/2 for antiferromagnetic fluctuations, or 5/3 for ferromagnetic fluctuations (see for example Lonzarich [1997]).

2.2.2 Magnetically mediated superconductivity

The large-amplitude spin fluctuations present around a magnetic QCP mean that an electron, which carries its own magnetic moment, will produce a large polarisation of its surroundings. This polarisation produces a local magnetic field which can be felt by a second electron, and if the relative orientation of the spins is appropriate, an attractive interaction will occur.

A phenomenological model for spin-fluctuation mediated superconductivity is discussed in Lonzarich [1997] and Mathur et al. [1998], with a critical temperature given by

$$T_c \sim T_{sf}[1 - (\frac{\xi}{\ell}^2)]\theta e^{-\frac{1+\lambda'}{g\lambda'}}. \tag{2.6}$$

T_{sf} is analogous to the Debye temperature in BCS theory, and is related to the relaxation rate Γ_q, of the spin fluctuations. This factor sets the overall scale for spin-mediated superconductivity in a given system.

The factor $1 - (\frac{\xi}{\ell}^2)$ describes the pair breaking due to impurities, illustrating the requirement in unconventional superconductors that the mean free path ℓ be greater than the coherence length ξ. θ depends on the form of Γ_q and partly represents the damping due to incoherent inelastic scattering from impurities and low frequency spin fluctuations.

The interaction strength g measures the effectiveness of the pair wavefunction in sampling the attractive part of the pair potential.

$\lambda' \sim \sum_q 1/\Gamma_q$ represents the effective mass enhancement due to the magnetic interaction. It diverges at the magnetic QCP, while away from the magnetic instability λ' becomes small and the T_c is strongly suppressed.

Apart from the pair breaking, most of these factors relate to the nature of the spin fluctuations, which interact with the conduction electrons and hence are visible in the normal state resistivity. If one can identify the presence of spin fluctuations in the normal state properties, along with correlations between these and the superconductivity, this is strong evidence that they are of the same origin.

2.3 Valence instabilities and valence-fluctuation mediated superconductivity

Ce-based heavy fermions owe their massively enhanced effective masses to the interaction between the spins of the conduction electrons and the dense array of Ce^{3+} ions, whose single $4f^1$ electron has its own magnetic moment.

There exists another class of Ce compounds, which display more normal metallic behaviour. They have properties close to that of the equivalent La compound, which lacks $4f$ electrons, and measurements to determine the valence of the Ce atom show an intermediate valence somewhere between three and four.

When placed under extremely high pressure, compounds such as $CeCu_2Si_2$ go from heavy fermion behaviour to that reminiscent of intermediate valence compounds, and the resistivity for instance is close to that of $LaCu_2Si_2$. In chapter five I will present evidence that this valence change happens suddenly at a pressure associated with the enhancement of superconductivity under pressure in $CeCu_2Si_2$.

The relationship between valence change and superconductivity was first put on a theoretical footing by Miyake in 1998, who introduced an extra term into the periodic Anderson model representing a Coulomb repulsion U_{fc} between the conduction c-, and f-electrons (see Miyake et al. [1999] onwards). The introduction of this term

causes the valence change to become much more abrupt, eventually of first order character for large enough values of U_{fc}.

Recently Monthoux and Lonzarich [2004] have proposed a phenomenological theory of density-fluctuation-meditated superconductivity, which encompasses valence fluctuations. They found that the robustness of the pairing increases gradually as the system goes from a cubic to a more and more anisotropic tetragonal structure.

In the following section I will explain the principal results from Miyake's valence fluctuation theory, including in more detail the recent developments presented in Holmes, Jaccard, and Miyake [2004b]. I will first describe the model itself, then its consequences relating to the valence instability, superconductivity, and enhanced impurity scattering.

The detailed derivation of the linear resistivity and enhanced Sommerfeld coefficient is based on Miyake's contribution to Holmes et al. [2004b].

Finally, I will present a qualitative microscopic picture of the valence instability. This is my own speculative interpretation of the theory, but it appears to explain intuitively several features, from the sudden change of f-occupation, to the attractive pairing interaction.

2.3.1 The extended periodic Anderson model

The model proposed to explain the rapid change of valence with pressure was parameterised in the following hamiltonian:

$$\begin{aligned}\mathcal{H} &= \sum_{k\sigma}(\epsilon_k-\mu)c^\dagger_{k\sigma}c_{k\sigma}+\epsilon_f\sum_{k\sigma}f^\dagger_{k\sigma}f_{k\sigma}+U_{ff}\sum_i n^f_{i\uparrow}n^f_{i\downarrow}\\ &\quad +V\sum_{k\sigma}(c^\dagger_{k\sigma}f_{k\sigma}+\text{h.c.})+U_{fc}\sum_{i\sigma\sigma'}n^f_{i\sigma}n^c_{i\sigma},\end{aligned} \tag{2.7}$$

where the first two terms denote the energy of the conduction and f electrons respectively, along with the chemical potential μ; the third term represents the on-site correlation energy which prevents the f-levels from being doubly occupied; the fourth term is the hybridisation between conduction and f electrons. The final term is the extra one, with U_{fc} representing the short range coulomb repulsion between f electrons and those in the conduction band.

The effect of pressure is introduced via the energy ϵ_f, which is assumed to rise towards the Fermi level E_F as the pressure is increased. At the point where $\epsilon_f + \langle n_f\rangle U_{fc} \simeq E_F$, the $4f^1$ and $4f^0$ states are nearly degenerate, giving rise to valence fluctuations.

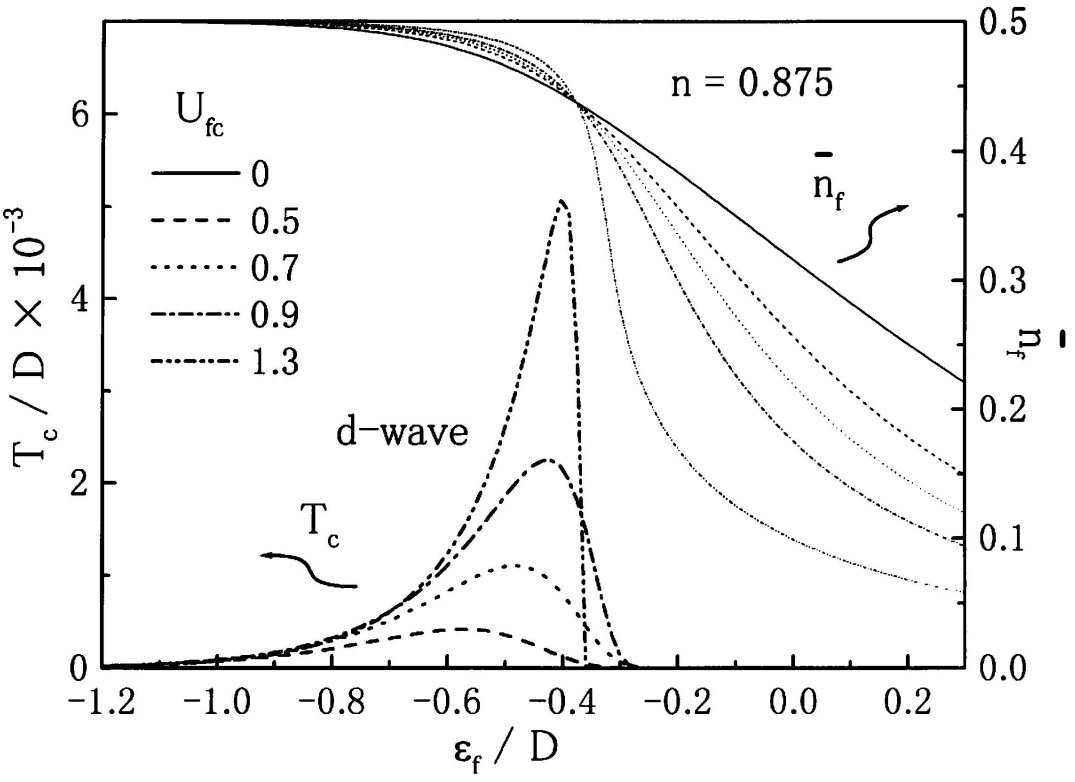

Figure 2.1: T_c for the d-wave channel and $\bar{n}_f$, f-electron number per site and 'spin' as a function of ϵ_f. The other parameters are as given in Onishi and Miyake [2000b].

2.3.2 The effect of U_{fc}: Rapid valence change and superconductivity

The introduction of U_{fc} produces a rapid charge transfer of f-electrons into the conduction band when $\epsilon_f + \langle n_f \rangle U_{fc} \simeq E_F$. The associated fluctuations can scatter from f and conduction electrons, and produce an attractive interaction in the d-wave channel, leading to superconductivity.

In figure 2.1, the number of f-electrons per site and 'spin' $\bar{n}_f$ is shown as a function of ϵ_f/D, where D is the conduction bandwidth. As U_{fc} increases, the drop in $\bar{n}_f$ becomes sharper and sharper, eventually revealing a discontinuous first order character (not shown). The valence susceptibility $\chi_{\rm v}$ is given by $-(\partial \bar{n}_{\rm f}/\partial \epsilon_{\rm f})_\mu$. Its maximum corresponds to the most rapid change of $\bar{n}_f$, and this is the point we define as the critical valence pressure $P_{\rm v}$.

The superconducting transition temperature T_c is shown in the same figure, and corresponds to d-wave pairing. It has a maximum slightly below $P_{\rm v}$, and is rapidly suppressed as $\bar{n}_f$ falls below about 0.4. The magnitude and sharpness of the peak in T_c increases with U_{fc}.

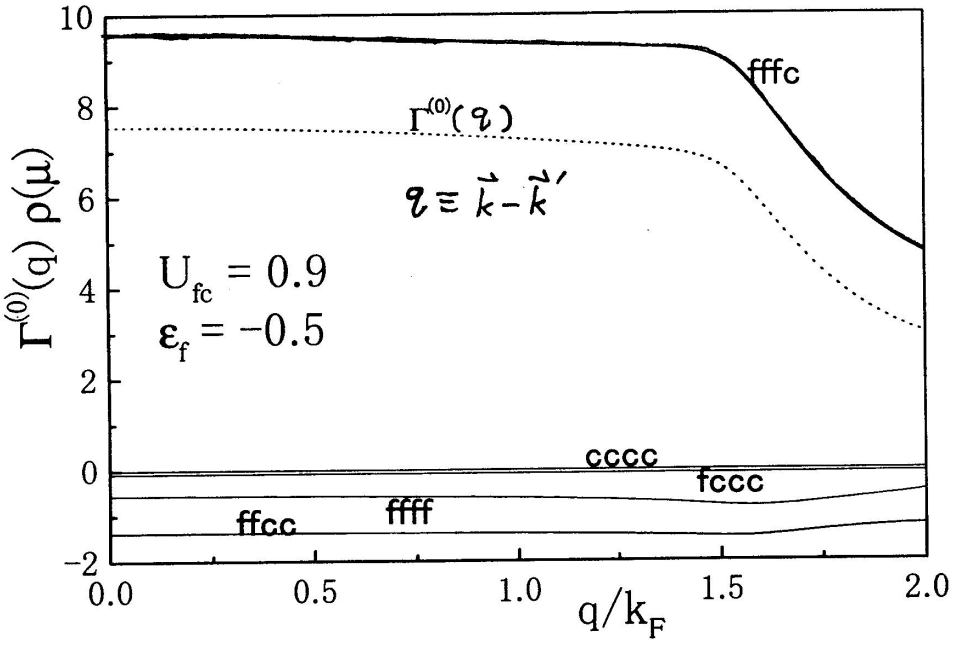

Figure 2.2: Scattering amplitude $\Gamma^{(0)}(q)$ as a function of momentum transfer q for various scattering channels. The total scattering amplitude is shown by the dotted line. Note that it remains roughly constant up to around $3k_F/2$.

In Fig. 2.2, the scattering amplitude $\Gamma^{(0)}(q)$ as a function of momentum transfer q is shown. It is formed from the sum of several different scattering processes, e.g. $ffcc$ represents two f electrons scattering off each other and into the conduction band. The major part of $\Gamma^{(0)}(q)$ is induced by the scattering process $(f,f) \rightarrow (f,c)$ or $(f,c) \rightarrow (f,f)$, in which the valence of f-electrons is changed directly. It is roughly constant up to $3k_F/2$, indicating that the interaction is largely localised.

2.3.3 Enhancement of the residual resistivity

The residual resistivity ρ_0 arises from scattering from defects and impurities. It was shown that impurity potentials can be renormalised by valence fluctuations, creating a giant enhancement of ρ_0 at the valence instability (Miyake and Maebashi [2002]).

According to the theoretical prediction, the residual resistivity ρ_0 is given as

$$\rho_0 = B n_{\rm imp} |u(0)|^2 \ln \left| \left(-\frac{\partial n_{\rm f}}{\partial \epsilon_{\rm f}} \right)_{\mu} / N_{\rm F} \right| + \rho_0^{\rm unit}, \tag{2.8}$$

where the coefficient B depends on the band structure of host metals, $n_{\rm imp}$ is the concentration of impurities with moderate scattering potential $u(q)$ coming from disorder other than Ce ions, $N_{\rm F}$ is the density of states of quasiparticles around the Fermi level, and the last term represents the residual resistivity due to unitary scattering mainly arising from any deficit or defect of the Ce ions.

This can be understood as the impurities nucleating a change of valence in the surrounding Ce ions, producing a greatly enhanced scattering cross section.

2.3.4 Theory of T-linear resistivity and enhanced Sommerfeld coefficient

In the preceding sections I presented results based on a series of theoretical investigations on the basis of an extended Anderson lattice model (Onishi and Miyake [2000a,b]; Miyake and Maebashi [2002]).

Various unconventional properties observed around $P \sim P_{\rm v}$ were explained, at least qualitatively, by these calculations. However, the T-linear temperature dependence of the resistivity observed in a narrow region around $P \sim P_{\rm v}$ remained unexplained before Holmes et al. [2004b].

In Onishi and Miyake [2000b], microscopic calculations showed that the static limit of the effective interaction $\Gamma^{(0)}(q)$ between quasiparticles is enhanced greatly around $P \sim P_{\rm v}$, and is almost independent of q, the momentum transfer, up to $\sim 3/2$ of $k_{\rm F}$, reflecting the local nature of critical valence fluctuations (this is shown in Fig. 2.2). This implies that the valence fluctuation response function $\chi_{\rm v}(q,\omega)$ is also almost q-independent in the low frequency region. Based on this observation, we can explain

phenomenologically the T-linear resistivity and the enhancement of the Sommerfeld coefficient γ around $P \sim P_{\rm v}$.

Valence-fluctuation propagator $\chi_{\rm v}$

We adopt an exponentially decaying phenomenological form, independent of q, for the valence-fluctuation propagator (dynamical valence susceptibility) $\chi_{\rm v}$:

$$\chi_{\rm v}(q,\omega) \equiv {\rm i}\int_0^\infty {\rm d}t e^{{\rm i}\omega t}\langle[n_{\rm f}(q,t), n_{\rm f}(-q,0)]\rangle \tag{2.9}$$

$$= \frac{K}{\omega_{\rm v} - {\rm i}\omega}, \quad \text{for } q < q_{\rm c} \sim p_{\rm F} \tag{2.10}$$

where $n_{\rm f}(q)$ is the Fourier component of the number of f-electron per Ce site, K is a constant of $\mathcal{O}(1)$, and $\omega_{\rm v}$ parameterizes the closeness to criticality. $\omega_{\rm v}$ is inversely proportional to the valence susceptibility $\chi_{\rm v}(0,0) = -(\partial n_{\rm f}/\partial\epsilon_{\rm f})_\mu$.

Quasiparticle effective mass and lifetime

The real and imaginary parts of the retarded self-energy $\Sigma^{\rm R}_{\rm vf}(p, \epsilon + {\rm i}\delta)$ respectively give a measure of the quasiparticle effective mass and lifetime. They can be calculated using a simple one-fluctuation mode exchange process (see Fig. 2.3) and are given as follows:

$$\begin{aligned}{\rm Re}\Sigma^{\rm R}_{\rm vf}(p,\epsilon) &= -\frac{K}{2\pi}\sum_{\mathbf{q}}|\lambda|^2\int_{-\infty}^{+\infty}{\rm d}x\frac{x}{\omega_{\rm v}^2+x^2} \\ &\quad\times\frac{\coth\frac{x}{2T}+\tanh\frac{\xi_{\mathbf{p}-\mathbf{q}}}{2T}}{-\epsilon+\xi_{\mathbf{p}-\mathbf{q}}+x},\end{aligned} \tag{2.11}$$

$$\begin{aligned}{\rm Im}\Sigma^{\rm R}_{\rm vf}(p,\epsilon) &= -\frac{K}{2}\sum_{\mathbf{q}}|\lambda|^2\frac{\epsilon-\xi_{\mathbf{p}-\mathbf{q}}}{\omega_{\rm v}^2+(\epsilon-\xi_{\mathbf{p}-\mathbf{q}})^2} \\ &\quad\times\left(\coth\frac{\epsilon-\xi_{\mathbf{p}-\mathbf{q}}}{2T}+\tanh\frac{\xi_{\mathbf{p}-\mathbf{q}}}{2T}\right),\end{aligned} \tag{2.12}$$

where λ is the coupling between quasiparticles and the valence fluctuation modes, and ξ_p is the dispersion of the quasiparticle. For simplicity, λ is assumed to be constant without wavenumber or frequency dependence.

In typical limiting cases, (2.12) can be straightforwardly calculated in the approximation $\xi_{\mathbf{p}-\mathbf{q}} \simeq -vq\cos\theta$, where θ is the angle between $\mathbf{p}$ and $\mathbf{q}$, v is the quasiparticle velocity, and p is assumed to be on the Fermi surface, i.e., $p = p_{\rm F}$:

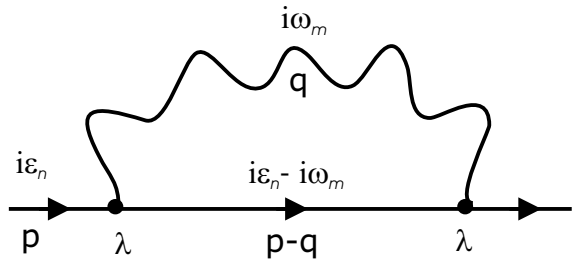

Figure 2.3: Feynman diagram for the self-energy given by eqs. (2.11) and (2.12). The solid line represents the Green function of the quasiparticles, the wavy line the propagator of the valence fluctuations, and the filled circle the coupling between valence-fluctuation modes and the quasiparticles. ϵ_n and ω_m are the Matsubara frequency of the quasiparticle and fluctuation propagators, respectively.

$T = 0$, $\epsilon \neq 0$:

$$\mathrm{Im}\Sigma^{\mathrm{R}}_{\mathrm{vf}}(p_{\mathrm{F}}, \epsilon) \simeq -\frac{|\lambda|^2 K q_{\mathrm{c}}^2}{32\pi^2 v} \ln\left(1 + \frac{\epsilon^2}{\omega_{\mathrm{v}}^2}\right), \tag{2.13}$$

where q_{c} is the cutoff wavenumber of the order of k_{F}.

$\epsilon = 0$, $0 < T \ll \epsilon_{\mathrm{F}}$:

$$\begin{aligned} \mathrm{Im}\Sigma^{\mathrm{R}}_{\mathrm{vf}}(p_{\mathrm{F}}, 0) \;\simeq\; & -\frac{|\lambda|^2 K}{8\pi^2 v} \int_0^{q_{\mathrm{c}}} \mathrm{d}q\, q \int_{-vq/2T}^{vq/2T} \mathrm{d}y \times \\ & \frac{y}{(\omega_{\mathrm{v}}/T)^2 + y^2} (\coth\frac{y}{2} - \tanh\frac{y}{2}), \end{aligned} \tag{2.14}$$

where $y = vq\cos\theta/2T$. Since $vq \gg T$ holds in the dominant region of q-space, the integration with respect to y can be performed, to a good accuracy, leading to

$$\mathrm{Im}\Sigma^{\mathrm{R}}_{\mathrm{vf}}(p_{\mathrm{F}}, 0) \simeq -\frac{|\lambda|^2 K q_{\mathrm{c}}^2}{4\pi^2 v} \frac{T}{\omega_{\mathrm{v}}} \tan^{-1}\frac{T}{\omega_{\mathrm{v}}}, \tag{2.15}$$

where we have made approximation that the range of integration is restricted as $-1 < y < 1$ in which the last factor in (2.14) is approximated as $2/y$. Then,

$$\mathrm{Im}\Sigma^{\mathrm{R}}_{\mathrm{vf}}(p_{\mathrm{F}}, 0) \simeq -\frac{|\lambda|^2 K q_{\mathrm{c}}^2}{4\pi^2 v} \begin{cases} \left(\frac{T}{\omega_{\mathrm{v}}}\right)^2, & T \ll \omega_{\mathrm{v}} \\ \frac{\pi}{2}\frac{T}{\omega_{\mathrm{v}}}, & T \gg \omega_{\mathrm{v}} \end{cases} \tag{2.16}$$

The latter result, $\mathrm{Im}\Sigma_{\mathrm{vf}}(p_{\mathrm{F}}, \epsilon = 0) \propto T/\omega_{\mathrm{v}}$ for $T \gg \omega_{\mathrm{v}}$, implies that almost all the critical valence-fluctuation modes can be regarded as classical at $T > \omega_{\mathrm{v}}$, and T-linear dependence stems from the asymptotic form of $\coth(x/2T) \simeq 2T/x$, essentially the classical approximation of the Bose distribution function.

The real part of the self-energy, (2.11), can be calculated easily at $T = 0$ and $\epsilon \sim 0$, leading to

$$\begin{aligned} \mathrm{Re}\Sigma^{\mathrm{R}}_{\mathrm{vf}}(p_{\mathrm{F}}, \epsilon) &- \Sigma^{\mathrm{R}}_{\mathrm{vf}}(p_{\mathrm{F}}, 0) \\ &\simeq -\frac{|\lambda|^2 K \epsilon}{4\pi^2} \int_0^{q_{\mathrm{c}}} \mathrm{d}q\, q^2 \int_{-1}^{1} \mathrm{d}t \\ &\quad \times \left[\frac{-1}{\omega_{\mathrm{v}}^2 + (vqt)^2} \ln \left| \frac{e\omega_{\mathrm{v}}}{vqt} \right| + \frac{\pi \omega_{\mathrm{v}} vq|t|}{[\omega_{\mathrm{v}}^2 + (vqt)^2]^2} \right. \\ &\qquad \left. + \frac{2\omega_{\mathrm{v}}^2}{[\omega_{\mathrm{v}}^2 + (vqt)^2]^2} \ln \left| \frac{\omega_{\mathrm{v}}}{vqt} \right| \right], \end{aligned} \tag{2.17}$$

where $t = \cos\theta$. In the limit $\omega_{\mathrm{v}} \ll v p_{\mathrm{F}}$, integration with respect to t in (2.17) leads to

$$\mathrm{Re}\Sigma^{\mathrm{R}}_{\mathrm{vf}}(p_{\mathrm{F}}, \epsilon) \simeq -\frac{|\lambda|^2 K q_{\mathrm{c}}^2}{2\pi^2 v} \frac{\epsilon}{\omega_{\mathrm{v}}} \int_0^1 \mathrm{d}u \frac{1-u^2}{u^2+1} \ln \left| \frac{1}{u} \right| \tag{2.18}$$

$$\propto -\frac{\epsilon}{\omega_{\mathrm{v}}}, \tag{2.19}$$

where $u = vqt/\omega_{\mathrm{v}}$.

Linear resistivity

The T-linear dependence of $\mathrm{Im}\Sigma^{\mathrm{R}}_{\mathrm{vf}}(p, 0)$, for $T > \omega_{\mathrm{v}}$, (2.16), implies T-linear resistivity, as the quasiparticles are subject to the large angle scattering by the critical valence-fluctuation modes. These are effective in a wide region in the Brillouin zone due to their local nature and easily couple to the Umklapp process of quasiparticle scattering. This result is consistent with the experimental fact that T-linear resistivity is observed in a narrow pressure region around P_{v}, which is considered to correspond to a nearly critical valence transition of the Ce ion.

Such a T-linear dependence has been discussed in the context of high-T_c cuprates with a marginal Fermi liquid (MFL) assumption (Varma et al. [1989]), and charge transfer fluctuations were once considered as an origin for MFL (Varma et al. [1987]; Perakis et al. [1993]), while further theoretical models have been put forth up to now (Varma et al. [2002]). Excepting the T-linear resistivity, the present result is different from MFL behavior. The self-energy exhibits different energy dependence, while the idea for the origin of our singular behavior shares aspects similar to the first idea of a charge transfer mechanism for high-T_c cuprates (Varma et al. [1987]; Perakis et al. [1993]). $\Sigma(\epsilon)$ in the MFL model is given as $\Sigma(\epsilon) \propto (\epsilon \ln \epsilon - \mathrm{i}|\epsilon|)$ (Varma et al. [1989]) which is indeed different from the present case [Eqs. (2.13) and (2.19)]. In any case, it is to be noted that T-linear resistivity is accompanied by the peak of T_c in both systems, high-T_c cuprates and $CeCu_2Si_2$.

Enhanced Sommerfeld coefficient

The result (2.19) implies that the mass enhancement $(1-\partial \mathrm{Re}\Sigma^{\mathrm{R}}_{\mathrm{vf}}(\epsilon)/\partial\epsilon)$ is expected around $P \sim P_{\mathrm{v}}$. Namely, the effective mass is given by

$$m^* \propto \bar{m}\frac{1}{\omega_{\mathrm{v}}}, \tag{2.20}$$

where $\bar{m}$ is the effective mass renormalized by the conventional correlation effect, leading to heavy electrons, i.e. not including the effect of critical valence fluctuations. This latter effective mass $\bar{m}$ exhibits a drastic decrease around $P \sim P_{\mathrm{v}}$, while the second factor in (2.20) is enhanced. Both effects should be reflected in the Sommerfeld coefficient γ, so that the peak of $\gamma \propto m^*$ is shifted to the lower pressure (larger $\bar{m}$) side, and the anomaly of γ due to the valence fluctuations may be smeared to some extent. Nevertheless, some trace should be observed. (The shift of peak of γ can be understood as the superposition of the two trends using a model P-dependence of $\bar{m}$ and ω_{v}.) Indeed, the present experimental result presented in Figs. 5.10 and 5.13 may be explained by this effect.

2.3.5 Microsopic description of valence fluctuations

It is worth addressing the physical interpretation of the valence fluctuation mediated pairing interaction. This intuitive explanation is rather speculative, but I think that it is sufficiently useful to merit inclusion.

A clue comes from the likely nearest neighbour pairing, implied by the largely local nature of the interaction, and the prediction of d-wave pairing symmetry. One can imagine an almost filled f-band, with each occupied f^1 site experiencing a Coulomb repulsion U_{fc} from the respective conduction electrons [Fig. 2.4 (a)].

Local reinforcement of valence change

As the pressure is increased and ϵ_f moves closer to the Fermi level E_F, there will come a point where $\epsilon_f + \langle n_f \rangle U_{fc} \simeq E_F$ and the f-band will start to empty. On an individual $4f^0$ 'hole' site, the repulsion caused by U_{fc} will be absent, thus an increased density of conduction electrons would be energetically favorable at this position. If this extra 'screening' conduction electron density is not strictly localized onto the atom itself, but spills onto neighboring sites, the f-electrons on Ce atoms around the original 'hole' site will feel an increased repulsion [Fig. 2.4 (b)]. The neighbouring $4f^1$ sites will be affected by the screening cloud of any $4f^0$ Ce atoms, raising the local Coulomb energy and favouring the transfer of their f electrons into the delocalised conduction band. This self-reinforcing tendency to transfer electrons from the f to conduction bands explains intuitively the increasingly catastrophic drop in n_f for larger U_{fc}, shown in Fig. 2.1.

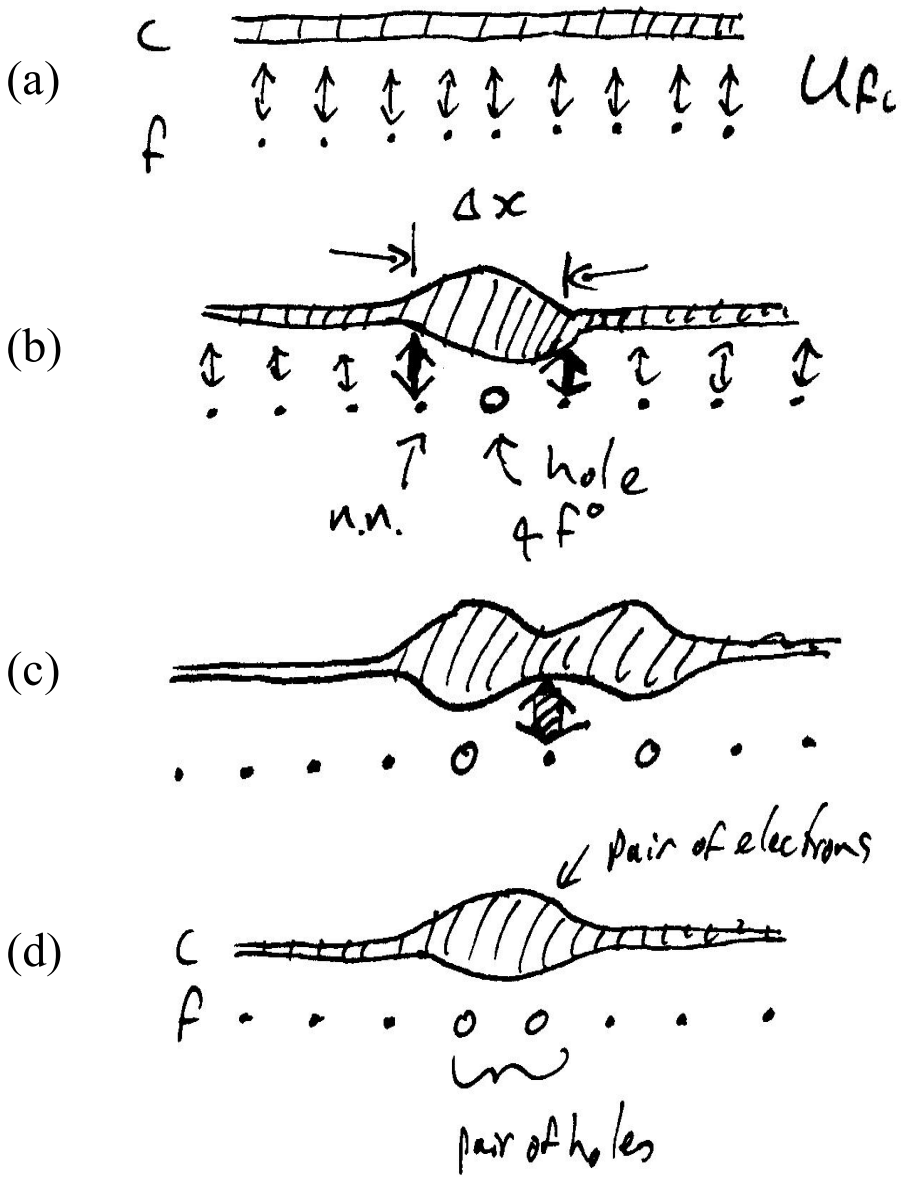

Figure 2.4: Graphical representation of valence transition at a local level. (a) $\epsilon_f + U_{fc} \ll E_F$, and all f sites are filled. (b) When $\epsilon_f + \langle n_f \rangle U_{fc} \simeq E_F$, f electrons start to transfer into the conduction band. Empty $4f^0$ sites will be screened by the conduction electrons, which are felt by neighbouring filled $4f^1$ sites via U_{fc}. (c) and (d) show how this can lead to an attractive nearest-neighbour pairing interaction. The extra repulsion from two overlapping screening clouds favours a $f^0 f^0 f^1$ configuration over $f^0 f^1 f^0$.

Attractive interaction

The attractive pairing interaction can be understood as follows [see Fig. 2.4 (b) and (c)]: Consider an isolated pair of $4f^0$ 'holes', accompanied by their cloud of conduction electrons. If these are separated by two lattice positions, with an intervening filled $4f^1$ site, the two screening clouds will overlap at the intermediate site, further increasing the Coulomb energy at that point. It would therefore be energetically favorable for the two 'holes' to be on neighboring atoms, thus the attractive interaction. The attractive interaction between 'holes' is equivalent to that between 'electrons', so that this argument would give an intuitive understanding of the origin of the valence-fluctuation mechanism of superconductivity.

Further consequences

If this model is correct, it would predict other effects. The attractive interaction is in real space, and not confined only to two electrons at a time. Therefore for large enough U_{fc}, phase separation might be expected to occur, given the right choice of other parameters such as V and ϵ_f.

This might explain why superconductivity disappears so rapidly when the $4f$ occupation drops much below 1/2. As the concentration of $4f^0$ sites increases, the chances of three or more interacting with each other increases rapidly.

The highly local and real-space nature of the interaction will also depend critically on the local charge distribution, and hence on the shape and orientation of the $4f$ orbitals. This may be why the excited crystal field split levels appear to be important, as P_{v} occurs where $T_K \sim \Delta_{CEF}$. An anisotropic interaction may also mean that the behaviour within the layers in the basal plane could be very different from that between them.

These thoughts are by no means certain, but they do have testable consequences, both through calculation and experiment.

2.4 Summary

In this chapter, after briefly addressing the mechanism of superconductivity in conventional systems, I have summarised the two main candidates for the superconducting mechanism in the systems presented in this thesis. These are namely spin-fluctuation and valence-fluctuation mediated pairing. Both have consequences for the normal state properties, observable through resistivity measurements. The latter has yet to gain widespread acceptance, but it appears to provide a convincing explanation for the phenomena observed in $CeCu_2Si_2$ at high pressure.

Chapter 3

Experimental methods

In this chapter I will outline the experimental methods used during the preparation of this thesis, with emphasis on new developments and refinements to existing procedures. The chapter has four main parts, describing the high pressure techniques, the measurement of resistivity and specific heat, the application of Bayesian analysis to power law behaviour in the resistivity, and a description of the pressure cells used to obtain the results presented in chapters four and five.

3.1 High Pressure

Static pressure techniques are commonly divided into two main categories, using anvil and piston-cylinder apparatus respectively. The latter permits larger volumes, but with a smaller maximum pressure, set by the tensile strength of the materials used to make the pressure cell. These techniques (and more) are discussed in great detail in Eremets [1996].

The high pressures attained in our experiments were produced using two different anvil cell methods:

Bridgman anvil cell Using tungsten carbide or sintered diamond anvils with a solid pressure medium, a pressure of up to 30 GPa can be obtained in quasi-hydrostatic conditions.

Helium-filled diamond anvil cell (DAC) This technique provides the best possible hydrostatic conditions, with pressures up to 10 GPa in our case. The use of a highly compressible pressure medium means that it is quite a lot more difficult to realise than the Bridgman technique.

3.1.1 Pressure Cells

For static pressures above 3 GPa, an opposed anvil design is usually required. The sample is embedded in a solid or liquid pressure medium, which is contained laterally by a gasket, and compressed between two anvils made from an extremely hard material (e.g. diamond, sapphire or tungsten carbide).

All of the experiments described below involve a clamp cell, where the force is applied using a hydraulic press, and maintained by four rods held under tension by a set of nuts. The load remains constant whilst measurements are carried out at low temperature. The pressure is then increased and the process repeated.

The body of the clamp is made from a non-magnetic material such as stainless steel in the case of the Bridgman cells, or Copper-Beryllium alloy in the diamond anvil cell.

Bridgman Anvil Cell

The pressure cell consists of two opposed anvils, a gasket and two discs of the pressure medium sandwiching the sample. For pressures up to 10 GPa, non-magnetic tungsten carbide anvils with a flat of 3.5 mm can be used. For higher pressures, up to 25-30 GPa, sintered diamond anvils with a flat of 2 or 1.5 mm are used.

The cylindrical gasket is made from pyrophyllite, chosen for its high friction coefficient with the anvils and itself. The pressure medium is the soft solid steatite (soapstone), in the form of two discs between which the sample and connection wires are sandwiched. Up to 12 wires can be introduced into the cell, for up to four samples plus a lead manometer. The electrical contacts are formed simply by physical pressure.

The main disadvantage of this technique compared to the DAC/He combination is the presence of pressure gradients, up to around 5% of the total pressure at 30 GPa. These can be identified by the width of the superconducting transition of lead, which is used as a pressure gauge. There are also uniaxial stresses present in the cell, whose magnitude is harder to evaluate. However we have taken advantage of these uniaxial stresses in compounds which are especially sensitive to anisotropic conditions. This is discussed in more detail in chapter 5. Further details about Bridgman cell construction can be found in, for example, Vargoz [1998].

Helium-filled Diamond Anvil Cell

The pressure cell was formed from a stainless steel gasket squeezed between two diamond anvils with 1.5 mm double bevelled culets, supported in a CuBe alloy clamp (see Fig. 3.1). Helium, introduced into the cell as a superfluid, was used as a

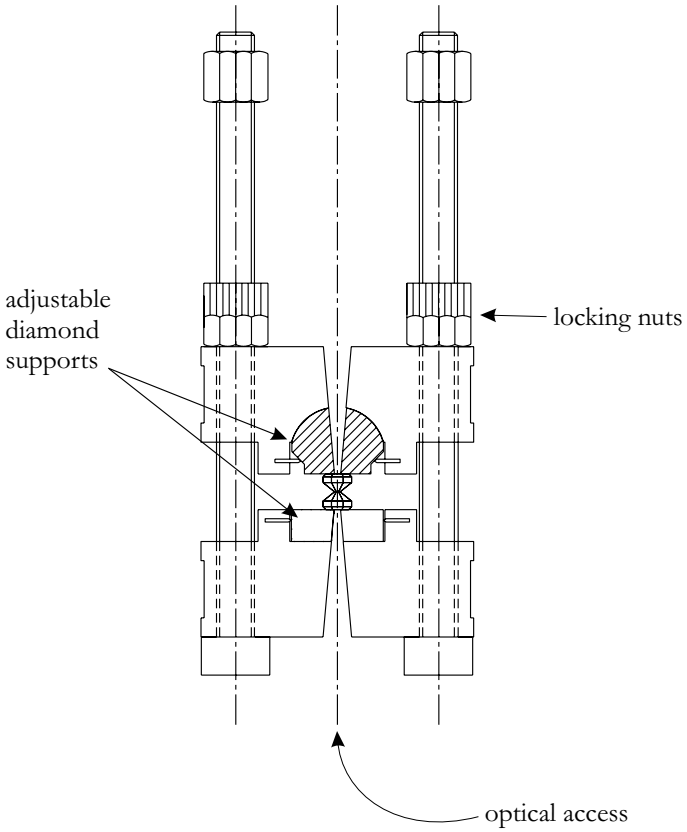

Figure 3.1: The diamond anvil clamp body is made from non-magnetic annealed CuBe alloy. The diamonds are adjusted to be precisely parallel, and perpendicular to the clamp axis. There is an additional copper plate between the two diamond support sections (not shown), which supports the gasket, electrical contacts, and thermometers. It is in good thermal contact with the rest of the cell. Pressure is applied by suspending the clamp from the upper nuts, applying the appropriate force to the upper diamond support, then tightening the locking nuts in as symmetrical a manner as possible. Pressure measurements are carried out using a ruby fluorescence method.

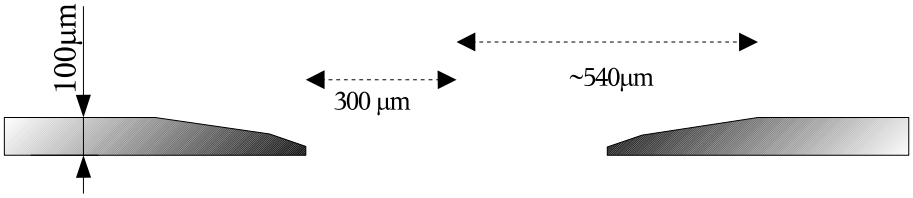

Figure 3.2: Profile of the stainless steel gasket used for the helium cell.

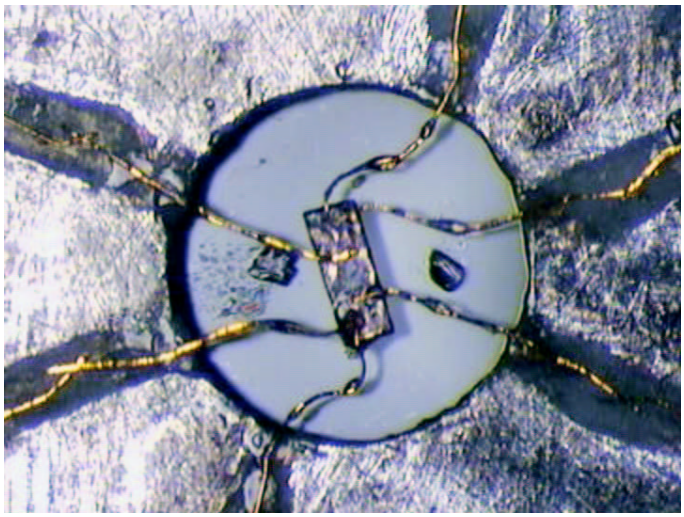

Figure 3.3: View from flat side of the helium cell gasket. The hole has a 600 μm diameter, and the monocrystalline $CeCu_2Si_2$ sample was cut and polished to $230 \times 80 \times 20\ \mu m^3$. One can also see the ruby chips used for pressure measurement, and the 5 μm wires with electrical insulation formed from 12-15μm deep grooves filled with an Al_2O_3/epoxy mixture. The gasket was electrically isolated from the clamp body, so that a single breach of the insulation would not cause an earth contact. The two ruby chips are used to determine the pressure. (Constructed in collaboration with D. Jaccard.)

pressure transmitting medium. Pressure could be applied to the cell both at room temperature and also in a glass cryostat that could be cooled down to 1.2 K.

Anvil alignment

The anvils must be precisely parallel, to avoid instability of the cell. If the diamonds are allowed to touch when the cell is under pressure, they will break! By observing the optical interference fringes produced when the diamonds were in contact with no gasket present, it was possible to align the diamonds to within 1 μm across the width of the culet.

Gasket

The gasket has to contain the pressure medium, keep the diamonds apart, and absorb any plastic deformation produced during the pressurisation process. It also has to allow passage of the measurement wires. Due to the high compressibility of both liquid and solid helium, there is a large reduction in volume of the pressure cell (up to a factor of eight at 10 GPa). The shape of the gasket allowed for this by starting with a hole with a truncated conical profile (see Fig. 3.2). This provides

a large initial volume which collapses as the pressure increased, and it also avoids scissoring the measurement wires.

Wires

The 5 μm Au or AuFe wires were spot welded to the sample and insulated from the gasket using Stycast 1266 epoxy resin saturated with Al_2O_3 powder in grooves on the flat site of the gasket. The grain size of the alumina powder was important for the integrity of the insulation, and a mixture of grain sizes ($< 1\mu$m and $< .3\mu$m) was used.

He pressure medium

The helium pressure medium was introduced into the cell by immersing the clamp in a bath of liquid helium, which was cooled by evaporation to below its superfluid transition temperature. Enough force to close the cell was applied to the clamp via a mechanical coupling to the room temperature hydraulic press. The force was blocked by tightening the nuts such that the pressure medium could not escape. The clamp was then allowed to warm to room temperature.

Low temperature vs. room temperature pressurisation.

It was possible to increase the pressure while the cell was still at liquid helium temperatures, using the same apparatus used to load the pressure cell. However, we found that the plastic deformation of the gasket was not continuous under these conditions, indeed there was often even an audible 'crack' followed by a sudden jump in the pressure. This is probably due to the lack of thermally activated dislocation movement at very low temperatures. In any case, it was not possible to change the pressure in-situ in the dilution cryostat, so the reported measurements were obtained by changing the pressure at room temperature. Precautions still had to be taken to avoid loss of helium pressure medium during the loading process.

3.1.2 Pressure measurement

Two different methods were used to measure the pressure inside the cell, depending on its type.

Bridgman cell — lead superconducting transition

In Bridgman cells, the superconducting transition temperature of lead provided the pressure scale. It decreases from a value of 7.2 K at ambient pressure to ~ 1 K at 32 GPa. The calibration used in this thesis came from Bireckoven and Wittig [1988]. However, more recent calibrations of lead (Schilling [2003], unpublished) indicate that there may be discrepancies, resulting from pressure inhomogeneities, of up to 1.7 GPa in the calibration. These are largest around 5 GPa. The quoted value of the pressures in the Bridgman cells may therefore be somewhat too large around this point.

There remained a small remnant field in the cryostat, which had to be corrected with a small opposing current in the cryostat magnet before an accurate value of T_c could be measured.

Helium cell — ruby fluorescence

With transparent anvils such as diamonds, optical methods can be used to determine the pressure. One such pressure gauge is the ruby scale. Ruby has a strong luminescent doublet at 694.2 and 692.8 nm. These shift more or less linearly with pressure, and they provide a useful pressure scale which has been calibrated up to 100 GPa.

An Ar laser was used to excite the ruby fluorescence, and a diffraction grating and CCD detector to determine the ruby emission lines. By fitting the top of the emission peak, the pressure could be determined to within 0.02 GPa at 4.2 K, assuming a temperature-independent shift of the ruby line of 2.746 GPa nm^{-1}. Further discussion of the ruby pressure scale can be found in Eremets [1996].

Figure 3.4 shows the V-T phase diagram of solid and liquid helium with isobars up to 20 kbar (2 GPa). This illustrates a problem with helium-filled pressure cells which is not present in Bridgman cells, i.e. there is a considerable pressure loss going from room temperature to cryogenic temperatures. Indeed, in the resistivity data it is possible to identify the He liquid-solid transition, and follow its variation with pressure. The bulk of the pressure loss occurs in the liquid phase however, and we can assume that the pressure remains constant below around 10 K.

We therefore measured the pressure at 4.18 K (and also at higher temperatures) for all experiments, using an optical fibre introduced into the dilution cryostat. Care was taken to thermally anchor the optical fibre, and to avoid signal losses from scratches or due to bending it about too small a radius of curvature.

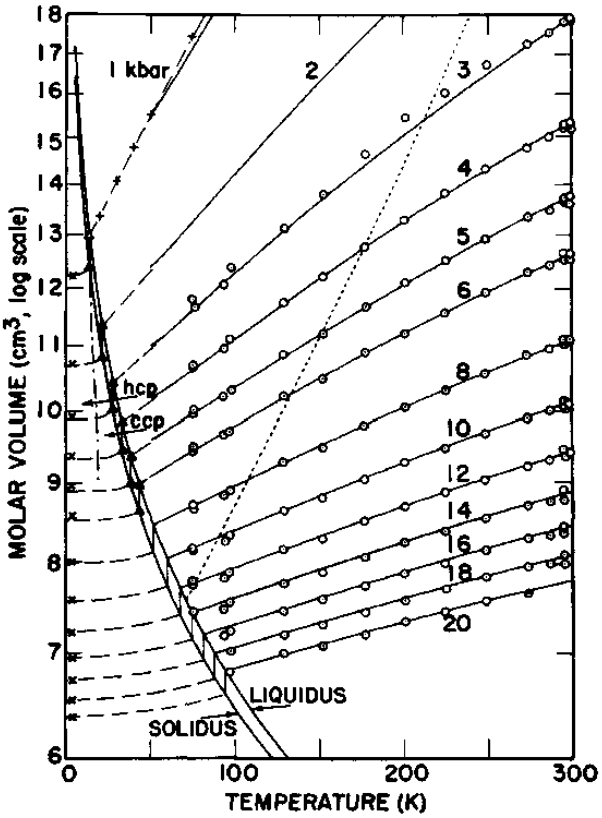

Figure 3.4: Plot of $\ln V$ vs T for 13 isobars in fluid and solid ^{4}He, from Mills et al. [1980]. Assuming the volume is constant in the pressure cell, around 1 GPa is lost on cooling from e.g. 2 GPa at 300 K. The pressure loss decreases as the pressure increases.

3.2 Cryogenics, thermometry, and magnetic field

The experiments were carried out in a ^{3}He/^{4}He dilution cryostat capable of going down to 15 mK in the absence of a payload. The lowest temperature attained with a pressure cell was around 30 mK.

Temperatures were determined below 4.18 K using calibrated RuO_2 resistance thermometers, with appropriate compensation when under magnetic field (detailed in Vargoz [1998]). Above 4.18 K cernox, Ge and Pt resistance thermometers were used. A high precision TRMC2 temperature controller was used for the resistance measurements.

The cryostat was fitted with a superconducting magnet capable of producing a field of up to 8 T.

3.3 Resistivity

The resistance measurements presented in the following chapters were obtained using a dc method with detection giving a precision of 0.05–1 nV, depending on the exact setup. Low impedance copper and superconducting connections from 300 K down the cryostat ensured the minimum possible thermal noise.

Four-point resistance measurements of the sample were carried out. The resistivity was determined from the geometry measured prior to loading the cell. After depressurisation the contacts were compared with their initial positions, which indicated that the absolute values of the resistivity were correct to within 10% or better.

Joule heating of the sample by the measurement current had to be avoided when measuring at the lowest temperatures. Smaller currents would accomplish this, at the expense of measurement noise, but the optimum sample geometry was therefore a matchstick form, with the minimum cross-section and maximum length compatible with the cell.

3.4 AC Calorimetry

The second experimental technique we used was ac calorimetry. This involves heating the sample with a periodic heat source, and following the resulting temperature oscillations. The phase and amplitude of these depends on the heat capacity of the sample, and on the thermal coupling to the surroundings. If the modulation frequency is sufficiently high, then the sample is effectively decoupled from its surroundings. In these conditions the ac calorimetry technique provides a sensitive measurement of the sample heat capacity even in highly non-adiabatic circumstances.

Traditional adiabatic calorimetry involves the subtraction of a background signal, due to the apparatus around the sample, and therefore works best with large samples. AC calorimetry can deal with situations where the surrounding apparatus is vastly more massive than the sample itself, so it is ideally suited to the high pressure environment. Our samples were typically smaller that 1 μg.

In comparison with adiabatic methods, the ac technique has less absolute accuracy, but it is extremely sensitive, enabling very small anomalies in the specific heat to be identified. The actual heat capacity measured may, however, include components from the anvils, pressure medium etc. as well as from the sample itself. The amplitude of the heating power may not be known precisely either, so this method is best used to identify anomalies at phase transitions, or to follow changes in specific heat with pressure, for example.

The technique was first tried in the helium-filled DAC system by Demuer [2000], using a laser heating method in a conventional ^{4}He cryostat, at temperatures down to 1.2 K, and has also been used in a Bridgman-type pressure cell (Bouquet et al. [2000]; Demuer et al. [2002]). The results in chapter five represent the first time that the ac calorimetry technique has been used in a helium medium below 1 K, in a dilution cryostat.

For a more general discussion of ac calorimetry, including its applicability to first order transitions, see Bouquet [1998].

3.4.1 Principles

The model used to extract the specific heat from the phase and amplitude of the temperature oscillations is based on a simplified version of that discussed in Sullivan and Seidel [1968] and Eichler and Gey [1979]. We consider a sample with heat capacity C connected via a thermal conductance K to a thermal bath at a temperature T_b. If a heating power $P = P_0[1 + \cos(\omega t)]$ is applied to the sample, then the amplitude of its temperature oscillations depend in part on C. We can describe the sample temperature T in general as

$$T = T_b + T_{DC} + |T_{AC}| \cos(\omega t + \phi), \tag{3.1}$$

where T_{DC} represents the average elevation of sample temperature above the bath, and $|T_{AC}|$ represents the amplitude of the temperature oscillations, which have a phase shift ϕ with respect to the heater.

The model is straightforward to solve, and gives, in complex notation,

$$T_{AC} = \frac{P_0}{K + i\omega C}. \tag{3.2}$$

This model does not take into account any decoupling of the thermometer and sample, which would result in a more rapid falloff in amplitude at frequencies above that

characterising the relaxation timescale between the sample and thermometer. This is considered in more detail in the above references. Given that our thermometer consisted of a thermocouple spot welded to the sample, it was assumed that they were in thermal equilibrium at our measurement frequencies, and that this was not the most significant imperfection in the model in any case.

For frequencies $\omega \gg \omega_c$, where ω_c is the cut-off frequency K/C, the sample contribution dominates the signal, and $|T_{AC}|$ can be considered to be inversely proportional to the heat capacity (which we assume to be dominated by the sample). For $\omega \ll \omega_c$, the signal approaches the dc limit and gives a measure of the mean elevation of the sample temperature over that of the bath. For intermediate measurement frequencies, information from the phase ϕ, can be used to extract the specific heat:

$$C = \frac{-P_0 \sin\phi}{\omega\,|T_{AC}|}\ . \tag{3.3}$$

Alternatively, one can subtract a background signal taken at a different frequency, with

$$C = \frac{P_0}{(\omega_2^2 - \omega_1^2)^{1/2}} \left(\frac{1}{|T_{AC,\omega_2}|^2} - \frac{1}{|T_{AC,\omega_1}|^2} \right)^{1/2}, \tag{3.4}$$

where ideally $\omega_2 > \omega_c > \omega_1$. The sample temperature must also be corrected for the constant dc component of the oscillatory Joule heating. This was done by repeating the measurement well below the cut-off frequency, also providing the background signal in order to estimate C_P using Eq. (3.4).

3.4.2 Measurement

The helium cell had both optical access for laser heating, and the possibility of electrical heating of the sample. We determined that electrical heating was the best method. It gave a larger contribution to the signal from the sample itself (this was determined by the relative size of the superconducting specific heat jump in $CeCu_2Si_2$ for similar magnitude of signal).

The temperature oscillations were detected using a Au/AuFe thermocouple, amplified by a transformer and preamp circuit (at room temperature), and measured using lock-in detection. The detection sensitivity was 0.2 nV using a 3 s filter.

By measuring the frequency response at a give temperature, it was possible to identify the cut-off frequency ω_c. In the helium cell this turned out to be very temperature dependent, varying between 200 Hz at 0.5 K and over 2 kHz at 1.5 K, presumably due to the thermal properties of the surrounding material. Fortunately, while complicating the data analysis, the reduction in ω_c at the lowest temperatures allows the technique to be used down to $\sim$100 mK. The two estimates of C_P using

Eqs. (3.3) and (3.4) are in good agreement below ∼2 K. The working frequency ω_2 was generally of the order of ω_c.

The sample temperature must also be corrected for the constant dc component of the oscillatory Joule heating T_{DC}. This was done by repeating the measurement well below the cut-off frequency, also providing the background signal used to calculate C_P using eq. (3.4). In helium the correction grows quickly at low temperature, as the thermal conductivity of the pressure medium rapidly decreases. This means (unsurprisingly) that the heating power must be reduced at low temperature. In general a given set of parameters ω, P_0 is only appropriate over a half decade in temperature.

3.4.3 Data analysis

To obtain $C_P(T)$ from the calorimetry data, the following steps were taken:

1. Measure the amplitude and phase of the thermocouple response at two frequencies: (a) at or above the cut-off frequency ω_c, and (b) well below it.

2. Convert the thermocouple voltage amplitude into temperature, using the AuFe thermopower $S(T)$. This gives T_{AC} and T_{DC} respectively for (a) and (b).

3. Correct the temperature scale — the mean sample temperature is given by $T + T_{DC}$.

4. Calculate C_P using either Eq. (3.3) (using the phase of T_{AC}) or (3.4) (using T_{DC}), taking into account the heating power.

An example is shown in Fig. 3.5, where the phase was used to calculate C_P. The superconducting specific heat jump at around 1.5 K is almost as large as the total amplitude, indicating that the sample provides the majority of the signal. If the specific heat is calculated using the two-frequency method [Eq. (3.4)], the result agrees ($< 5\%$) with that calculated using the amplitude and phase up to at least 2 K.

3.4.4 Possibilities and Limitations

The results shown above, and presented in chapter five, show that the ac calorimetry technique can provide very high quality data, representing something closely resembling the sample specific heat under pressure. We are therefore tempted to analyse these results quantitatively, to determine for example the temperature dependence of C_P, or the size of the superconducting specific heat jump.

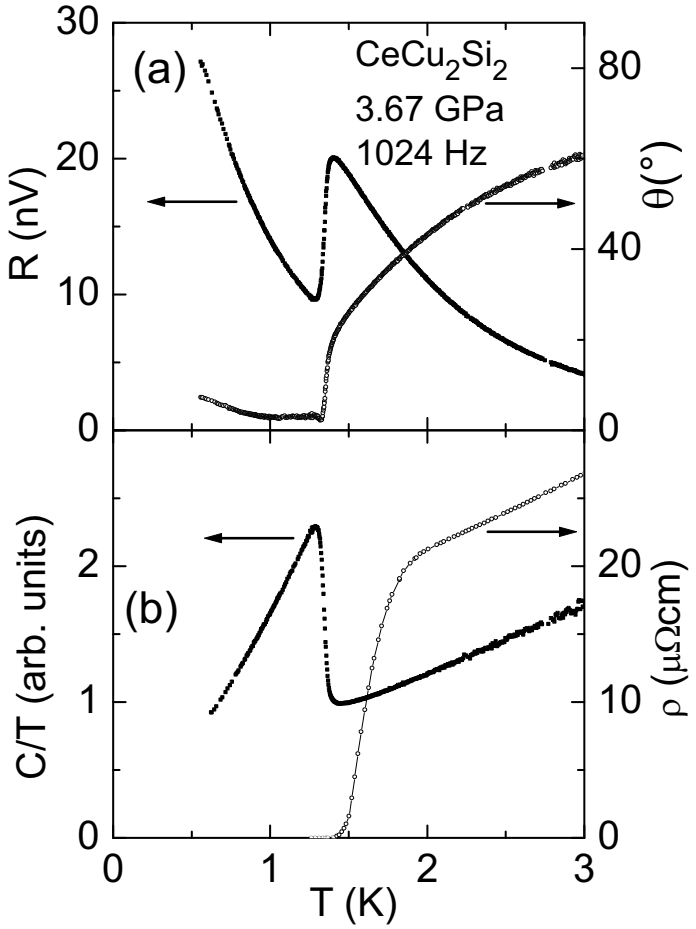

Figure 3.5: Raw and processed ac calorimetry data showing the superconducting transition in $CeCu_2Si_2$ in a helium pressure medium. The superconducting transition in specific heat occurs at the completion of the resistive transition.

Before we can draw quantitative conclusions, we must examine the sources of systematic error in the result. These might come from:

- Variation of the AuFe thermopower under pressure.
- Temperature and/or frequency dependent addenda to the measured specific heat due to the pressure medium, gasket and/or anvils.
- Any irreversibility or first-order character in the transitions being observed.
- Deviations from the simple model described in section 3.4.1.

These could explain, for example, the linear positive temperature dependence of C/T in the normal state seen in Fig. 3.5, which we would expect to be constant, or decreasing near a QCP. Indeed there is some evidence that this changes its form (becoming quadratic), at high pressure, beyond P_{v}.

We can, however, attempt to determine how much these errors are likely to affect the final result. For example, the thermopower of the AuFe thermocouple was assumed not to vary with pressure. Wilhelm and Jaccard [2002] found that it varies by no more than 20% up to 12 GPa.

The model used to extract the specific heat from the amplitude and phase of the temperature oscillations takes no account of the heat capacity of the solid helium, diamonds, or surrounding pressure apparatus, or the essentially three-dimensional nature of the situation. Nevertheless, the superconducting transition observed corresponds to $\sim$ 100% of the signal amplitude, indicating that the addenda are a minority contribution to the total signal at T_c. Runs at several different frequencies agree to within 10–20% after the amplitude and phase are combined, with the discrepancy possibly due to frequency-dependent addenda. Kapitza resistance between the sample and helium is likely to better decouple the sample from its surroundings at very low temperature.

There is good agreement between C_P extracted from the amplitude and phase at a single measuring frequency, and that calculated using Eq. (3.4) along with data taken at two frequencies. This is good evidence for the validity of the model proposed above.

Given these observations, it seems reasonable to accept our results as a good first approximation to C_P, to within a constant scaling factor, and with an unknown and temperature dependent but relatively small component due to addenda.

To refine the model, a detailed analysis of the frequency response at different temperatures using a system whose specific heat was well understood would be required.

3.5 Bayesian parameter estimation

In this section, I will briefly touch on a statistical technique that has applications in an enormous variety of fields, from artificial intelligence to epidemiology to philosophy. However in this thesis, it serves as a tool for a particulary tricky bit of curve fitting.

Bayesian analysis is essentially a consequence of probability theory. The concept was invented by the Rev. Thomas Bayes [1763], and later used by Laplace [1774] in the analysis of planetary motion. It has been subject to a certain amount of controversy in the past among professional statisticians, mostly due to its emphasis on the subjective nature of any conclusions, but has gained a loyal following among a large group of physicists, amongst others.

3.5.1 Bayes' theorem and marginalisation

Bayes' Theorem is a simple restatement of the law of conditional probability, namely that

$$P(B|A) = \frac{P(A|B)P(B)}{P(A)}, \tag{3.5}$$

Where $P(A|B)$ means 'the probability that A is true, given knowledge of the state of B'. This becomes of great interest when we realise that most scientific inference follows this pattern, namely:

$$P(\text{Hypothesis}|\{Data\}, I) = \frac{P(\{Data\}|\text{Hypothesis}, I)P(\text{Hypothesis}|I)}{P(\{Data\}|I)}, \tag{3.6}$$

where the additional term I represents our background knowledge of the situation.

$P(\text{Hypothesis}|\{Data\}, I)$ is the posterior probability of the hypothesis, i.e. our state of knowledge of it after having considered the data. The term $P(\{Data\}|\text{Hypothesis}, I)$ is known as the likelihood, and is a measure of how well the data can be explained by the hypothesis under consideration. The term $P(\text{Hypothesis}|I)$ is known as the prior probability, and it is a measure of our subjective opinion of the hypothesis *before* any data has been considered. The denominator is usually determined by the constraint that the total probability for all possible hypotheses must add up to 1.

This explicit statement of our prior beliefs has been the basis of a huge amount of discussion, which I do not propose to reproduce here, but among other things Bayes' theorem can be used to derive a mathematical formulation of the adage 'extraordinary claims require extraordinary evidence'.

The second piece of probability theory needed is the technique known as marginali-

sation, i.e.

$$P(B) = \sum_i P(B|A_i)P(A_i), \tag{3.7}$$

where $\{A_i\}$ form a complete set with

$$\sum_i P(A_i) = 1. \tag{3.8}$$

This can be extended to a continuous distribution of A giving the probability density

$$P(B) = \int P(B|A)P(A)dA, \tag{3.9}$$

where $P(A)dA$ is the probability that A lies between A and $A + dA$.

For a much more complete and rigorous (and also very entertaining) review of these concepts, see Jaynes [2003]. A more concise selection of concrete examples of the application of Bayesian data analysis to real problems can be found in Sivia [1996].

3.5.2 The problem

A recurring problem when dealing with so-called non Fermi-liquids, is the fitting of power laws to the resistivity. Generally we wish to determine the exponent n in an expression

$$\rho = \rho_0 + AT^n, \tag{3.10}$$

for

$$T_{\min} \leq T \leq T_{\max}. \tag{3.11}$$

with n typically taking a value somewhere between 1 and 3.

There are various ways to determine n, ranging from simply plotting ρ against T^n and looking for a straight line, to taking a logarithmic derivative:

$$n(T) = \frac{\partial}{\partial \ln T} \ln(\rho(T) - \rho_0). \tag{3.12}$$

The latter method of course depends on the choice of ρ_0, but if one finds that $n(T, \rho_0)$ remains at a particular value over a large range in temperature, then that can be assumed to be the correct exponent. Usually ρ_0 is determined experimentally by the resistivity for $T \to 0$.

There remains an essential problem, especially in the presence of noisy data. For virtually any given n, appropriate choice of the parameters ρ_0 and A will allow us to fit at least a subset of the data arbitrarily well (though the range of validity will be reduced for very poor fits). This is of course nothing other than the observation that any simple curve resembles a straight line when approached closely enough.

Because the exponents of interest are typically close to 1, the deviation from a straight line is often very small, and the problem can become very ill-posed indeed, with strong correlations between the fitting parameters. The Bayesian approach allows us to take into account all possible values of the 'nuisance' parameters ρ_0 and A, weighted by the goodness-of-fit. This gives a distribution $P(n)$ for a given set of data. Its maximum represents the exponent which fits the data best over its entire temperature range without making any assumptions about the other parameters, and the width of the distribution indicates the uncertainty on its determination.

3.5.3 Application of Bayesian analysis to power law resistivity fits

We wish to determine $P(n|\{D\})$[1] for a set of noisy data $\{D\} = \{\rho_i, T_i\}$, under the assumption that the true relationship between ρ and T is in the form of a power law $\rho = \rho_0 + AT^n$. The values of ρ_0 and A do not concern us, at least for this problem, and will be treated as nuisance parameters to be integrated out.

Applying (3.9) twice gives

$$P(n|\{D\}) = \iint P(n|\rho_0, A, \{D\})P(\rho_0)P(A)dAd\rho_0, \tag{3.13}$$

where $P(A)$ and $P(\rho_0)$ correspond to our prior probabilities for A and ρ_0. We will assume them to be uniform, simply providing the limits of integration and a multiplicative constant.

Now applying Bayes' theorem (3.5) to the integrand we have

$$P(n|A, \rho_0, \{D\}) = \frac{P(\{D\}|n, \rho_0, A)P(n)}{P(\{D\})}, \tag{3.14}$$

where $P(\{D\}|n, \rho_0, A)$ is the likelihood, $P(n)$ is the prior probability for the value of n, and $P(\{D\})$ can be considered as a normalising constant.

The likelihood for a given parameter set $\{\rho_0, A, n\}$, is given by

$$P(\{D\}|n, \rho_0, A) \propto \prod_i \exp\left\{-\frac{[\rho_i - \hat{\rho}_i(T_i; \rho_0, A, n)]^2}{2\sigma_i^2}\right\} \tag{3.15}$$

$$= \exp[-\chi^2(\rho_0, A, n)/2], \tag{3.16}$$

where

$$\chi^2(\rho_0, A, n) = \sum_i \frac{[\rho_i - \hat{\rho}_i]^2}{\sigma_i^2} \tag{3.17}$$

[1]The background knowledge I will be omitted for clarity.

and

$$\hat{\rho}_i = \rho_0 + AT_i^n. \tag{3.18}$$

We are making the simplifying assumption that the temperature T_i of each data point is known exactly, and the corresponding resistivity ρ_i has a known gaussian measurement error σ_i. These assumptions could be included in the analysis if necessary, but it would add considerably to the computational effort involved.

Combining Eqs. 3.13, 3.14, and 3.15, we get

$$P(n|\{D\}) = CP(n) \iint_{\rho_0^{min},A_{min}}^{\rho_0^{max},A_{max}} \exp[-\chi^2(\rho_0, A, n)/2] dA d\rho_0, \tag{3.19}$$

where C is defined such that $\int P(n|\{D\})dn = 1$.

The prior probability $P(n)$ is actually fairly important. If we wish to be guided entirely by the data, we can use an uninformative prior, with our initial guess of $P(n)$ constant between some broad limits, say $1 \leq n \leq 3$. This in fact gives a result very similar to that produced by a traditional least squares fit in a program such as Origin. The best estimate of n is that which gives the maximum likelihood, i.e. that which minimises χ^2.

This approach, letting n take on any value within a certain range, fails to make use of all the information at our disposal. We are usually trying, in fact, to distinguish between a small set of alternative hypotheses, each of which specifies a particular value of n, e.g. 3/2 for antiferromagnetic fluctuations or 5/3 for ferromagnetic. In chapter four I will show that choosing between three or four discrete values of n requires much less data than if n is allowed to vary continuously.

3.5.4 Implementation

The determination of $P(n|\{D\})$ requires a relatively large amount of computational effort, for which the software Matlab was used. The essential task is to evaluate 3.19 for each value of n of interest, be it a discrete set or a large number of points to trace out the continuous distribution.

The basic steps were as follows:

1. Select a subset $\{T_i, \rho_i\}$ from the entire resistivity data, for a window $T_{\min} \leq T \leq T_{\max}$.
2. For a particular value of n, calculate $\chi^2(\rho_0, A, n)$ using this data, for a range of ρ_0, A which encompasses all plausible fits (i.e. which have a non-negligible value of $\exp[-\chi^2/2]$).
3. Numerically integrate the resulting $\exp[-\chi^2/2]$ over ρ_0, A.

4. Repeat for the next value of n.
5. Normalise to ensure that $\sum_j P(n_j) = 1$.

In order to calculate χ^2, the experimental error σ_i on each ρ_i is required. The measurement noise was not constant, particularly across the superconducting transition of the cryostat connection wires at around 8K. σ_i was therefore estimated for a given data point ρ_i in a very non-Bayesian way, using the standard error in the resistivity of the surrounding ten points. A smoothing procedure was then applied to the result to give the $\sigma(T)$ used to calculate χ^2.

Because there were only two integration variables, ρ_0 and A, a simple grid and sum method could be used to numerically integrate $\chi^2(\rho_0, A, n)$. For a model with more parameters, this would rapidly become very inefficient. In that case a more effective solution would be to approximate the likelihood by a multi-dimensional gaussian form, with the moments determined by the second derivatives around the maximum likelihood.

3.5.5 Is this really worth the effort?

In chapter four I present some results using this method to determine the exponent in ε-Fe.

It is reassuring that the Bayesian method of estimating the non Fermi-liquid exponent gives very similar results to more traditional least-squares fitting used in programs such as Origin. This is not surprising, as in both cases the optimum parameters are found by minimising χ^2 with respect to the fitting parameters. The only difference with more traditional methods being the explicit removal of the 'nuisance' parameters ρ_0 and A, which will not affect the best fit if the likelihood is symmetrical about its maximum. The sophisticated fitting routines in Origin also calculate the second derivatives of χ^2 about the maximum, thus giving a consistent estimate of the uncertainties on the fitting parameters.

Given that the results are very similar to more simple least-squares fitting methods, the advantage of the Bayesian approach when n is allowed to vary freely is more philosophical than practical, as it forces us to explicitly define our assumptions, and lacks the arbitrary nature of more ad-hoc approaches.

The real power of the Bayesian approach comes when we can make use of our prior knowledge. That is that we are trying to distinguish between a small number of models for the resistivity, i.e. only considering a few possible values of n. For example the presence of ferromagnetic or antiferromagnetic fluctuations would give $n = 5/3$ or $3/2$ respectively. This massively reduces the parameter space we are searching, and allows us to use noisier data, or fewer data points to come to a firm conclusion.

We have yet to apply the Bayesian analysis technique very broadly, but it is a very useful and convincing way to approach a rather difficult but important aspect of the analysis of resistance data.

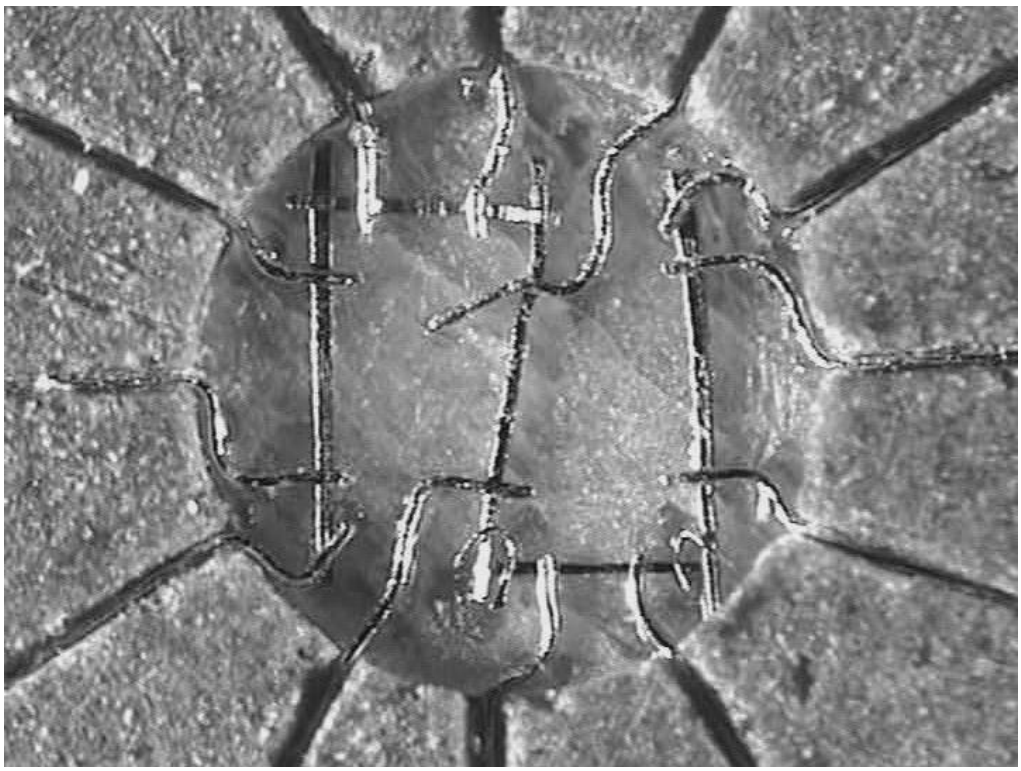

Figure 3.6: Bridgman cell #1 containing four iron samples and a lead manometer. The samples, labelled as in table 4.1 are, from left to right: #5, Pb manometer, #6, #3, and #4.

3.6 Pressure cells

The results presented in chapters four and five consist of five pressure runs, one using the helium-filled DAC technique, and the rest Bridgman cells. They are summarised in table 3.1. Figure 3.6 shows the contents of cell #1 before compression. The four Fe samples along with the lead manometer are arranged so that the current flows in series through them all, and independent voltage contacts are formed by pressure on each.

Helium cell setup

The DAC containing a single $CeCu_2Si_2$ sample is shown on page 20, in Fig. 3.3, before pressurisation. The small monocrystal was cut and polished to $230 \times 80 \times 20\ \mu m^3$, and six $5\,\mu m$ ϕ wires (four gold and two Au + 0.07% at. Fe) were spot welded to the sample. The c-axis of the tetragonal structure was parallel to its smallest dimension. The magnetic field, when applied, was parallel to the c-axis.

The six wires spot-welded to the sample allowed multiple redundant measurements

#	Cell type	Anvil size (mm)	Samples	Measurement methods
1	Bridgman	2.0	Fe ×4	resistance
2	Bridgman	1.5	Fe ×1	resistance & calorimetry
3	DAC/He	1.5	$CeCu_2Si_2$ ×1	resistance & calorimetry
4	Bridgman	2.0	$CeCu_2Si_2$ ×4	resistance
5	Bridgman	2.0	$CeCu_2Si_2$ ×2	resistance

Table 3.1: Pressure cells used to produce the results reported in this thesis (not in chronological order). Cells #1 and 2 are discussed in chapter four, and #3–5 in chapter five.

to be performed. This improved reliability and enabled us to verify the calorimetry measurements using several different configurations. The sample resistance could be measured by a four-point method.

The two thermocouple junctions were formed from an Au/AuFe pair at either end of the sample. An alternating resistive heating current was passed through one (to avoid passing the current through the sample), while the signal from the other was measured using a lock-in amplifier.

3.7 Summary

I have described in this chapter the principal experimental tools used to obtain the results presented in chapters four and five.

Several of these techniques are technical innovations: ac calorimetry has not, to my knowledge, been used in such extreme conditions of temperature and pressure before the work presented in this thesis. The Bayesian approach to the analysis of resistivity data is something of a personal hobby-horse, and as such may turn out perhaps to be an example of using a sledgehammer to crack a nut, however, I personally hope and believe that it may turn out to be of some use to the wider community.

Chapter 4

Iron

4.1 Introduction

4.1.1 The properties of iron under pressure

Discovery of superconductivity

In early 2001, iron was discovered to be superconducting in its high pressure *hcp* ε phase (Fig. 4.1, Shimizu et al. [2001]). It thus became the 52nd element found to be a superconductor, the 23rd under pressure.

The phase diagram of iron is shown in Fig. 4.2. In ambient conditions, iron is in its ferromagnetic α phase, and has a *bcc* structure. Above a pressure of around 13 GPa at 300 K, it transforms to the *hcp* ε phase. This is believed to be non-magnetic, Mössbauer measurements for example showing a fixed moment of less than 0.05 μ_B at 20 GPa in an ethanol/methanol pressure medium (Nasu et al. [2002]).

The discovery of superconductivity in a metal which is ferromagnetic in ambient conditions is intriguing, as superconductivity and magnetism are usually antagonistic, with the presence of one excluding the other. This therefore prompted several theoretical investigations (Mazin et al. [2002]; Jarlborg [2002b]; Bose et al. [2003]; Thakor et al. [2003]).

The results of these calculations implied that the superconductivity is likely to be due to an unconventional pairing mechanism. The presence of superconductivity itself could be explained by phonon-mediated BCS type pairing, but its rapid disappearance with pressure can not. The authors suggested that the pairing mechanism may be of magnetic origin, where the attractive interaction between electrons is due to the exchange of ferromagnetic (FM) or antiferromagnetic (AFM) fluctuations.

The gradual emergence of superconductivity at the α-ε transition also stands in

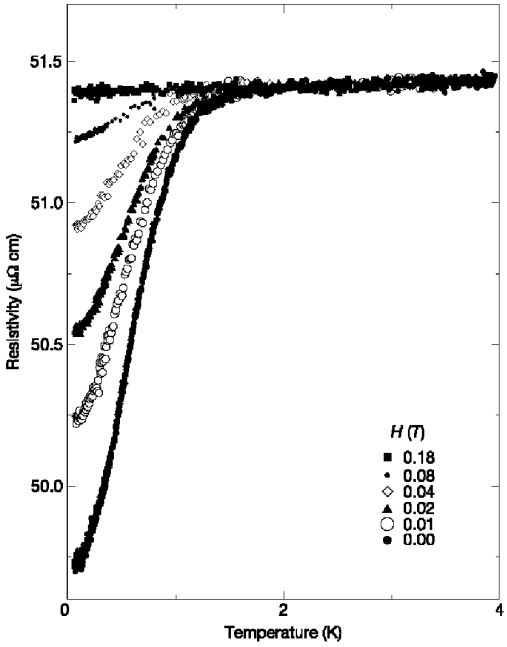

Figure 4.1: The first evidence of superconductivity in iron is shown here (Shimizu et al. [2001]), a tiny kink in the magnetic susceptibility was found at the same temperature.

contrast to other elements such as Si where a superconducting phase appears after a structural transition. In that case, the superconducting phase appears suddenly, with a finite transition temperature.

Aside from the calculations mentioned above, there were several reasons to believe that such an unconventional, magnetically mediated, pairing mechanism is likely. Firstly magnetism plays an extremely important role in the physical properties of iron; for example the ferromagnetic *bcc* structure found in ambient conditions is not predicted by theory unless magnetic correlations are taken into account (Cohen [2003]). Secondly, the partial resistive transitions observed indicated that sample quality may be a factor in the appearance, or otherwise, of superconductivity. This is a salient feature of unconventional pairing, where the electronic mean free path is required to be larger than the superconducting coherence length ξ.

α-ε transition

The α-ε transition is martensitic (Wang and Ingalls [1998]), i.e. it is a non-diffusive structural transition with the *bcc-hcp* transformation occuring by atomic plane slippage, with crystal orientation preserved. The transition is shear driven; the pressure conditions, including the shear strength of the pressure medium, determine its pres-

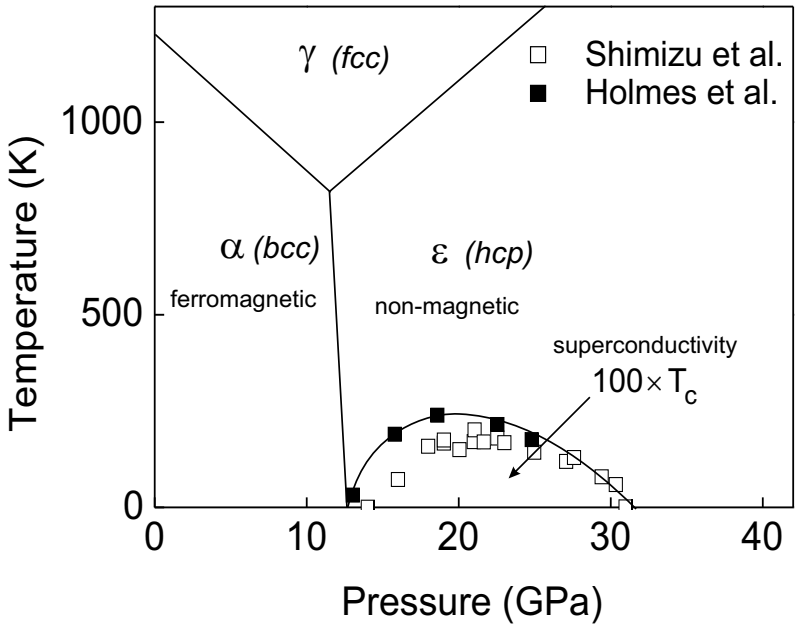

Figure 4.2: Phase diagram of iron showing superconducting region in the ε phase. White squares show T_c values from Shimizu et al. [2001] while black symbols indicate the values of T_c reported below. Note the emergence of superconductivity at the α-ε phase boundary.

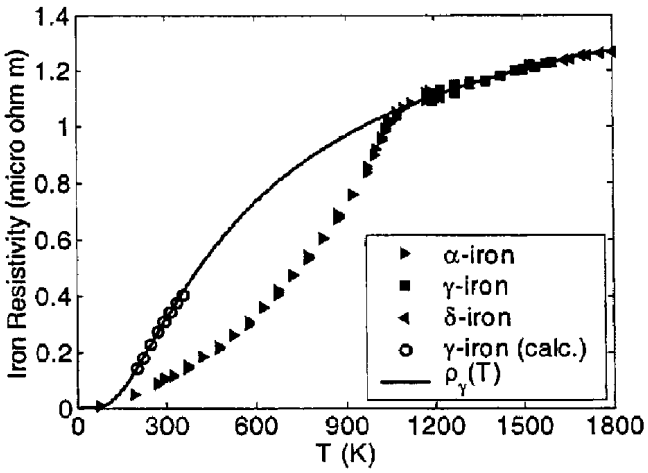

Figure 4.3: Resistivity of non-magnetic and ferromagnetic iron at ambient pressure, up to and above the Curie temperature. (Bohnenkamp et al. [1992])

sure width and hysteresis. One reason for this is that a 5% volume reduction occurs from the α to the ε phase (Jephcoat et al. [1986]), and the medium has to readjust itself to occupy extra space made available. For a given pressure medium, the width of the α-ε transition is about 10 times the pressure gradient ΔP.

The gradual nature of the phase transition means that both α and ε phases likely coexist over the entire superconducting pressure range. The superconductivity may well be intrinsic to the ε phase, but ferromagnetic remnants of the α phase are likely to have some influence on its properties. The pressure conditions strongly influence the proportion of the two phases at any given pressure.

Magnetism

The importance of magnetic scattering on the electron properties is illustrated in Fig. 4.3. Bohnenkamp et al. [1992] extrapolated the resistivity of non-magnetic fcc γ-Fe around room temperature from alloys which stabilise the fcc structure. Iron goes through several structural transitions above the Curie temperature, where the resistivity is more or less continuous, but below the Curie temperature, the magnetically ordered state has a much lower resistivity. This indicates that scattering from spin disorder is a major contribution to the resistivity, and plays a much larger role than changes in phonon scattering at a structural transition.

Magnetism also plays an important role at the lowest temperatures. Taylor et al. [1968] observed that the magnetic domain configuration in single crystals with very high RRR[1] values had an extremely large effect on the resistivity at very low tem-

[1]The residual resistivity ratio (RRR), defined by $\rho(293\text{K})/\rho(T \to 0)$, is widely used as a measure

peratures.

In this chapter, I will describe how resistivity measurements under pressure can help to identify the nature of the superconducting phase. There are several questions that need answering:

- Can we confirm the phase diagram determined by Shimizu, especially the emergence of T_c from zero around 15GPa and its disappearance around 30GPa?
- What is the relationship between T_c and the residual resistivity ρ_0?
- What does the normal state tell us about the electronic scattering mechanisms present in ε-Fe?
- Is there any evidence for a quantum critical point in the vicinity of the superconductivity?

4.1.2 Experimental background

Discovery of superconductivity

The initial discovery of superconductivity by Shimizu et al. [2001] was carried out in a diamond anvil cell both without a pressure medium, and with NaCl as a pressure medium. It was identified by a small resistance drop (up to 10%), which could be suppressed by a magnetic field, and a kink in susceptibility.

Signs of unconventional pairing

In Geneva, Didier Jaccard then attempted to reproduce this observation using a Bridgman anvil technique. The Fe sample used (which will be referred to as sample #0) was a high purity (4N, i.e. 99.99% pure[2]) commercial sample from Goodfellow metallurgical suppliers. The sample was rolled in mangle down to the appropriate thickness for the pressure cell. This significantly increased the residual resistivity. On cooling to 50 mK, no superconducting transition could be found.

Jaccard had determined that the residual resistivity for very pure samples (>3N) was dominated by the structural disorder, introduced for example by the rolling process. With this in mind, he made another attempt to observe superconductivity in two samples, referred to as #1 and #2. The first was provided by Y. Onuki and Y. Inada, in Osaka, from the same batch used by Shimizu. The second was from a large-grained rod produced over 30 years ago in Dresden by G. Behr. Pieces cut from these samples were also used in subsequent experiments by myself.

of sample quality.

[2]Impurities (ppm): Ag < 1; Al < 1; Cu < 1; Si 1

The samples were not rolled, but cut to a size compatible with the pressure cell. Resistivity measurements were performed at two pressures, one in the α phase on one in the ε phase. The latter at 22 GPa, a pressure coinciding with the maximum $T_c(P)$ found by Shimizu. At the higher pressure complete resistive superconducting transitions were found (Jaccard et al. [2002]).

There were several other noteworthy results. The variation of the normal state resistance with temperature was found to change between the two states (see Fig. 4.4). α-Fe behaves as a typical ferromagnet at low pressure, i.e. a largely linear resistance below room temperature, with a small magnon scattering term, and a quadratic temperature dependence at very low temperature[3]. In the ε phase, the magnon term was gone, with a largely linear behaviour above $\sim$ 100 K. Below 35 K however, a temperature variation of the form $\rho = \rho_0 + AT^{5/3}$ was found. This power law behaviour points to a nearly ferromagnetic Fermi liquid state, where critical ferromagnetic fluctuations are expected to dominate the scattering.

The superconducting state itself also exhibited peculiar behaviour. The resistive transition width was very broad, much larger for example than the superconducting transition in lead, which is used as a pressure measurement and whose width reflects pressure gradients in the cell. The resistivity drop itself was also highly dependent on the current density used, with a complete resisitive transition found only for very small current densities (0.25 Acm^{-2}), however even for current densities several orders of magnitude larger, a partial transition could be observed.

4.1.3 Sample preparation and experimental setup

The observations described above prompted us to clarify the effect of sample quality on the superconducting state. I present results from two pressure runs. The first cell contained four samples (#3–6) from three different sources, and the second contained a single crystal Fe whisker, #7 (see below for more details). Results from the first cell have been published in Holmes et al. [2004a].

It was noted above that in very pure iron, the residual resistivity of the purest samples depended mainly on the metallurgical state of the sample, i.e. the concentration of defects, dislocations, and grain boundaries introduced by cold work. This provides a useful mechanism for varying the quality of the samples without affecting the impurity concentration. We can increase ρ_0 by rolling, or reduce ρ_0 by annealing.

We attempted to destroy superconductivity in a sample that had previously shown it by rolling, hence raising ρ_0, and to induce it in a sample from a previously non-superconducting source. Table 4.1 summarises the treatment each sample received.

In order to avoid oxidation, the annealing was carried out in a high vacuum ($< 10^{-7}$

[3]Note however that the temperature dependence below 4 K can be heavily dependent on the magnetic domain structure, see Taylor et al. [1968] for more details.

Sample	Origin	Preparation	Final RRR
#3	Onuki	rolled	35
#4	Onuki	rolled & annealed	259
#5	Goodfellow	rolled & annealed	247
#6	Behr	rolled & annealed	279
#7	Onuki	whisker	800

Table 4.1: Samples used in cells 3 and 4, showing preparation method and final RRR [i.e. $\rho(293\,\mathrm{K})/\rho(\mathrm{T} \to 0\,\mathrm{K})$]. Samples #3–6 were all rolled down to a thickness of 15–20 μm before any further treatment. Sample #7 was cut to the right length from a single crystal Fe whisker grown by vapour deposition.

torr) using a high frequency induction furnace. The samples were suspended from a tungsten hanger, and maintained at 1000°C for 24 hours. After annealing, about 10% of the original mass had been lost, and grains with sizes up to 1mm were visible. No attempt was made to orient them, as at $P = 0$ ρ is not very anisotropic.

It is worth noting that if the temperature is too high (1200°C) the samples are completely evaporated!

The pressure cell used in the first experiment was constructed by D. Jaccard. It contained the four samples connected in series, with a pair of voltage contacts on each, and a lead manometer. It was a Bridgman type clamp cell with sintered diamond anvils.

The second set of experiments was carried out on a single crystal iron whisker (sample #7), prepared by Y. Onuki, Y. Inada and H. Kohara. A whisker is in principle a perfect single crystal formed by vapour deposition (reduction of $FeCl_2$) around a single screw dislocation. Taylor et al. [1968] shows that whiskers have remarkably high RRR's (up to 3000!) when their magnetic domains are aligned by field. This is because the principle source of scattering is from magnetic domain boundaries.

The whisker selected was already of more or less the right cross-section for the pressure cell (though it turned out to have been slightly too big), and smaller sintered diamond anvils with a 1.5 mm flat was used. The cell was again constructed by D. Jaccard. The aim was to go to higher pressures and see the disappearance of T_c, and to see whether higher values of T_c could be obtained by using a single crystal.

Thermocouples were connected to both the iron and the lead manometer and heating circuit was included in the cell in view of carrying out an ac-calorimetric study.

Unfortunately this experiment proved to be of limited use, as the pressure cell was unstable, there was an extremely large pressure gradient, and not all the wires provided good electrical contact. This resulted in very broad lead transitions, and

was evident visually when the cell was depressurised.

The lead transition at all pressures in this cell had a broad high-temperature tail, consisting of about 40% of the resistance drop, and about 80% of the temperature width, with the rest of the resistance drop much steeper. As dT_c/dP is negative, this implies that the upper limit on the pressure, given by the temperature at which $R(\mathrm{Pb}) = 0$, is likely to be the most representative of the majority of the cell.

4.1.4 Results

I will present together here the results of all the work carried on superconducting iron in Geneva. The results from cells 1 and 2 (samples #0–2) were obtained entirely by D. Jaccard, while the measurement and analysis of data from cells 3 and 4 (samples #3–7) was my own work. In samples #3–6, the measured form factors were corrected slightly to obtain a resistivity of 9.71 $\mu\Omega$cm at 293 K and ambient pressure. This normalisation was kept constant as the pressure was increased.

The normal state properties will be presented first, showing the large increase in electronic scattering as the $\alpha \rightarrow \varepsilon$ transition is crossed, and the evolution of the temperature dependence of the resistivity with pressure. I will then show the results pertaining to the superconducting transition and the effect of pressure, current and magnetic field.

Figure 4.4 shows the temperature dependence of the resistivity ρ of iron in the α and ε phases. Following Matthiessen's rule, the resistivity ρ can be assumed to be a sum over all different scattering mechanisms

$$\rho(T) = \rho_0 + \rho_{e-e}(T) + \rho_{ph}(T) + \rho_{mag}(T) + \rho_{dev}(T) \tag{4.1}$$

where ρ_0 represents the scattering from impurities, ρ_{e-e} the electron-electron scattering, ρ_{ph} the contribution from phonons, and ρ_{mag} that from spin waves. ρ_{dev} represents any deviation from a simple additive rule, and is assumed to be negligible. It is often very difficult, or even impossible, to separate these different contributions empirically, as they may have very similar temperature dependencies, or one component may dominate to the extent that it is impossible to resolve the others. However I will comment on Fig. 4.4 as far as is possible.

At 3.5 GPa, the resistivity has a textbook ferromagnet temperature dependence. At high temperature, above 100K or so, $\rho_{ph} \sim aT$ is dominant, with $a = 0.033\mu\Omega\mathrm{cmK}^{-1}$, with a small additional magnon component $\rho_{mag} \sim bT^{2.2}$, up to the Curie temperature where magnetic ordering is lost. The coefficient b of the magnon scattering is 8.5×10^{-6} $\mu\Omega\mathrm{cmK}^{-2.2}$.

At low temperature, when phonon scattering is frozen out, the resistivity has a quadratic temperature dependence AT^2 with a coefficient $A = 2 \times 10^{-5}$ $\mu\Omega\mathrm{cmK}^{-2}$ reflecting the electron-electron scattering.

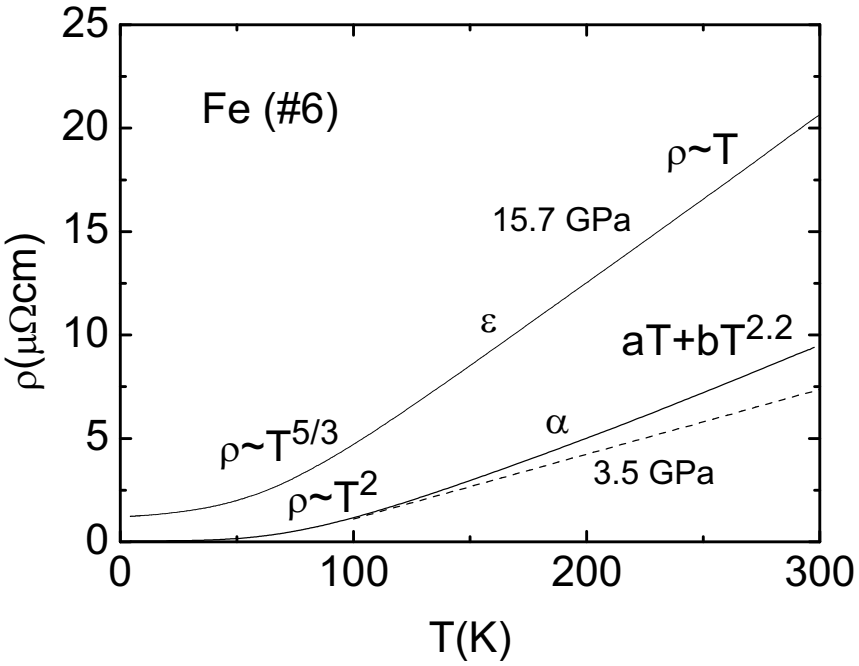

Figure 4.4: Temperature dependence of the resistivity ρ of iron in the α and ε phases. The dashed line shows the linear phonon component aT in the α phase. The resistivity at 3.5 GPa is typical of a ferromagnet, while that in the ε phase shows many unusual features, discussed in the text.

In the ε phase the resistivity is much larger, and strictly linear from 300 K down to around 100 K, with no trace of the $T^{2.2}$ magnon term seen in the α phase. A first reflex would be to assume that this is due to phonon scattering, however the slope, 0.081 $\mu\Omega$cmK^{-1}, is much larger than the phonon component deduced in the α phase. If we assume that ρ_{ph} is more or less unchanged at the transition, this implies that there is also a linear magnetic scattering component at high temperature, corresponding to 41% of the total resistivity. A linear magnetic contribution would obviously be impossible to separate empirically from a phonon term, but by comparing the two different phases of the same material, it is brought to light.

If we compare this with Fig. 4.3, and draw a parallel between the non-magnetic γ phase, and the ε phase, we are moving from the lower to the upper curve, which indeed appears linear around room temperature.

A linear magnon contribution, analogous to phonon scattering well above the Debye temperature, might be possible near to a magnetic instability, where low energy spin wave modes are available, so long as the spin wave disperson relation resembles that of phonons.

Signs of the phase transition in resistivity

During the $\alpha \rightarrow \varepsilon$ transition in iron, the most significant change, other than the *bcc-hcp* transformation, is the loss of magnetic order. The importance of magnetic scattering in the electronic properties of Fe has been established, so it is not surprising that the resistivity shows significant features as the phase boundary is crossed with increasing pressure.

Figure 4.5 shows the resistivity vs. pressure at 293 K. The resistivity initially decreases slowly and linearly with pressure. This is followed by a sharp kink as the transition starts to manifest itself, then a broad maximum and a slow decrease above $\sim$ 16 GPa as the pressure is increased further.

The α-ε transition should start at $p < 10$ GPa in a steatite medium according to Mössbauer effect experiments (Taylor et al. [1991]). The sharp kink observed in ρ at higher pressures, around 13 GPa, with no precursor signs is therefore unexpected (the sharpness is more clearly visible in the data presented in Jaccard et al. [2002]). The kink could be attributed to the disconnection of the conducting α region by the growing amount of ε phase. A complimentary, and more likely explanation is that the kink in $\rho(P)$ corresponds to the pressure at which long range magnetic order is lost, which may occur well after the ε phase first appears.

At 4.18 K the phonon components of the resistivity are suppressed. Fig. 4.6 shows ρ(4.18 K, P) for samples #3-6. The pressure dependence of ρ_0 is remarkably similar to that of ρ(300 K).

In addition to the common increase in resistivity in all samples, the sample which has

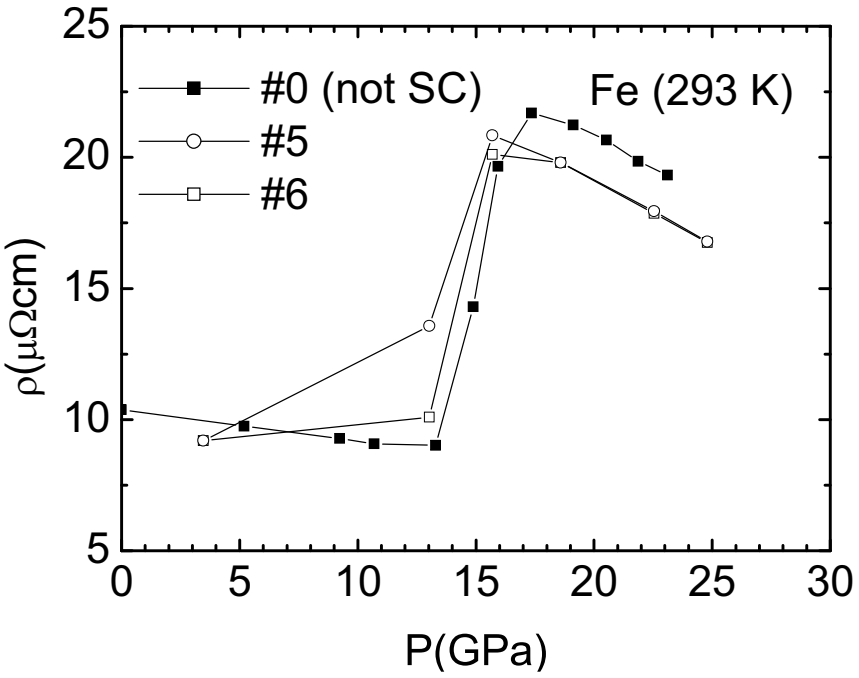

Figure 4.5: Evolution of the resistivity at room temperature in Fe with pressure. Note the abrupt increase associated with the $\alpha \rightarrow \varepsilon$ transition, which is already under way in sample #5 at 13 GPa.

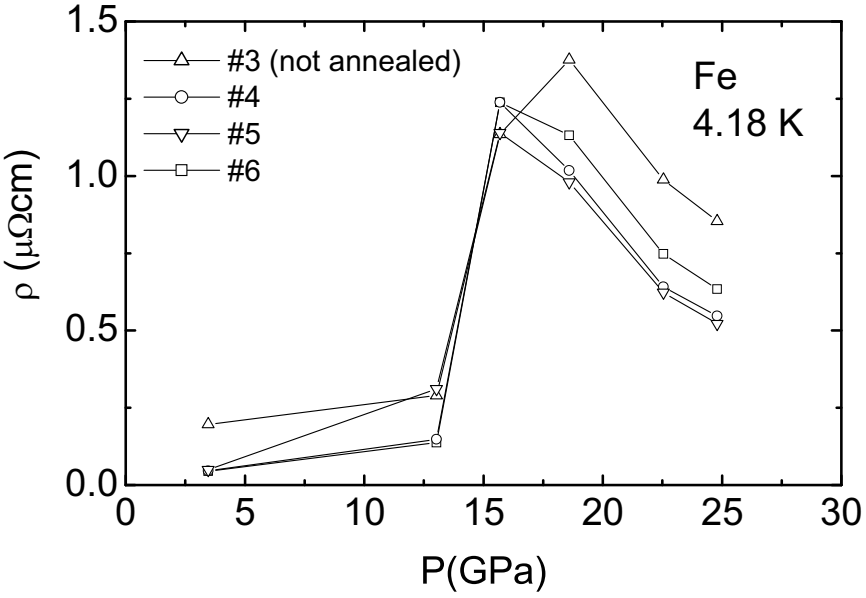

Figure 4.6: Evolution of the residual resistivity (measured at 4.2 K) in samples #3-6. Note the similarity to Fig. 4.5, and the influence of structural disorder in #3 at all pressures.

the highest residual resistivity at ambient pressure, #3, also has a larger increase at the $\alpha \rightarrow \varepsilon$, and the differences between samples at $P = 0$ are somewhat amplified. This may be due to the effect of defects and impurities on either the nucleation or growth of the ε phase, a hypothesis supported by the fact that the unannealed sample has a maximum ρ_0 at a higher pressure than the others.

On increasing the pressure further one can extrapolate the residual resistivity back down to its value in the α phase at a pressure just above 30 GPa, which corresponds to the disappearance of superconductivity.

These observations are strong evidence that the large increase in resistance at the α-ε transition can be attributed to the introduction of static and dynamic spin disorder with the loss of ferromagnetic correlations. The alternative explanation would be a large change in phonon scattering between the two phases, which one would not expect to see at very low temperature. The precise origin of the low temperature scattering is not completely obvious however.

A spin disorder scattering explanation for the resistivity is supported by Fig. 4.3. The structural transitions above the Curie temperature have very little effect on the resistivity, while there is a large difference between the magnetically ordered and non-magnetic state. We can again imagine that we are moving from the lower to

the upper curve in Fig. 4.3, drawing a parallel between the ε phase and γ-Fe.

Non-Fermi liquid behaviour

The temperature dependence of the resistivity provides important information about the scattering processes taking place in a material. At low temperatures, below about 20 K, phonon scattering is strongly suppressed and the resistivity is dominated by electronic interactions. In normal metals, this gives rise to a quadratic temperature variation, though sometimes with an enhanced prefactor reflecting a larger effective mass due to correlation effects. In certain compounds, so-called non-Fermi liquid behaviour is found, where the resistivity varies as $\rho = \rho_0 + AT^n$, and the exponent n is less than 2.

This behaviour is often linked with the disappearance of magnetic order, for example as the electronic bands are broadened under pressure and the magnetic ordering temperature driven to zero. In this case, the lowest energy excitations are critical fluctuations of the magnetic order parameter. This has been modelled (e.g. Millis [1993]), and these same interactions may also lead to superconductivity, mediated by the exchange of magnetic fluctuations, rather than phonons, as in the case of BCS type superconductivity (Lonzarich [1997]).

The exponent n depends on the nature of the fluctuations and the dimensionality of the system. For a 3D system close to a quantum critical point, antiferromagnetic fluctuations would give rise to $n = 3/2$ while in a nearly ferromagnetic material, an exponent of 5/3 would be expected. My experiments confirmed the observation of $T^{5/3}$ resistivity found in samples #1 and 2. The fitted exponent varied between 1.67 and 1.75, but it is clear from Fig. 4.7, where ρ is plotted against $T^{5/3}$ and $T^{3/2}$ that $\rho \sim T^{1.5}$ does not adequately describe the situation.

If a magnetic field sufficient to suppress the superconductivity is applied, NFL scaling persists down to the lowest measurable temperatures (Fig. 4.8).

While Fig. 4.7 shows that a $T^{5/3}$ power law fits better over a larger temperature range than $T^{3/2}$, they are both virtually indistinguishable to the eye over a small range in temperature, below 20K for example on the scale shown. Thus the question is posed: down to what temperature range can we identify a particular exponent?

This is a subtle question, the fitting coefficients ρ_0, A, and n are often highly correlated, especially in the presence of experimental noise, so that equally good fits can result from rather different parameter sets.

Figure 4.9 helps to give an answer. It shows the probability density $P(n)$ (i.e. the probability that n lies between n and $n+dn$) for the exponent n in a fit $\rho = \rho_0 + AT^n$ to a subset of the data from sample #6 at 22.5 GPa. For each fit, data is selected from a temperature range whose size and average temperature varies. As we are essentially measuring the curvature of $\rho(T)$, the fit is intrinsically non-local, so a

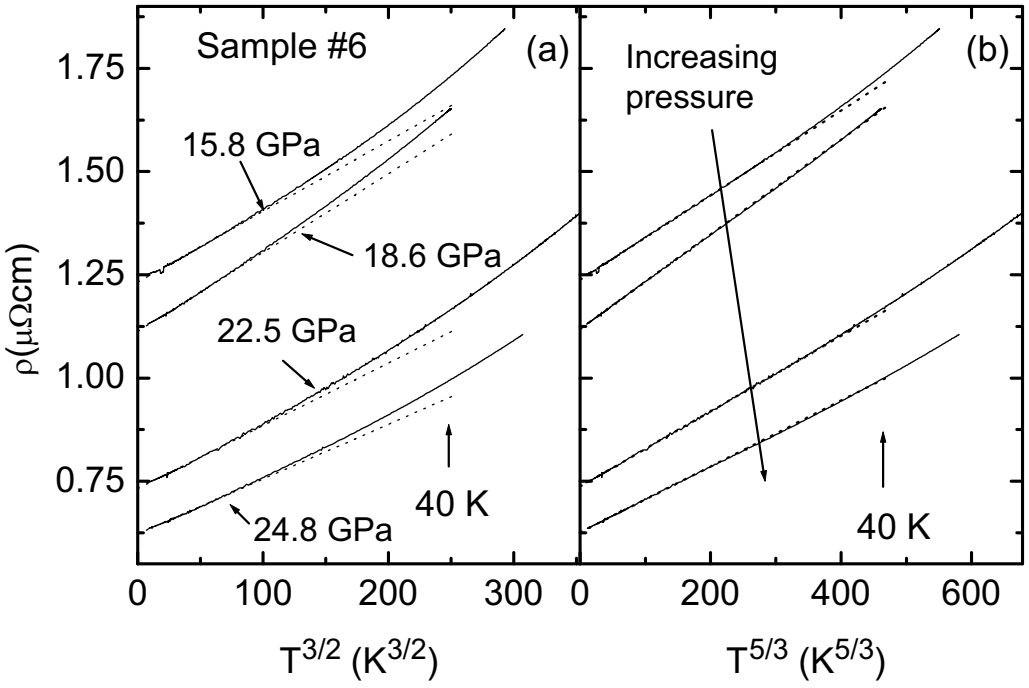

Figure 4.7: Resistivity ρ plotted against (a) $T^{3/2}$ and (b) $T^{5/3}$. At all pressures, $\rho = \rho_0 + AT^{5/3}$ is clearly a better fit. Note also the evolution of ρ_0 and A with pressure. The dotted lines represent perfect $T^{3/2}$ or $T^{5/3}$ dependence.

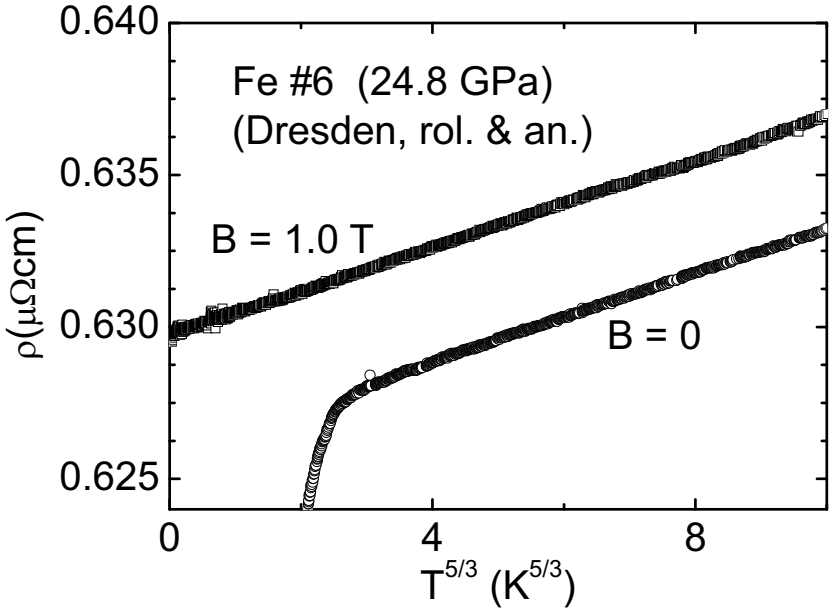

Figure 4.8: In a magnetic field of 1 T, strong enough to supress superconductivity completely, the $T^{5/3}$ temperature variation of ρ appears to be preserved down to the lowest measurable temperatures (though at the very lowest temperatures, below 1 K, a good argument could be made for a different exponent).

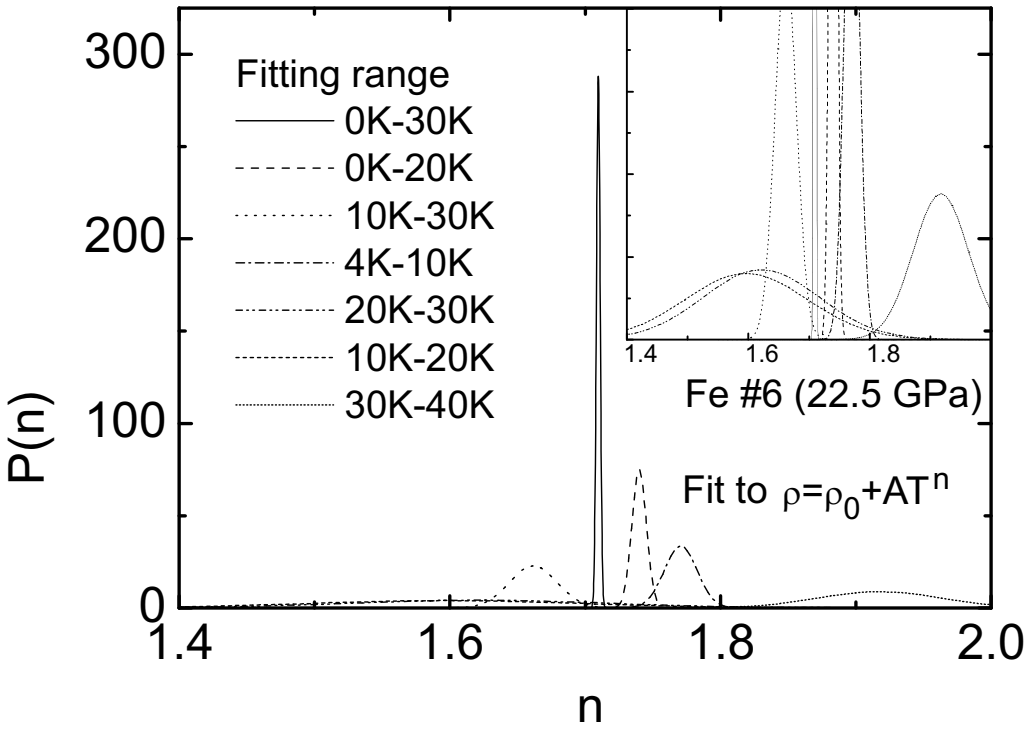

Figure 4.9: Posterior probability for the exponent n in a fit $\rho = \rho_0 + AT^n$ to the resistivity of sample #6 at 22.5 GPa. The very broad peaks, seen best in the zoomed inset, correspond to a 10 K window, swept between 10 K and 40 K. The medium sized peak just below 1.8 corresponds to a window of 4 K to 10 K, where there are more data points with lower noise level. The two peaks either side of the sharp peak at 1.70 correspond to a temperature window 20 K, either starting from the lowest temperature data, or from 10–30 K. The sharp central peak results from using the entire $\rho(T)$ data up to 40 K

larger temperature range will lead to a better determination of n.

$P(n)$ for a given value of n is obtained by integrating $e^{-\chi^2(\rho_0,A,n,\{data\})/2}$ over the parameters A and ρ_0 so that all possible combinations of A and ρ_0 are taken into account, weighed by the goodness-of-fit of the entire curve (see section 3.5 for details).

As more data is added, or the resolution improves, the curves sharpen and converge on the best fit, found to be $n = 1.70$. When a temperature window of 10 K is used for the fit, the result is very unstable when swept over the entire curve up to 40 K, and n is poorly determined. However the 4–10 K fit is obviously better than higher temperature windows, due to the lower noise in the data below 8 K, where the connecting wires become superconducting, and there is a higher density of measurement points.

For a 20 K window the result is better defined, yet it is clear that even for such a temperature window, the range of n found its not completely stable as the window is shifted. For a 30 K window a much sharper peak is found.

To improve the determination of n, there are several possibilities. Firstly, more data points could be taken, or the measurement noise reduced (these are statistically equivalent), or a larger temperature window used for the fit. Figure 4.9 shows that the latter is a more effective solution.

There is a much more powerful method of determining n, if we explicitly take into account our theoretical assumptions. In the preceding analysis we simply assumed that the resistivity had a power-law temperature relation, and that the exponent was somewhere between 1 and 3 with uniform prior probability. Our prior information about n is completely neglected in this case. However if one assumes that n can take a finite set of values, for example 1, 3/2, 5/3 or 2, it is possible to compare these four possibilities for a given data set. In effect we are multiplying a curve similar to those in Fig. 4.9 by four delta functions at the positions that interest us.

A Bayesian analysis using this information requires much less data to identify the most likely value of n than the discussion above would suggest when we allowed n to vary freely. As an example, using the same data up to only 6 K (with data down to 3.7 K), it is possible to say that an exponent of 5/3 is 352 times more likely at 22.5GPa than the nearest possibility, which is $n = 2$, and more than 10^{12} times more likely than $n = 3/2$!

We can apply this technique to the low temperature data shown in Fig. 4.8. In that case, only the in-field data provide a consistent exponent, perhaps indicating the influence of superconducting fluctuations above the temperature identified as T_c^{onset}. For the resistivity with $B = 1$ T, an exponent of 5/3 is the best fit above 1.5 K. Below 1 K, down to 150 mK, the lowest measurement temperature, an exponent of 3/2 is required. This result should be taken with a certain amount of skepticism, as, for example, the magnetoresistance of the thermometer has not been taken into

account. However if it can be confirmed it would be very significant, as one of the major discrepancies between our results and theoretical models is that we do not find the expected exponent 3/2, over a large range of temperature.

On applying a magnetic field up to 8 T, the magnetoresistance of the normal state at 4.18 K and 700 mK was determined to follow the relation $\rho(B) - \rho(0) = \alpha B^{1.54\pm0.03}$, with $\alpha = 0.023 \pm 0.002 \mu\Omega\text{cm}\text{T}^{-1.54}$. This is unexpected as the usual d-band metal magnetoresistance varies as B^2.

The shift is virtually identical at all temperatures, indicating that the temperature coefficient A is virtually independent of magnetic field on a scale of 8 T. This implies that any magnetic fluctuations present have a large characteristic energy scale.

While there is a large variation of ρ_0 with pressure, shown in Fig. 4.6, the temperature coefficient A also evolves with pressure. This can be seen from the change in slope with pressure in Fig. 4.7(b).

The variation of the temperature coefficient A with pressure is shown in Fig. 4.10. The results are from a fit to $\rho = \rho_0 + AT^n$, where n was either fixed at 5/3 or allowed to vary (results shown on the graph). Both methods show a maximum around 19 GPa, coinciding with the highest T_c. A, or more comparably $(\rho - \rho_0)/T^2$, is very large compared to that in the α phase, being enhanced by a factor of about 30. As the effective mass m^* scales with $A^{1/2}$, this indicates a mass enhancement of a factor of around 6. There is also an increase of the quadratic coefficient in the α phase by a factor of two between 3.5 and 13 GPa, perhaps a sign of the softening of phonon modes as the first order transition is approached, however, there is no sign of any quantum critical behaviour in the α phase.

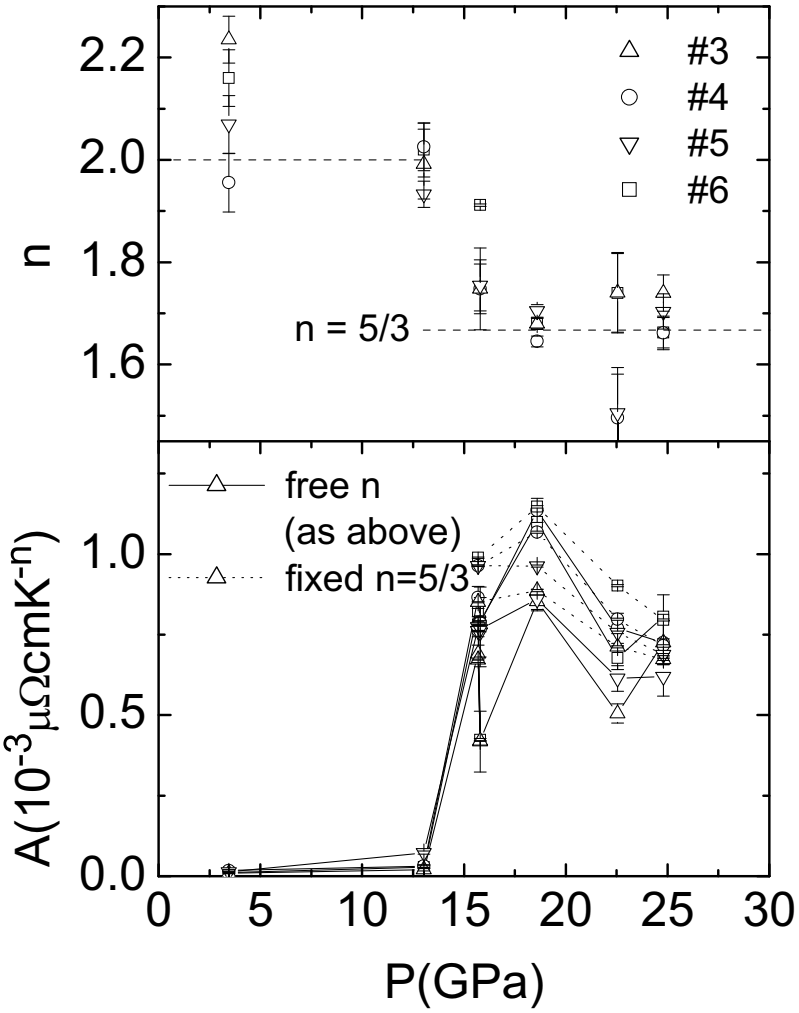

Figure 4.10: Coefficient A, and n from a fit to $\rho = \rho_0 + AT^n$ up to around 25 K. A is shown with n variable and fixed at 5/3.

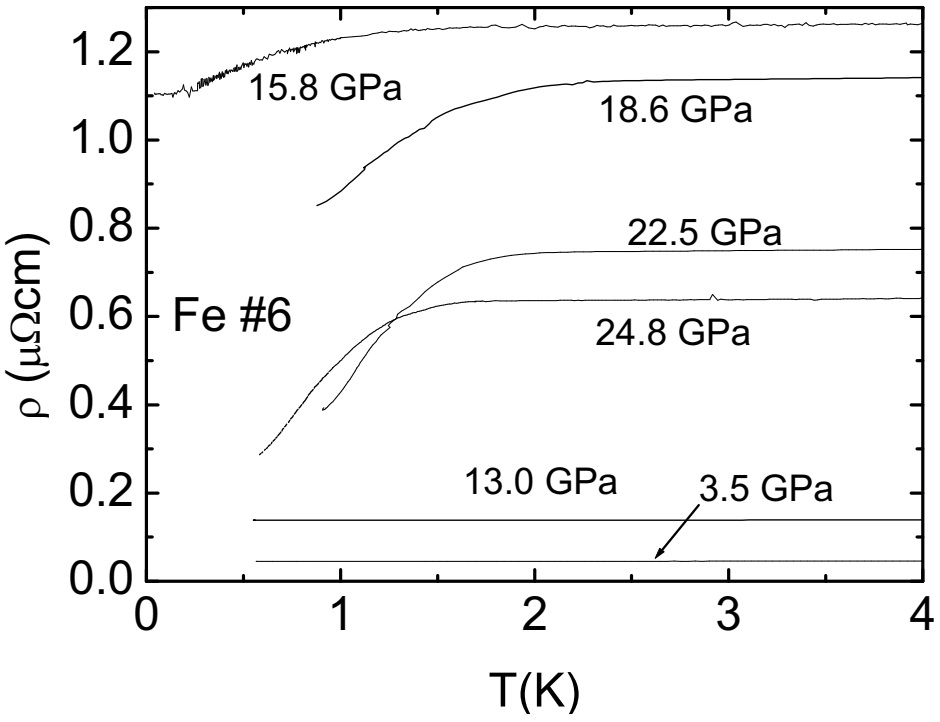

Figure 4.11: Evolution with pressure of the resistive superconducting transition in sample #6. Further measurements with a lower current down to 80 mK showed traces of superconductivity at 13 GPa.

4.1.5 Superconducting properties

The evolution of the resistivity in sample #6 below 4 K can be seen in Fig. 4.11. One can note both the evolution of ρ_0 shown in Fig. 4.6, and the superconducting transitions in the high-pressure curves.

At the lowest pressure, 3.5 GPa, iron is still fully in its α form and the resistivity from 4 K down to 0.6 K was found to be completely featureless. At 13 GPa, on the boundary of the ε phase, ρ_0 has already started to increase. At this pressure the resistivity was measure down to 80 mK (not shown), and a very small kink could be observed in the resistivity of this sample at 0.3K, with a total resistance drop slightly larger than the experimental noise (0.01%). On further increasing the pressure, T_c has a maximum at 18.6 GPa. The superconducting resistivity drops were smaller than in samples #1 and 2, but they became more complete as the pressure was increased. The current dependence within the transition, to be discussed below,

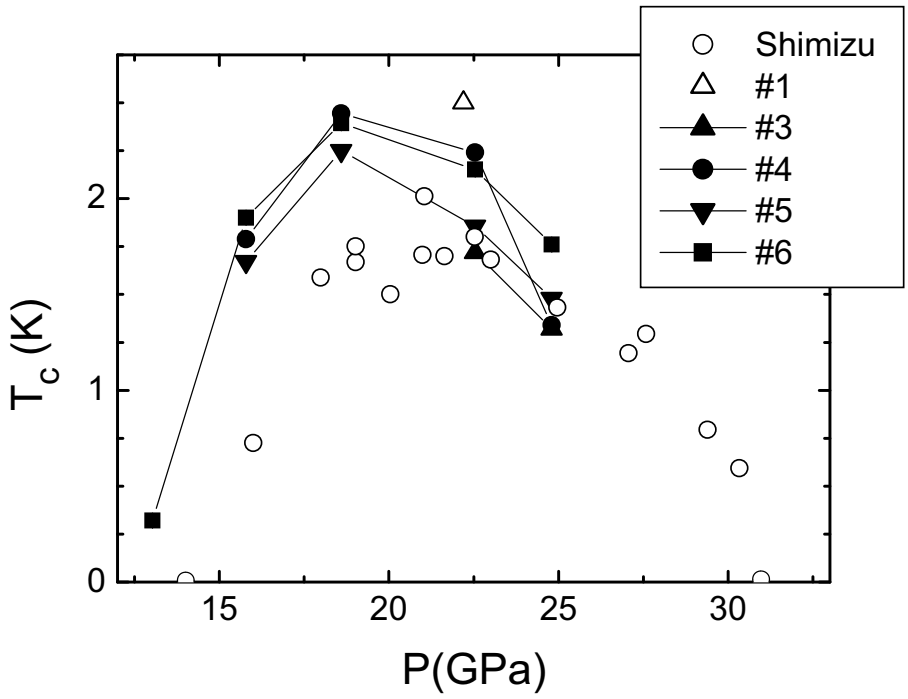

Figure 4.12: Superconducting critical temperature T_c^{onset} in many different samples as a function of pressure. Note that in sample #3, no trace of superconductivity was observed at pressures lower than 22 GPa, and its transitions were much less complete than the other samples.

became less pronounced at higher pressure.

T_c versus P

In Fig. 4.12, T_c vs. pressure is shown for samples #3–6, along with previous results. We confirm the phase diagram established by Shimizu, and show that slightly higher critical temperatures can be obtained from purer samples.

Only sample #6 showed any trace of superconductivity at 13GPa. At higher pressure the purified samples #4 and #6 behave very similarly. The commercial Goodfellow sample, #5, was almost as good.

The rolled sample #3, which had a significantly higher ρ_0 than the annealed samples, showed no trace of superconductivity below 22 GPa, though for the final two pressures, a drop in resistance was observed, though smaller than that in the other samples.

In comparison with previous results, the original carefully cut Osaka sample #1 had a higher T_c than any in this cell. Shimizu's T_c maximum was also found at a higher pressure.

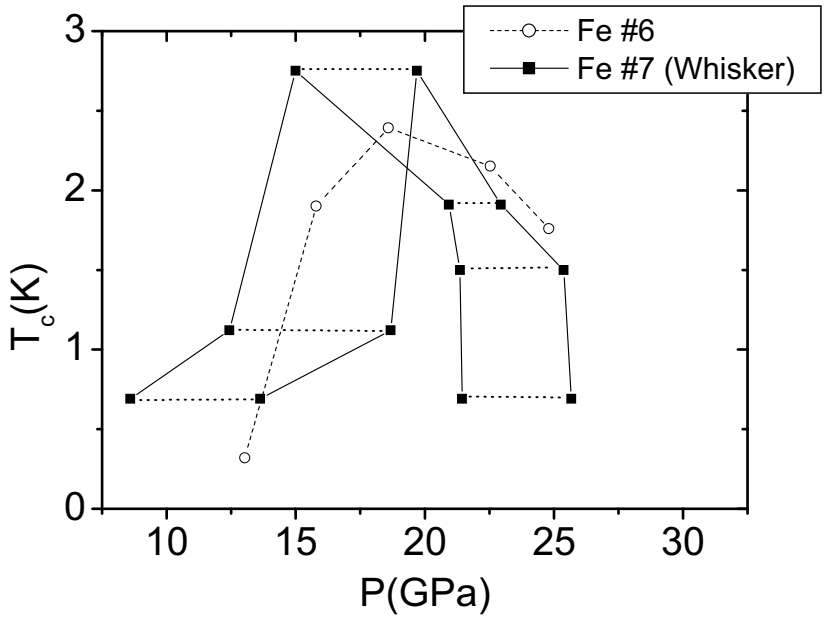

Figure 4.13: T_c^{onset} of the single crystal sample #7. Problems with the cell lead to extremely large pressure gradients, (the horizontal dotted lines represent ΔP), but the largest maximum T_c^{onset} observed was seen in this sample.

The results for sample #7, the single crystal whisker, are shown in Fig. 4.13. Broad superconducting transitions of the lead manometer indicated that large pressure gradients were present in the cell containing this sample. Despite the fact that the pressure conditions were far from ideal, the record highest T_c^{onset} ever observed in iron (so far) was found in this sample.

As T_c^{onset} reflects the highest transition temperature found in the sample, it may be appropriate to take the high pressure limit as T_c is increasing, and the low pressure limit as it goes back down to zero. If this is the case, then the superconducting pocket is significantly narrower than in any of the other samples. Comparing with previous results, there is therefore some evidence for a trend towards a narrower superconducting pocket with increasing sample quality.

Despite the non-ideal conditions, the transitions in #7 were more complete than those that had been annealed, i.e. for small enough current, a complete transition was observed, and a 73% drop in resistance was still obtained with a current density of 94 Acm^{-2}. The smaller resistance drops in samples #4–6 may indicate that the annealing process introduces some chemical impurities.

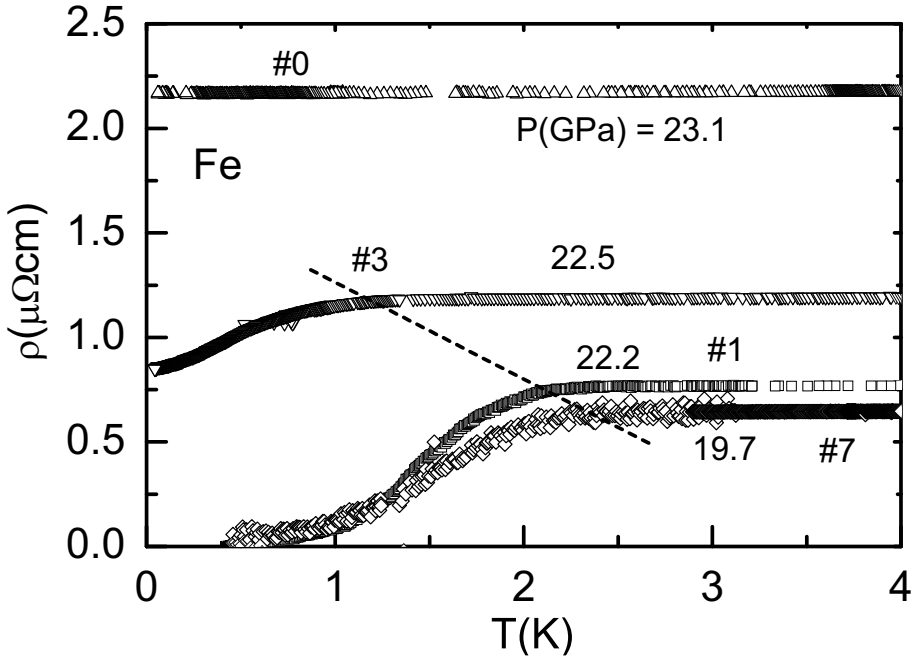

Figure 4.14: Superconducting transitions in samples with varying ρ_0, at a pressure near the maximum of T_c. The dashed line corresponds to a resistivity drop of 1% of the normal state.

AC calorimetry

There was a measurable ac calorimetry signal, which varied with pressure and temperature, from the setup using sample #7. However there was no visible anomaly connected with the superconducting transition in either the phase or the amplitude of the signal, either for the iron transition or that of the lead. The lack of transition in specific heat is not necessarily a purely experimental problem in the iron, given the very broad transition widths and the difficulties in observing such an anomaly in other magnetic superconductors such as $ZrZn_2$.

T_c vs. ρ_0

In the triplet superconductor Sr_2RuO_4, one of the principal pieces of evidence for unconventional pairing was a strong dependence of T_c on scattering from non-magnetic impurities. The suppression of T_c with increasing scattering, and hence ρ_0, was fitted to the Abrikosov-Gork'ov functional form (see Mackenzie et al. [1998]). This essentially gives the requirement that the mean free path ℓ be of the same order than the superconducting coherence length ξ and for the case of Sr_2RuO_4 led to superconductivity disappearing completely for ρ_0 above 1 $\mu\Omega$cm.

Figure 4.14 shows the superconducting transitions in samples with ρ_0 varying be-

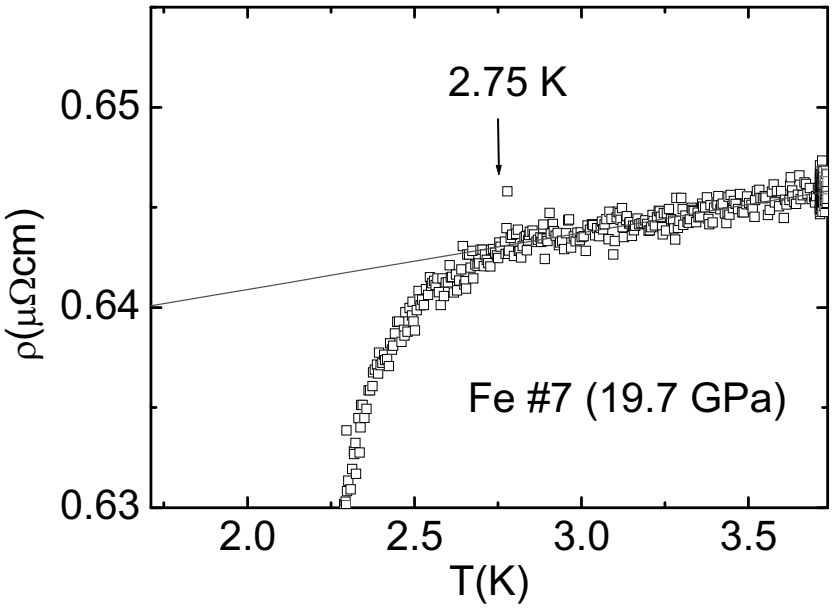

Figure 4.15: T_c^{onset} is defined as the temperature where ρ starts to deviate from its normal state behaviour. Shown here for example is the highest T_c so far observed, in sample #7, at 2.75 K. The pressure of 19.7 GPa quoted is likely to be an upper limit, determined from the completion of the Pb manometer transition, as there were large pressure gradients in the cell.

tween about 0.6 and 2.2 $\mu\Omega$cm. The differences in ρ_0 between samples are amplified from the situation at P=0. This means perhaps that for higher sample quality at ambient pressure, fewer defects are produced during the martensitic α-ε transformation process.

There is clearly an anticorrelation between ρ_0 and T_c, shown by the dashed line. A fit to the theoretical relation was not carried out, as the absolute value of the resistivity has an error around 10-15%, and T_c is too ill-defined. By simple extrapolation however it seems that a residual resistivity of under 1.7 $\mu\Omega$cm is required to see any trace of superconductivity, and a maximum T_c just over 3 K might obtained for the purest samples.

The highest T_c so far observed, at 2.75 K, can be seen in Fig. 4.15. This figure also shows how T_c^{onset} is defined, as a visible negative deviation from the normal state resistance. This criterion is obviously fairly subjective, and would be sensitive to superconducting fluctuations above the bulk value of T_c (if they are present). However it seems to be a more useful and reproducible criterion than others, such a 1% or 5% drop in resistance, indeed the latter may be almost 1 K below T_c^{onset}, and will vanish quickly in a magnetic field.

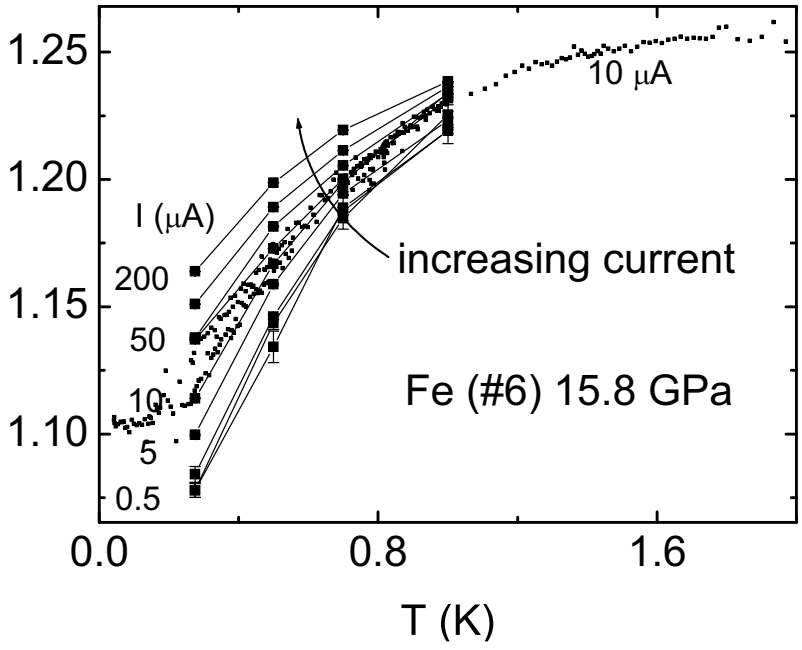

Figure 4.16: Effect of measurement current on partial superconducting transition. To convert to a current density, divide by the cross section of the sample, which was $15\times20\ \mu\mathrm{m}^2$.

Current dependence

To observe a complete resistive transition, a very small current density was required (Jaccard et al. [2002]). The effect of current on the superconducting transition in is shown in Fig. 4.16. Note that the closer to T_c^{onset} is resistance drop, the smaller the current dependence. This is another reason why T_c^{onset} is used as the principal definition for T_c.

It was suggested[4] that the partial, current-dependent transitions resemble flux-flow resistivity in a type II superconductor in a magnetic field (Kim et al. [1965]). This is where the potential drop measured is produced by vortex motion induced by the current. If this is the case, then the voltage/current relationship within the transition should be $V = a(I - I_0)$. An attempt to fit a flux-flow form to the resistivity is shown in Fig. 4.17. A small quadratic term in V(I) was required in addition to the linear term for a proper fit, but there was an extremely good agreement with $V = a(I - I_0) + bI^2$.

[4]by J.-P. Brison

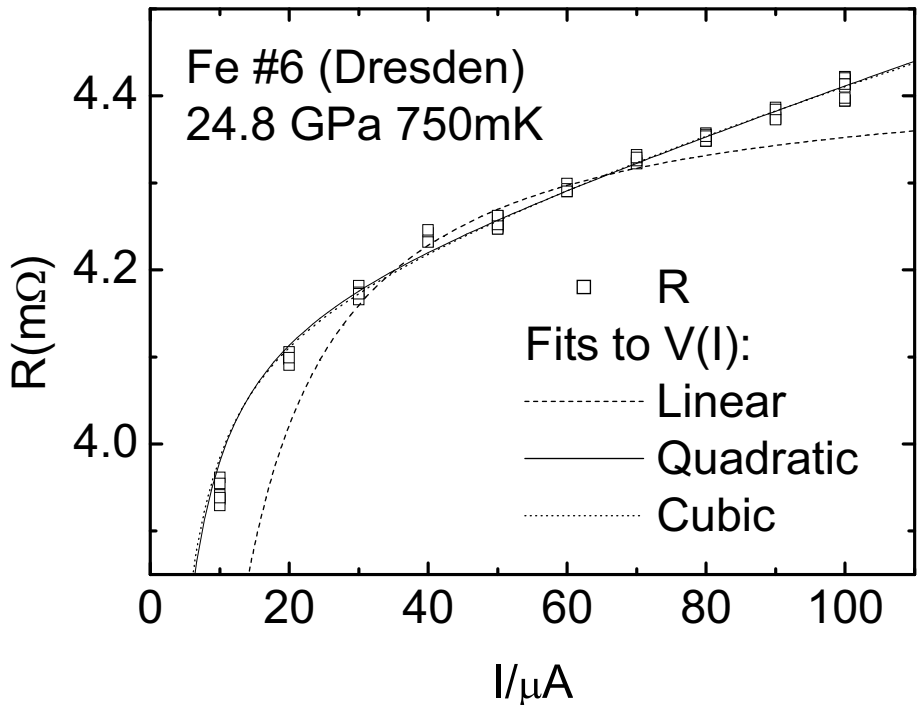

Figure 4.17: Current dependence at fixed temperature. The resistance R could be fitted to $R = a(1 - I_0/I) + bI$, i.e. voltage V quadratic in I.

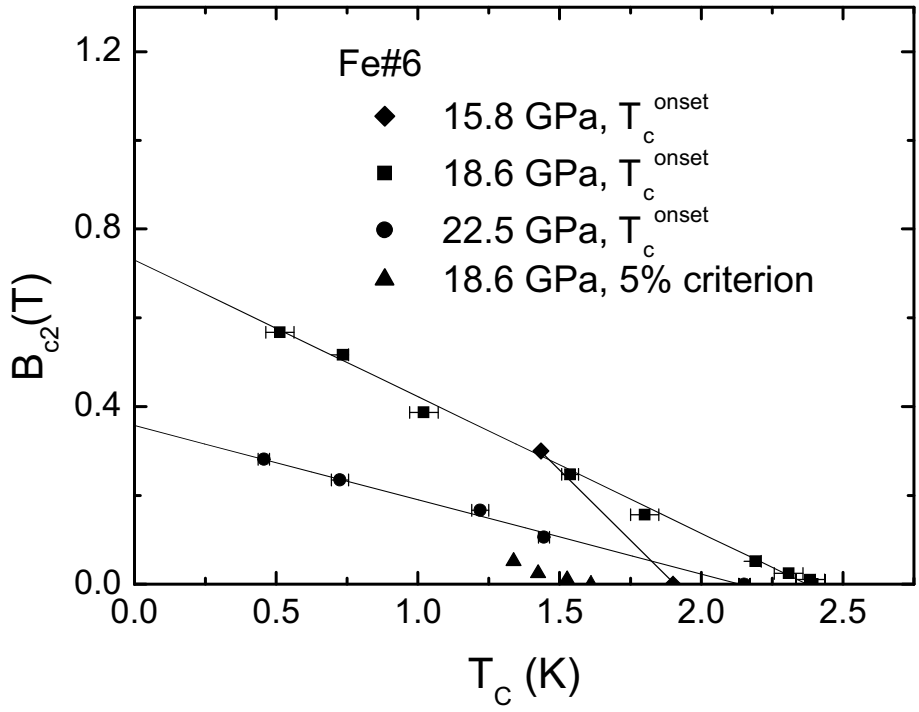

Figure 4.18: The critical field of ε-Fe at selected pressures. Two T_c criteria are used at 18.6 GPa.

The depinning current I_0 in this model is the minimum current required to activate the motion of flux lines. It was found to be very small, with an equivalent current density of 0.17 A cm^{-2}. For the transitions shown, there is no external applied field, but it is quite possible that remnants of the ferromagnetic α phase provide a substantial internal magnetic field. The internal field of pure ferromagnetic iron is very large (2.2 T), so it is far from out of the question that an internal field large enough to affect the superconductivity is present.

Critical field

Figure 4.18 shows the upper critical field B_{c2} for sample #6 determined using an onset criterion for T_c, at 15.8, 18.6 and 22.5 GPa. For comparison, a 5% resistance drop criterion at 18.6 GPa is also shown. While using a different criterion for T_c reduces both T_c and B_{c2} significantly (triangles vs. squares), both criteria have similar slopes.

B_{c2} is very large and linear down to at least $T_c/5$; the extrapolated value of $B_{c2}(T = 0)$ (0.73 T at 18.6 GPa and $\sim$ 0.35 T at 22.5 GPa) is much larger (by a factor of up to 70) than that of the lead manometer, which has a nearly identical T_c. This large critical field implies that ε-iron is almost certainly a type II superconductor. If, as

discussed above, we do observe flux-flow resistance in zero applied magnetic field, then there are internal fields present which mean that the true value of B_{c2} may be even bigger than that reported here. Although large, $B_{c2}(0)$ is still much lower than the Pauli limit of s wave superconductors $H_P(0) = \frac{\sqrt{2}}{g\mu_B}\Delta_0 = 1.85T_c$ in Tesla.

The initial slope $B'_{c2}(T_c)$ is proportional to the square of the effective mass in the clean limit, and its large magnitude, compared to that of lead for example, confirms the mass enhancement mentioned above.

While T_c has a dome-shaped pressure dependence, with a maximum around 20 GPa, B_{c2} appears to decrease continuously with pressure. We must bear in mind that this is based on only one observation, and that the internal field is unknown (though likely decreasing with pressure). Despite these caveats, this may be evidence for a QCP situated at a pressure below the α-ε transition.

Taking a value of 0.73 T for $B_{c2}(T = 0)$, the coherence length ξ, given by $H_{c2}(T) = \frac{\Phi_0}{2\pi\xi^2(T)}$ is around 20 nm, which is comparable to the mean free path ℓ. This can be derived from band structure calculations, which give the conduction electron density and the Fermi velocity, along with the residual resistivity. These calculations give ℓ=12 nm (Jarlborg [2002a]). A requirement for the clean limit, i.e. $\xi < \ell$, is another feature of unconventional superconductivity.

4.2 Discussion

The relationship between the normal state properties and T_c is shown clearly in Fig. 4.19, where T_c, A, and ρ_0 are plotted together against pressure. It is clear from this plot that A and ρ_0 have maxima coinciding with the maximum of T_c. They can be extrapolated back down to their values in the α phase at a pressure close to the disappearance of superconductivity. These similarities suggest a common mechanism relating all three properties.

What do these results tell us about the superconducting mechanism? The two possibilities are BCS-type phonon-mediated pairing, perhaps with an unconventional (i.e. non-s-wave) order parameter, or spin-fluctuation mediation.

If spin fluctuations are indeed responsible for the pairing, then T_c is given by

$$T_c \sim T_{sf}[1 - (\frac{\xi}{\ell}^2)]\theta e^{-\frac{1+\lambda'}{g\lambda'}} \tag{4.2}$$

where all terms are defined in chapter two. Of particular interest in this case are the factor $[1 - (\frac{\xi}{\ell}^2)]$, which represents pair-breaking due to impurities, and T_{sf}, which is analogous to the Debye temperature in BCS theory. T_{sf} is related to the relaxation rate of spin fluctuations, i.e. their scattering from conduction electrons, and thus also shows up in the resistivity coefficient A.

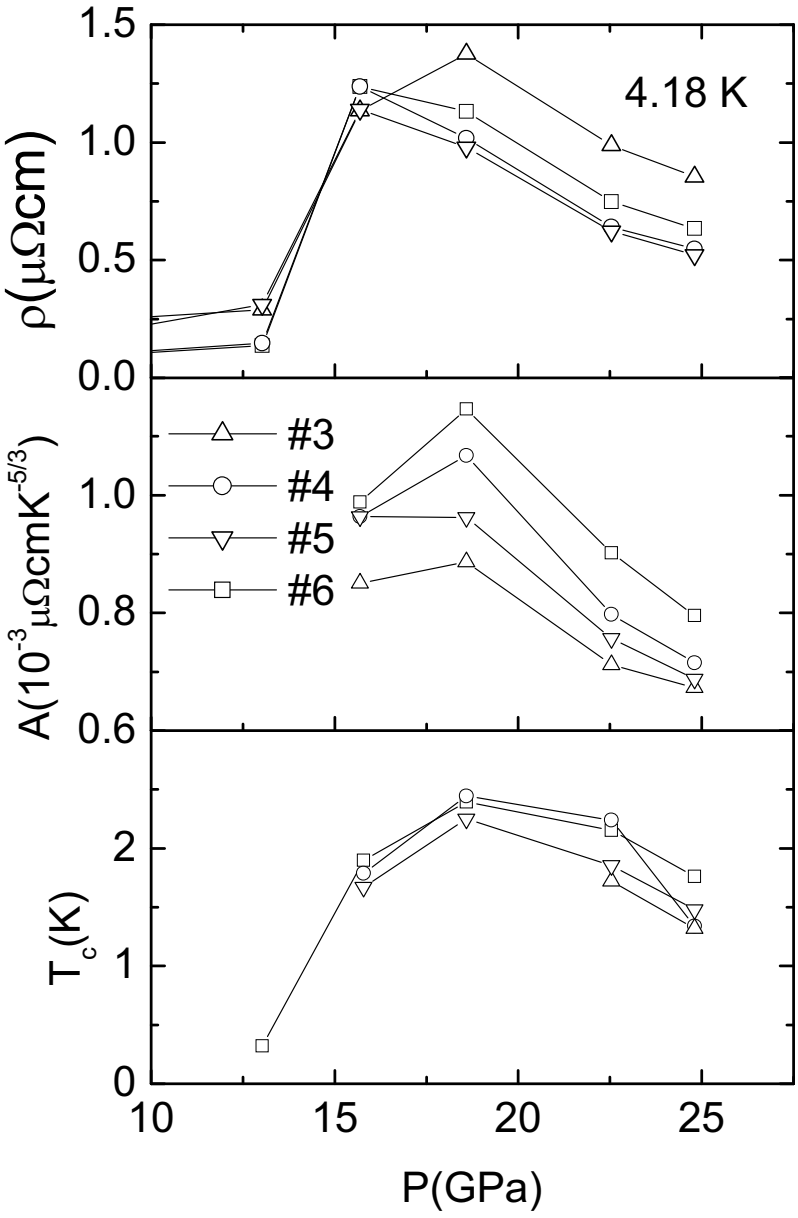

Figure 4.19: Pressure dependence of (a) the residual resistivity ρ_0, (b) the A coefficient in the $\rho = \rho_0 + AT^{5/3}$ power law, compared with (c) the superconducting critical temperature T_c.

The sensitivity to disorder strongly implies an unconventional order parameter. The small pressure range also makes a phonon mediated scenario unlikely, and there is strong evidence for the presence of critical spin fluctuations, whose energy scale is correlated with T_c. All of these point towards spin-mediated superconductivity.

There are, however, several problems with this scenario: critical spin fluctuations should be associated with a QCP, where an ordering temperature is driven to zero by an external parameter such as pressure. There is no evidence for such a critical point, though it may be hidden in the α phase.

The dominant fluctuations predicted for ε-Fe by most theoretical models are antiferromagnetic, which appears to be inconsistent with a 5/3 resistivity exponent.

The anomalous resistivity exponents associated with such a QCP are expected to be found in its immediate vicinity, whereas we find these spread over a large range in pressure and temperature. This is similar to the case of MnSi, where an exponent of 3/2 is found over a much larger pressure range than expected (Doiron-Leyraud et al. [2003]).

In fact, the QCP concept corresponds to a second order transition at $T = 0$, whereas in MnSi, a complex magnetic order is suppressed by pressure, ending in a first order transition. Perhaps this first order character, leading to a quantum critical region, rather than a single point, is relevant in iron.

Finally, soft lattice modes associated with the martensitic transition have not been specifically taken into account by theoretical models, so they could provide a phonon-based mechanism.

I will address these questions in more detail below, with specific reference to our results, and attempt to answer the questions posed in the introduction to this chapter.

- We have confirmed that superconductivity is observed in ε-Fe over a pressure range around 13–30 GPa, though we have not obtained high enough pressures to observe its complete disappearance. T_c emerges from $T = 0$ along with the first evidence for the presence of the ε phase in resistivity. The likely presence of a large internal magnetic field due to ferromagnetic clusters may suppress T_c from its intrinsic value at low pressure. However, we found a similar superconducting pressure range to that found by Shimizu, despite using different pressure medium. It therefore likely that the superconductivity is intrinsic to the ε iron, rather than some intermediate or mixed α/ε phase which would be sensitive to the pressure conditions.
- We have shown that T_c can be raised or lowered by manipulating intrinsic disorder in samples with a chemical impurity level lower than 100ppm. While fitting the relationship to a theoretical expression would provide more concrete proof of the nature of the pair-breaking, experimental constraints prevent this.

The requirement that $\ell \sim \xi$ for superconductivity to occur is consistent with our results. If however there is a QCP situated at a pressure p_c corresponding to the maximum of T_c, we would expect ξ to be proportional to $(p - p_c)^2$ (Demuer [2000]; Yuan et al. [2003b]). This would imply that the pressure width of the superconducting region would be smaller for more impurity scattering, which seems not to be the case.

- There is a large increase in resistivity going from the FM to the non-magnetic state, seen both at room temperature, and 4.18 K. This is probably due to a significant introduction of both static and dynamic (temperature dependent) scattering at the transition. At room temperature, this could conceivably come from differences in the phonon coupling, but a very similar structure is seen at 4.18 K, implying that both have the same, magnetic, origin. $\rho(4.18\,\mathrm{K})$ can be extrapolated to its low pressure value just above 30 GPa, coinciding with the disappearance of superconductivity. The reason for this relationship at low temperature is not clear, to me at least.

- The $\rho \sim AT^{5/3}$ resistivity law, valid up to about $15T_c$, signals the presence of spin fluctuations, probably of FM nature. The large value of A, corresponding to an effective mass m^* of about $6m_e$ shows that the charge-carrying quasi-particles are strongly renormalised by these interactions. The 5/3 exponent is predicted by a nearly FM model. This would imply that there is a triplet pairing symmetry. However, all calculations of *hcp* iron predict an AFM ground state.

- The value of A appears to track T_c. This is strong evidence that the same fluctuations responsible for the non-fermi liquid behaviour in resistivity are also responsible for the pairing interaction.

- The upper critical field observed is very large (70 times that of Pb, with an almost identical T_c), and it appears to have very little curvature. It is below the Pauli limit of around $1.85\,T_c$ (T), so it is not conclusive proof of triplet superconductivity. However the magnitude of B_{c2} demonstrates that ε-Fe is strongly type II, and confirms the high effective mass deduced from the resistivity coefficient A.

- There is a strong dependence of the resistivity on measuring current within the broad superconducting transitions. This may be explained by the flux flow resistance due to an intrinsic magnetic field produced by remnants of the α-phase.

This evidence shows that there is a strong possibility that ε-Fe is a triplet superconductor with pairing mediated by exchange of ferromagnetic fluctuations. These

are rare, as AFM-mediated singlet pairing is more robust than FM triplet superconductivity, as in the latter only longitudinal modes contribute to the pairing (see Lonzarich [1997]). However, anisotropy or the presence of a magnetic field can favour triplet pairing, where the Cooper pair has a non-zero total spin.

Other examples of triplet superconductors are Sr_2RuO_4 and $ZrZn_2$. These systems are all close to disappearance of ferromagnetic order, Sr_2RuO_4 is a paramagnet, with a highly anisotropic static susceptibility, and $ZrZn_2$ is a weak ferromagnet, with an ordered moment of $0.12\,\mu_B$ and a Curie temperature of 29 K. They share similar features with superconducting ε-Fe, including sensitivity to disorder, partial transitions, and NFL power laws (the exponent of which often varies between publications!). However for more conclusive proof of triplet status in ε-Fe, the spin susceptibility would have to be measured, not an easy task at these pressures. Mackenzie and Maeno [2003] describe in detail the physics of spin-triplet superconductivity.

There are other problems related to the α-ε transition which make it difficult to obtain a full picture of what is going on in superconducting ε-Fe. The martensitic nature of the transition means that over a broad range of pressure there is likely to be a rich microstructure, with microscopic coexistence of a ferromagnetic phase and non-magnetic one with a large susceptibility. However the similarity in results between different pressure media suggests that the superconductivity is intrinsic to the ε phase. Other more quantitative features should be interpreted bearing these qualifications in mind.

Further work to clarify the situation could involve measurement in different pressure media, such as helium, in which the $\alpha \rightarrow \varepsilon$ transition is likely to occur instantaneously. The extension, or not, of NFL behaviour to higher pressures should be investigated. It is also possible to stabilise non-*bcc* phases at ambient pressure in the form of thin films, for example on a Cu substrate. By varying the lattice mismatch, uniaxial strain can be introduced into a film. Given that triplet pairing is reinforced by anisotropy, it may conceivably be possible (though unlikely) to observe superconductivity and/or NFL behaviour at lower, or even ambient pressure using this technique.

The microscopic coexistence of the α and ε phases, and the role of ferromagnetic clusters should be explored with x-ray and magnetisation measurements, in collaboration with other labs.

We have shown that it is possible to induce superconductivity in Fe by using very pure samples, and tuning the electronic coupling by pressure. This raises the question, what about other ferromagnetic elements? Jarlborg [2003] has indeed predicted that cobalt will become superconducting at 50 GPa...

4.3 Summary

In this chapter, I have described resistivity measurements under pressure on superconducting iron. Using samples of varying quality, it was possible to observe the effect of disorder on the superconducting state. We showed that the highest T_c's and the most complete transitions required samples of very high quality, both in terms of their purity, and their metallurgical state.

These observations, and evidence from the normal state resistivity implies strongly that ε-Fe is an unconventional superconductor, with spin fluctuation mediated pairing the most likely mechanism. The nature of the Cooper pairs (triplet or singlet), and the associated fluctuations (ferromagnetic or antiferromagnetic respectively) is less firmly established, but our results support a ferromagnetically mediated triplet scenario.

Update

K. Miyake suggests a further possible explanation for the observed behaviour in superconducting Fe:

During the martensitic α-ε transition, there is likely to be an inhomogeneous coexistence of the two phases. Kadau et al. [2002] show a microscopic view of this from simulated shock-induced transitions. In the *bcc* α regions, ferromagnetic ordering has the lowest free energy, while in the *hcp* ε regions paramagnetism is the most stable state.

As one crosses the boundary from one phase to the other, the free energies of these two magnetic configurations will cross. In a boundary region (not necessarily coinciding with or the same width as the structural boundary zone), there will be significant magnetic fluctuations, which perhaps account for most of the electronic scattering.

If this is the correct microscopic picture, the superconductivity might be confined to this boundary region, explaining its fragile nature. The maxima in the residual resistivity and the A coefficient may also be explained if the electronic scattering is dominated by ferromagnetic fluctuations in this boundary zone, which may make up a small fraction of the sample.

Chapter 5

$CeCu_2Si_2$

5.1 Introduction

In the previous chapter we examined the case of iron, a transition metal whose properties are dominated by its d electrons. Superconductivity and non-Fermi liquid behaviour were found close to a phase boundary, where different ground states compete, and fluctuations between these configurations give rise to exotic scattering mechanisms.

The idea of competing ground states is very relevant to heavy fermions. These are usually rare earth intermetallic compounds, whose properties are dominated by their f electrons. An important class of these materials are cerium compounds.

Ce has a $[\mathrm{Xe}]4f^1(5d6s)^3$ electronic configuration. In most compounds the d and s electrons hybridise to form a conduction band, while the f electron may or may not remain localised on the Ce atom, giving Ce^{3+} or Ce^{4+} respectively. The level scheme of Ce^{3+} is shown in Fig. 5.1.

5.1.1 Magnetism

In the case of Ce^{3+}, the remaining $4f$ electron has a magnetic moment, which plays a crucial role in its electronic properties. This localised moment interacts with the conduction electrons via a coupling J. There are two different and competing effects which result from this. The first is the Kondo effect, where the spin of the conduction electrons is polarised to compensate for the f moment, and below a temperature $T_K \sim e^{-1/J}$, a singlet state is formed, quenching the magnetism. The second is the Rudermann-Kittel-Kasuya-Yosida (RKKY) interaction, where neighbouring f electrons interact indirectly, via the conduction electrons, and (anti)ferromagnetic ordering results, with characteristic temperature $T_{RKKY} \sim J^2$.

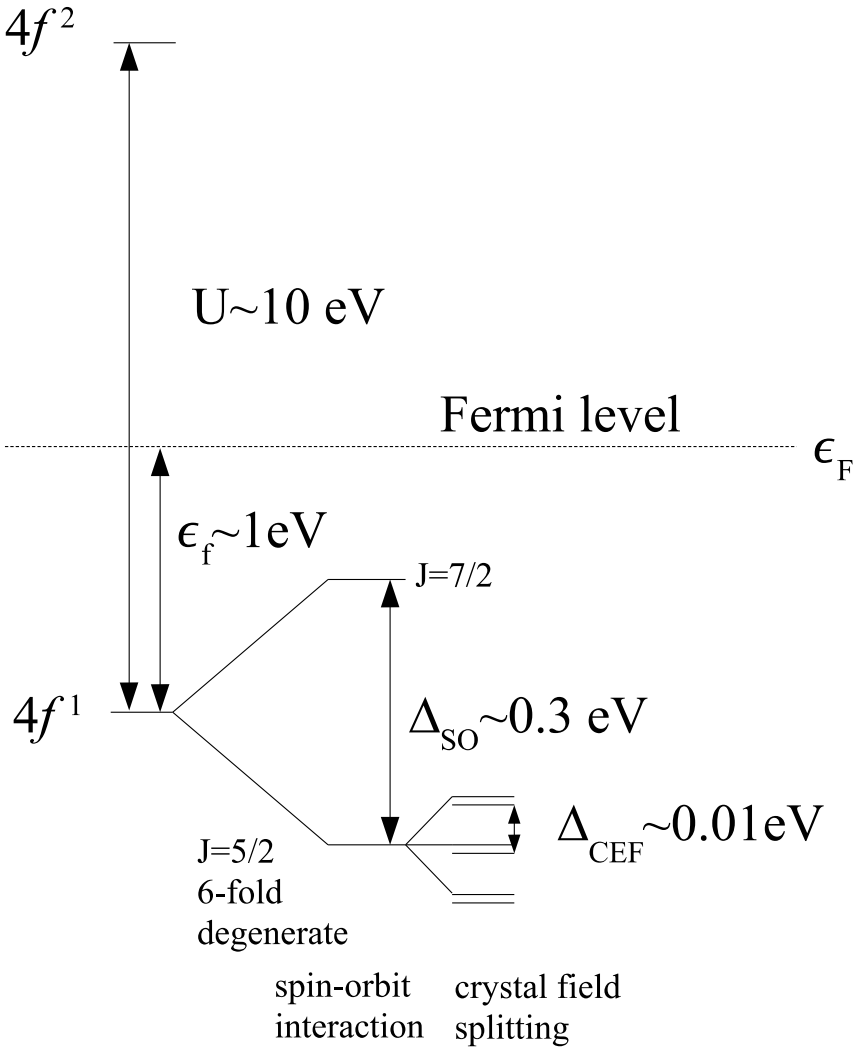

Figure 5.1: Electronic levels for the f electron in Ce^{3+}. In a tetragonal structure the sixfold $J = 5/2$ multiplet is split into three doublets by the crystalline electric field (CEF) effect. The large value of U ensures a maximum of one f-electron per atom, while hybridisation between the f-level and conduction band broadens the ground state doublet by an energy of order $k_B T_K$. Pressure affects the system by raising the f level ϵ_f, and increasing T_K.

The coupling J depends on the cell volume, which can be varied via chemical substitution or pressure. For a particular value of J, the effect of the Kondo and RKKY interactions will be equal and opposite, and the magnetic ordering temperature will approach zero. At this point, known as a magnetic quantum critical point (QCP), both magnetically ordered and non-magnetic ground states are degenerate. The associated critical fluctuations are thought to cause both superconductivity, and non-Fermi liquid behaviour, where a simple quasiparticle picture breaks down, in compounds such as $CePd_2Si_2$ and $CeIn_3$.

In both quasi-localised f electron compounds, such as Ce-based heavy fermions, and delocalised d electron materials such as iron, superconductivity and unconventional normal state scattering properties are produced by large amplitude, low energy fluctuations around a set of competing ground states. These may be critical spin fluctuations near a second order QCP, or they may involve a first order transition, a scenario which seems more and more likely in a variety of systems.

5.1.2 Valence transition

A magnetic phase boundary is not the only type of transition seen in Ce systems. In metallic Ce under pressure, there is an isostructural volume discontinuity, known as the α-γ transition. This corresponds to a valence change, where the $4f$ electron is transferred into the conduction band and becomes delocalised. This is a first order transition in elemental Ce, with a critical endpoint well above room temperature.

In $CeCu_2Si_2$, and other heavy fermion (HF) compounds, the Ce atoms are diluted in a lattice which reduces the coupling between f electrons. The chemical properties, such as atomic radius, electronegativity and valence of the ligand atoms, along with the pressure, affect the electronic environment of the Ce atom. As discussed above this can lead to changes in the magnetic coupling between f and conduction electrons, leading to different possible magnetic ground states.

The valence of the Ce ion also depends on the local environment, an important part of which is the unit cell volume, which can be varied with pressure. With increasing pressure $CeCu_2Si_2$ passes from a nearly trivalent $4f^1$ behavior, with Kondo coupling between conduction and f-electrons, to behavior at very high pressure characteristic of intermediate valence (IV) systems, whose valence fluctuates between the $4f^n$ and $4f^{n-1}$ + [5d6s] electronic configurations. As a result, deep in this IV regime, the resistivity, for instance, resembles that of $LaCu_2Si_2$, which lacks $4f$ electrons.

In this chapter, I explore the idea that an abrupt delocalisation of the Ce f electron is a general feature of Ce compounds, using the case of $CeCu_2Si_2$ as an example.

What form does this delocalisation take? It might be a gradual crossover, or it might be more sudden, as in metallic Ce. I will make the case for an intermediate scenario, where the delocalisation is abrupt and close to first order, but the critical end point is

at sufficiently low temperature that there are strong fluctuations between the $4f^1$ and $4f^0$ ground states. These fluctuations are responsible for a series of anomalies around the delocalisation pressure P_v, including a new mechanism of superconductivity!

5.1.3 Superconductivity

Superconductivity and magnetism

Following the discovery of superconductivity in $CeCu_2Si_2$ over twenty years ago (Steglich et al. [1979]), the relationship between superconductivity and magnetism has been extensively investigated in various d and f heavy fermion (HF) compounds. A consensus developed that HF superconductivity is mediated by spin fluctuations (Mathur et al. [1998]; Miyake et al. [1986]; Scalapino et al. [1986]; Monthoux and Lonzarich [2002]), mainly because superconductivity was found close to a magnetic instability at $T = 0$, sometimes described as a quantum-critical point (QCP), often attained by applying pressure.

$CeCu_2Si_2$ has a superconducting ground state at ambient pressure with a critical temperature T_c, around 0.7 K. It is firmly believed that the compound is close to an antiferromagnetic QCP at slight negative pressure, accessible for example by partial substitution of Si with Ge (Yuan et al. [2003a,b]).

As the Ce^{3+} moment is quenched by the Kondo effect just below the QCP, a rich variety of magnetic order appears (see for example Stockert et al. [2003]). The coexistence of superconductivity and antiferromagnetism also raises questions; a recent development is that an essentially gapless superconducting (SC) state has been identified by NMR/NQR measurements in the region where the SC state coexists with antiferromagnetism (Kawasaki et al. [2001, 2002]) consistent with a theoretical prediction by our collaborators (Fuseya et al. [2003]).

Superconductivity and the valence instability

The superconducting region of $CeCu_2Si_2$ is not confined to the antiferromagnetic QCP. In fact it extends well beyond the magnetic instability, and indeed appears to be enhanced at a pressure quite unrelated to the disappearance of magnetism. In this chapter I will argue that the enhancement of superconductivity is due to a second QCP, associated with f-electron occupation number, at a pressure $P_v \simeq 4.5$ GPa. Around P_v, critical valence fluctuations provide the SC pairing mechanism.

This idea is not new, indeed the link between valence change and superconductivity was proposed by Jaccard as far back as 1984 (Bellarbi et al. [1984]), developed in (Vargoz [1998]; Jaccard et al. [1999]) and a theoretical interpretation was developed by Miyake in the same year (Miyake et al. [1999]), but the new results reported here

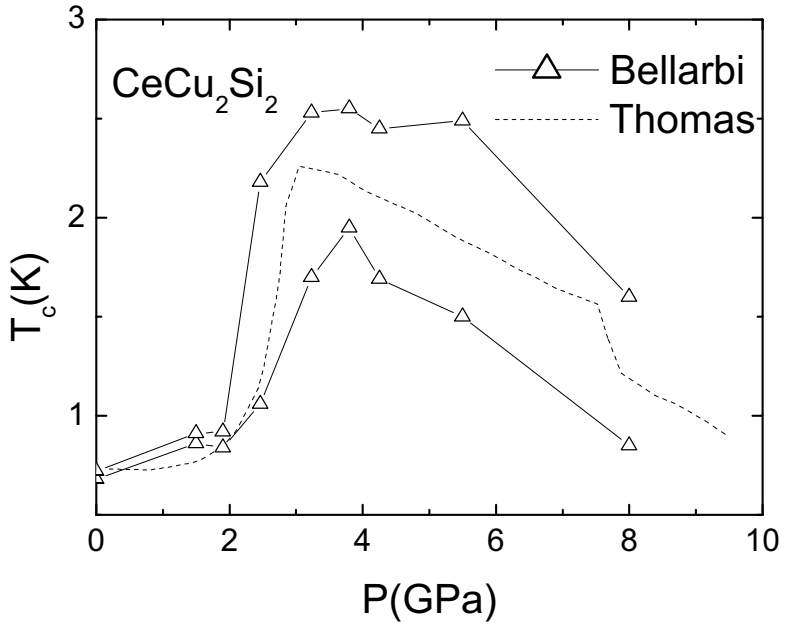

Figure 5.2: Superconducting critical temperature vs. pressure in $CeCu_2Si_2$, measured by susceptibility (dashed line, Thomas et al. [1996]) and resistivity (triangles, Bellarbi et al. [1984]). The two sets of resistive measurements come from the same sample, but reflect two different criteria for T_c. These broad resistive transition widths appear to be a characteristic feature, and will be discussed in detail the text.

confirm and extend these previous assertions.

T_c versus pressure

When pressure is applied to $CeCu_2Si_2$, T_c initially remains close to its ambient pressure value, followed by a sudden increase to around 2 K at about 3 GPa. Further increase in pressure results in a slower suppression of T_c to zero. This non-monotonous behavior of $T_c(P)$ was first explored by resistivity in the quasi-hydrostatic conditions of Bridgman anvil cell (Bellarbi et al. [1984]), see Fig. 5.2. Subsequent investigations by susceptibility (Thomas et al. [1996]) and resistivity (Vargoz et al. [1998]; Thomasson et al. [1998]) were carried out in various pressure media, and showed considerable variation in T_c between samples, especially at high pressure.

Similar $T_c(P)$ dependence to that found in $CeCu_2Si_2$ is seen in the isoelectronic sister compound, $CeCu_2Ge_2$, offset by about 10 GPa due to the larger atomic volume of Ge (Vargoz and Jaccard [1998]). Apart from this shift of the pressure scale, the two compounds share the same phase diagram.

5.1.4 Valence instability - a theoretical point of view

There exist at least three theoretical reasons to believe that critical valence fluctuations are at the origin of the pressure-induced peak of the SC transition temperature T_c.

First, the A coefficient of the T^2 resistivity law decreases drastically by about two orders of magnitude around the pressure corresponding to the T_c peak (Jaccard et al. [1999]). Since A scales as $(m^*/m)^2$ in the so-called Kondo regime, this implies that the effective mass m^* of the quasiparticles also decreases sharply there. This fall of m^* is possible only if there is a sharp change of Ce valence, deviating from Ce^{3+}, since the following approximate formula for the renormalization factor q holds in the strongly correlated limit (Rice and Ueda [1986]; Shiba [1986]):

$$\frac{m^*}{m} \simeq q^{-1} = \frac{1 - n_f/2}{1 - n_f}, \tag{5.1}$$

where n_f is the f-electron number per Ce ion.

Second, the so-called Kadowaki-Woods (KW) ratio A/γ^2 (Kadowaki and Woods [1986]), where γ is the Sommerfeld coefficient of the electronic specific heat, crosses over quickly from that of a strongly correlated class to a weakly correlated one (Miyake et al. [1989]). The inverse of the Sommerfeld coefficient, γ^{-1}, scales with the Kondo temperature T_K, which is experimentally accessible by resistivity measurements. This indicates that the mass enhancement due to the dynamical electron correlation is quickly lost at around $P \sim P_{\rm v}$, in agreement with the previous point. The phenomenon can be understood if we note the fact that γ consists essentially of two terms:

$$\begin{aligned} \gamma &= \gamma_{\rm band}\left(1 - \frac{\partial\Sigma(\epsilon)}{\partial\epsilon}\right), \\ &\equiv \gamma_{\rm band} + \gamma_{\rm cor}, \end{aligned} \tag{5.2}$$

where $\gamma_{\rm band}$ is due to the so-called band effect and $\gamma_{\rm cor} \equiv -\gamma_{\rm band}\partial\Sigma(\epsilon)/\partial\epsilon$ is due to the many-body correlation effect, with $\Sigma(\epsilon)$ being the self-energy of the correlated electrons. $\gamma_{\rm cor}$ and A are related to each other through the Kramers-Krönig relation, leading to the large value of the KW ratio (Miyake et al. [1989]), and when $\gamma_{\rm cor} \gg \gamma_{\rm band}$, this is indeed seen. On the other hand, if $\gamma_{\rm cor} \sim \gamma_{\rm band}$, the ratio A/γ^2 should be reduced from the KW value considerably because the effect of $\gamma_{\rm band}$ cannot be neglected in its denominator.

Third, there is a sharp peak in the residual resistivity ρ_0 at around $P \simeq P_{\rm v}$ (Jaccard et al. [1999]), which can be understood as a many-body effect enhancing the impurity potential (in fact we define the pressure $P_{\rm v}$ experimentally by the maximum of ρ_0). In the forward scattering limit, this enhancement is proportional to the valence susceptibility $-(\partial n_f/\partial\epsilon_f)_\mu$, where ϵ_f is the atomic f-level of the Ce ion, and μ is

the chemical potential (Miyake and Maebashi [2002]). Physically speaking, local valence change coupled to the impurity or disorder gives rise to a change of valence in a wide region around the impurity which then scatters the quasiparticles quite strongly, leading to the increase of ρ_0. The enhancement of ρ_0 can be thus directly related to the degree of sharpness of the valence change, because the variation of the atomic level ϵ_f is considered to be a smooth function of the pressure.

These circumstantial clues to the importance of critical valence fluctuations have been backed up by a microscopic calculation of T_c for d-wave pairing as a function of ϵ_{f} (Onishi and Miyake [2000b]). This showed that sudden valence change occurs if a moderately sized Coulomb repulsion U_{fc} is taken into account between the conduction c-, and localised f-electrons, with the peak structure of T_c being qualitatively reproduced. See Fig. 2.1 in chapter two for more details.

5.1.5 Experimental evidence for a valence instability

Table 5.1 summarizes the experimental evidence, of anomalies seen in $CeCu_2(Ge/Si)_2$ around P_{v}. References to the relevant observations are given in the table.

Part **(i)** of table 5.1 refers to direct evidence for a valence transition of the Ce ion:

Cell volume and L_{III} X-ray absorption measurements depend directly on the Ce valence. Both these properties show discontinuities as a function of pressure (in $CeCu_2Si_2$ and $CeCu_2Ge_2$ respectively). For example, Fig. 5.3, shows the volume discontinuity at P_{v} in $CeCu_2Ge_2$. The lack of discontinuity at room temperature implies that the critical end point lies somewhere between 10 K and room temperature.

The drastic decrease of the A coefficient of the T^2 resistivity law, along with the A vs $T_1^{\max}$ scaling relation, indicate that the system is leaving the strongly correlated regime characterized by a f-occupation number close to unity. ($T_1^{\max}$ is defined in Fig. 5.13 and assumed to be proportional to T_K.)

Part **(ii)** refers to anomalies observed close to the maximum of T_c predicted by critical valence fluctuation theory (Onishi and Miyake [2000b]; Miyake and Maebashi [2002]). These are the maximum of T_c itself and the enhanced residual resistivity, ρ_0.

Part **(iii)** refers to properties following from the extended treatment of the critical valence fluctuations published in Holmes et al. [2004b], and described in chapter two. This includes the linear resistivity, and the maximum in γ, both found around P_{v}.

In part **(iv)** are listed the remaining features that are observed in $CeCu_2Si_2$ and $CeCu_2Ge_2$ around the maximum in T_c but which are so far not fully explained. For example the merging of $T_1^{\max}$ and $T_2^{\max}$, where the latter (also defined in Fig. 5.13)

		$CeCu_2Si_2$	$CeCu_2Ge_2$
(i)	Volume discontinuity	-	1
	L_{III} X-ray absorption	2	-
	Drastic change of A by two orders of magnitude	This work, 3	3
	Change of $A \propto (T_1^{\max})^{-2}$ scaling	This work, 3	3
(ii)	Maximum in $T_c(P)$	This work, 4	5
	Large peak in ρ_0	This work, 3	3
(iii)	Maximum in $\gamma \simeq (C_P/T)$	This work, 6	-
	$\rho \propto T^n$ from $T_c < T < T^*$, with $n(P_v) = 1$ minimum	This work, 4, 7	3
(iv)	Sample dependence of T_c	This work, 4, 8, 9, 11, 3, 12	3
	Enhanced $\frac{\Delta C_P}{\gamma T}\Big\vert_{T_c}$	This work	-
	Resistivity and thermopower indicate $T_1^{\max} \simeq T_2^{\max}$	3, 7	3, 13
	Broad superconducting transition widths ΔT_c	This work, 4	3

[1] Onodera et al. [2002]; [2] Roehler et al. [1988]; [3] Jaccard et al. [1999]; [4] Bellarbi et al. [1984]; [5] Vargoz and Jaccard [1998]; [6] Vargoz et al. [1998]; [7] Jaccard et al. [1985]; [8] Thomas et al. [1996]; [9] Thomasson et al. [1998]; [11] Jaccard et al. [1998]; [12] Vargoz [1998]; [13] Link et al. [1996]

Table 5.1: Anomalies in $CeCu_2Si_2$ and $CeCu_2Ge_2$ associated with valence transition, with references. Symbols explained in the text.

Part **(i)**: Direct evidence for sudden valence change.
Part **(ii)**: Anomalies explained by published valence fluctuation theory (Onishi and Miyake [2000b]; Miyake and Maebashi [2002])
Part **(iii)**: Anomalies explained by extended treatment of the critical valence fluctuations (section 2.3.4, Holmes et al. [2004b]).
Part **(iv)**: Other anomalies observed around crossover to intermediate valence with pressure.

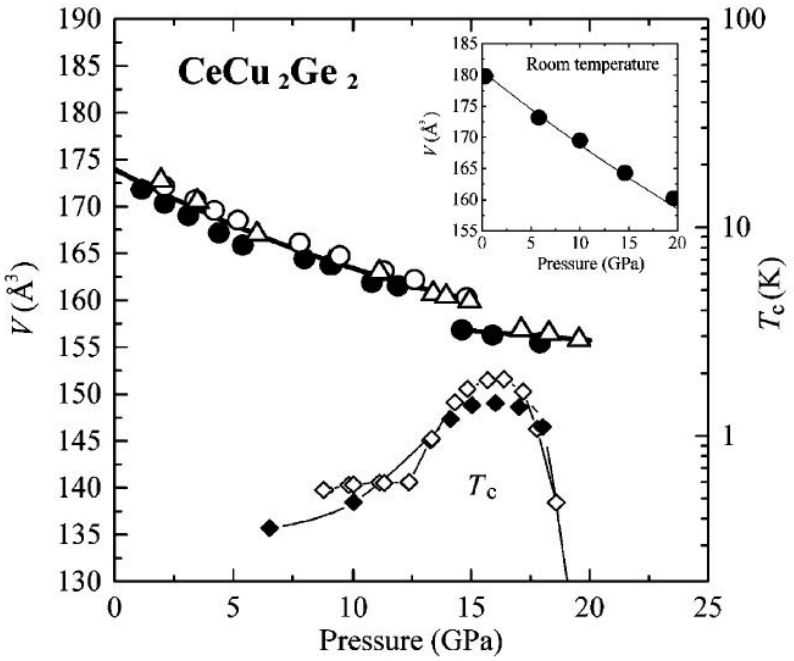

Figure 5.3: Cell volume at 10 K of $CeCu_2Ge_2$ up to 25 GPa. There is a volume discontinuity of 2%, which is not present at room temperature, coinciding with the maximum of T_c.

is believed to reflect the effect of the excited crystalline electric field (CEF) split f-levels. Many of the anomalies noted in table 5.1 have also been observed to coincide with the maximum of T_c in other HF superconductors, from $CePd_2Si_2$ (Demuer et al. [2002]) to $CeCu_5Au$ (Wilhelm et al. [2000]), the latter showing traces of superconductivity under pressure.

5.1.6 Different phases of $CeCu_2Si_2$ at ambient pressure

Previous work on $CeCu_2Si_2$ has shown a lot of variation in low-temperature behavior between different samples, and indeed large variations in the electronic properties of $CeCu_2Si_2$ are well known to result from extremely small differences in composition (see Ishikawa et al. [1983]; Modler et al. [1995]; Steglich et al. [1996]; Louca et al. [2000]).

$CeCu_2Si_2$ is often classified into the types A, A/S, and S. The labels denote the presence of a magnetically ordered 'A' phase and/or a superconducting 'S' phase at ambient pressure. The exact stoichiometry determines the phase obtained, but an excess of copper, for example, usually leads to an S phase sample. Ishikawa recently reported measurements on so-called 'high-T_c' and 'low-T_c' samples, where T_c was observed to increase or decrease with pressure, respectively (Ishikawa et al. [2003]).

The extension of all these variations with pressure has not previously been systematically explored up to now, but almost all samples so far studied have shown an enhancement of T_c, along with effects such as the enhancement of the residual resistivity, to be discussed below.

5.1.7 Pressure cells

The results presented below are from three pressure runs. The first was carried out in a diamond anvil cell (DAC) with a helium pressure medium, and the others in Bridgman anvil cells:

1. **DAC/helium** Single A/S sample (source: Geneva), spot welded contacts, hydrostatic conditions. Resistivity and ac calorimetry measurements.
2. **Bridgman cell #1** Four samples: 'high T_c' and 'low T_c' polycrystals (source: Ishikawa, ISSP, Chiba, Japan), and two A/S type single crystals (source: Jeevan, MPI, Dresden, Germany).
3. **Bridgman cell #2** Two A/S samples (same source), oriented differently with respect to cell axis.

Variability under pressure may be due to the samples themselves, or to pressure inhomogeneities caused by non-hydrostatic pressure media, which for example could lead to broad superconducting transitions if T_c varies rapidly with pressure.

We were therefore motivated to use solid helium as a pressure medium in our first run, due to its near-ideal hydrostaticity at low temperature. By simultaneously probing resistivity and specific heat in the same sample, we were able to explore both percolative transport and bulk evidence for superconductivity.

The $CeCu_2Si_2$ sample used in the DAC/He cell was prepared by reaction of its constituent elements with a slight excess of Cu, with a nominal initial composition $CeCu_{2.1}Si_2$. The product was then melted in an induction furnace and slowly allowed to crystallize under 50 bars Ar in a $BaZrO_3$ crucible (see Ref. Vargoz et al. [1998] for more details).

Having carefully studied the behaviour of one sample in ideal hydrostatic conditions, in the second run we explored the effect of composition, and orientation relative to the current and cell axis. Four samples were used, 'high-T_c' and 'low-T_c' polycrystals, provided by Ishikawa's group, and crystalline A/S type samples from Geibel's group. The A/S crystals were placed with their c-axis perpendicular and parallel to the current direction.

The final experiment was intended to isolate the effect of uniaxial stress on two A/S crystalline samples. This effect was shown to be important in $CePd_2Si_2$ (Demuer

et al. [2002]), and the results from the second run, mentioned above, suggested that this would be a fruitful area to explore.

5.2 Experimental results

The results obtained in the helium cell provide a comprehensive and coherent argument for the existence of a valence instability at $P_v \simeq 4.5$ GPa, and that valence fluctuations are responsible for the enhancement of superconductivity around that pressure. This has been published in Holmes et al. [2004b], and I will present the results therein in more or less the same form below; the subsequent experiments explored the details of the novel region around P_v, and those results follow afterwards.

5.2.1 Helium Cell

There are five principal results from the sample measured in the helium cell. By drawing on previous work, I will aim to place these results in a broader context. I will try to highlight common features found in many samples of $CeCu_2Si_2$, one of the defining characteristics of which is its variability.

- I will present the superconducting phase diagram obtained using various criteria for T_c, and compare it to the widely quoted phase diagram determined under hydrostatic conditions by susceptibility.

- I will examine the details of the superconducting transition, which provides some insight into the nature of the SC state and into the sample itself.

- I will estimate the variation of the Sommerfeld coefficient γ, with pressure, and compare it to previous results obtained by analysis of the upper critical field.

- I will report the pressure dependence of the residual resistivity ρ_0, and exponent n, determined by a fit to the normal state resistivity of $\rho = \rho_0 + \tilde{A}T^n$ ($\tilde{A}$ denoting a free exponent as opposed to the quadratic coefficient A). A comparison of $\rho_0(P)$ between different samples reveals a scaling relation which can be related to the theoretical enhancement of impurity scattering.

- Finally, I will explore the deviation from the scaling relation $A \propto T_K^{-2}$, which indicates the sharp change in f-electron occupation number described in the introduction. The enhancement of T_c and the other results described above are shown to occur around the same pressure.

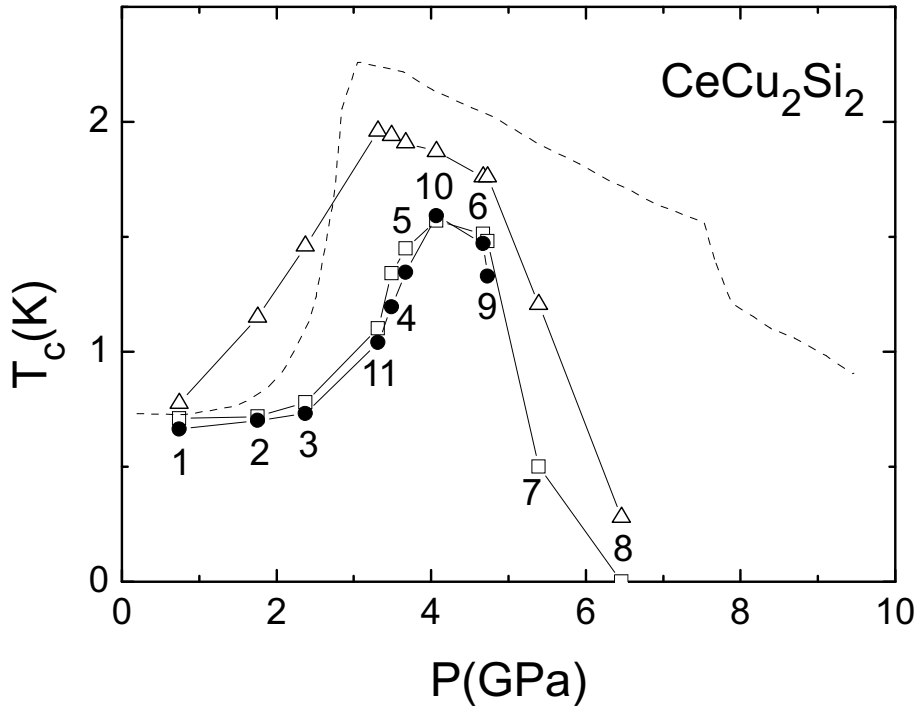

Figure 5.4: $T_c(P)$ in $CeCu_2Si_2$ determined from resistivity and specific heat measurements. The triangles show T_c determined from the onset of the resistive transition (T_c^{onset}), the squares show its completion ($T_c^{R=0}$), and the filled circles show the midpoint of the specific heat jump. The numbers indicate the sequence of pressures. The dotted line shows T_c determined by susceptibility in a different sample (Thomas et al. [1996]), also in a helium pressure medium.

T_c versus pressure

Figure 5.4 shows the superconducting phase diagram determined by both resistivity and specific heat, both on increasing and decreasing the pressure. Two qualitatively different types of behavior can be seen in the same sample, represented by the onset and completion of the resistive transition.

If we follow the transition onset $T_c^{\text{onset}}(P)$, one sees the sharp kinks similar to those seen in by Thomas et al. [1996] (dashed line), along with a linear decrease of T_c between 3.3 and 4.8 GPa at a rate of $0.14\,\text{K}\,\text{GPa}^{-1}$. Superconductivity is observed however over a much smaller pressure range in our sample.

The temperature $T_c^{R=0}(P)$, at which the resistance vanishes, behaves differently from $T_c^{\text{onset}}(P)$. It has a narrower peak with a maximum at slightly higher pressure. $T_c^{R=0}$ agrees closely however with the transition seen in the specific heat (see below). When a magnetic field was applied, $T_c^{R=0}$ and the specific heat anomaly shifted in agreement. The large resistive transition widths found in $CeCu_2Si_2$ at high pressure, seen more clearly in Fig. 5.5, are often blamed on a lack of hydrostaticity due to

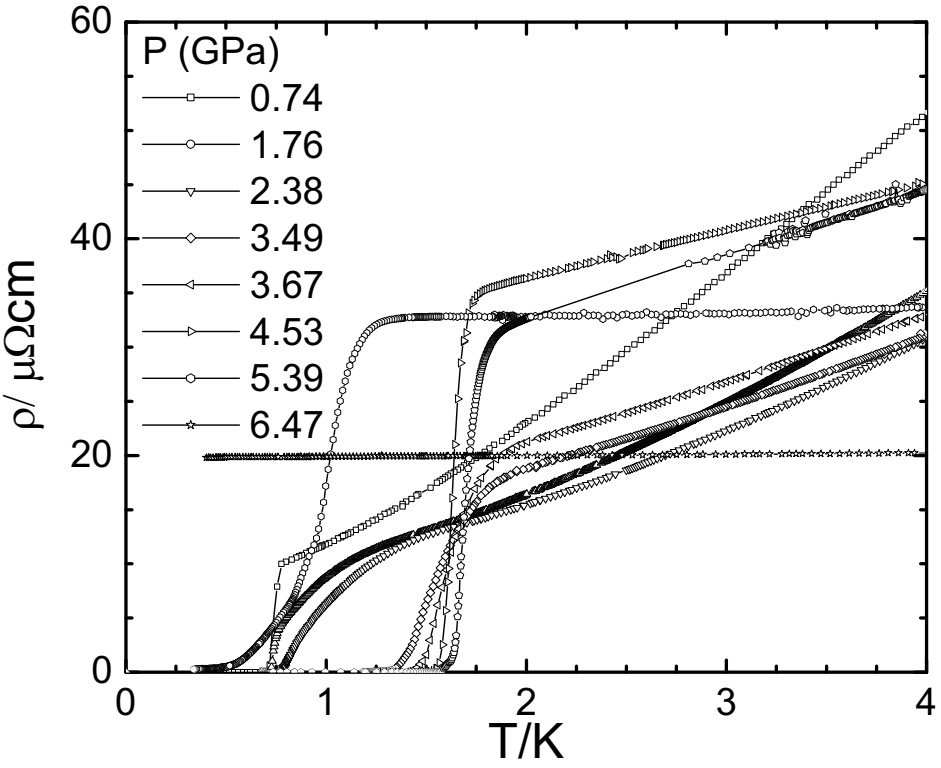

Figure 5.5: Resistivity in the helium cell below 4 K up to 6.5 K. Note the sharp transitions at 0.74GPa and around 4GPa, with broad transitions where T_c changes rapidly with pressure, despite the lack of pressure gradients.

the pressure medium. As helium was used in this case, we can rule out pressure inhomogeneities and concentrate on the sample itself.

Filamentary superconductivity above $T_c^{R=0}$

Further information about the SC state comes from the effect of measurement current and magnetic field on the transition width (see Figs. 5.6 and 5.7). For example, at 1.78 GPa high current led to the upper part of the transition disappearing, and a resistive transition can even be recovered with a narrow width comparable to that close to ambient pressure. This is presumably due to the presence of filamentary superconductivity, with a higher T_c, whose critical current density is exceeded. When a magnetic field is applied, the reverse happens, with the upper part of the transition being more robust due to its higher critical field.

These broad resistive transitions appear to be a universal feature of $CeCu_2Si_2$ at high pressure. Let us recall that even for the highest T_c^{onset} measured in a single crystal, at 2.4 K, a tail of 1% of the normal state resistivity remained well below 2 K, vanishing only at 1.5 K (see Vargoz et al. [1998]). The status of the superconductivity of $CeCu_2Si_2$ between T_c^{onset} and $T_c^{R=0}$ remains mysterious.

Specific heat jump at T_c

The ac calorimetry technique provided an extremely clear view of the superconducting transition in specific heat. Fig. 5.8 shows how the size and shape of the jump in C/T varies with pressure. One should notice that the jump starts off relatively small and sharp, then grows much bigger as T_c increases,[1] while remaining sharp. Before T_c reaches a maximum, the specific heat peak starts to broaden and then collapses in amplitude as the pressure is increased further and T_c is driven to zero. On reducing the pressure, the specific heat jump reversibly regains its shape, so we can rule out a disintegration of the sample.

Figure 5.9 compares in detail the superconducting transition in resistivity and specific heat at three different pressures. At 2.38 GPa the resistive transition is broad and the sharp specific heat jump at 0.73 K begins at the point where the resistance falls to zero. At 3.67 GPa the specific heat jump, at 1.35 K, is much larger, and remains sharp (and did so at intervening pressures), while the corresponding resistive transition has narrowed considerably. At 4.07 GPa (not shown in this figure) where $T_c^{R=0}$ has a maximum around 1.6 K in both ρ and C_P, the specific heat peak has already started to broaden and collapse in amplitude, while at the same pressure the

[1] N.b. the measurement frequency changes between these two temperature domains. This is accounted for in the normalisation, but this is the first ever measurement under these conditions, and there remains the possibility that there are problems with the model used to extract the specific heat.

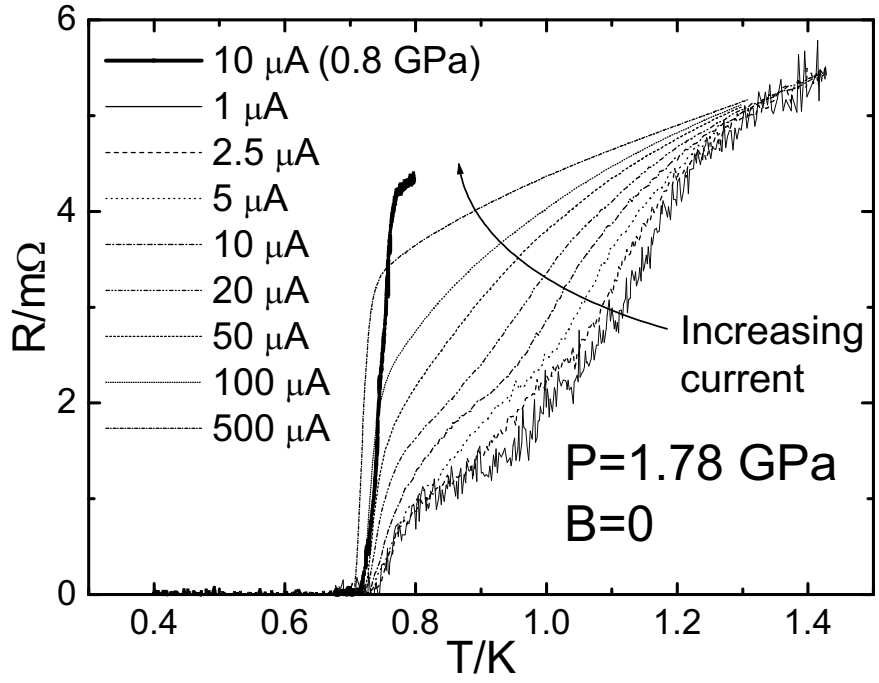

Figure 5.6: Resistive transition at 1.78 GPa, where increasing current suppresses the upper part of the transition, and a narrow width is recovered.

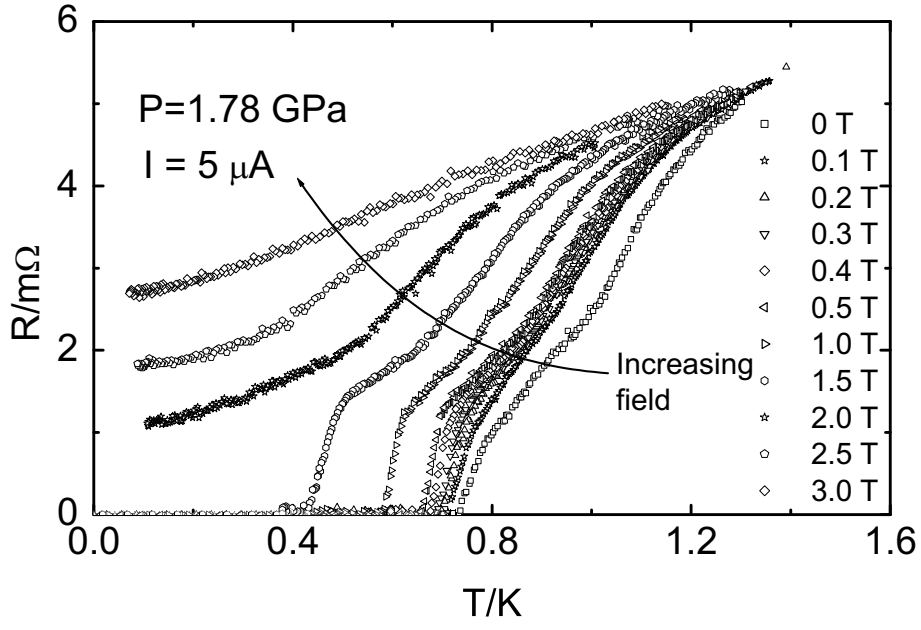

Figure 5.7: Resistive transition at 1.78 GPa, showing the effect of magnetic field, where the lower part of the transition, having a lower critical field, becomes normal.

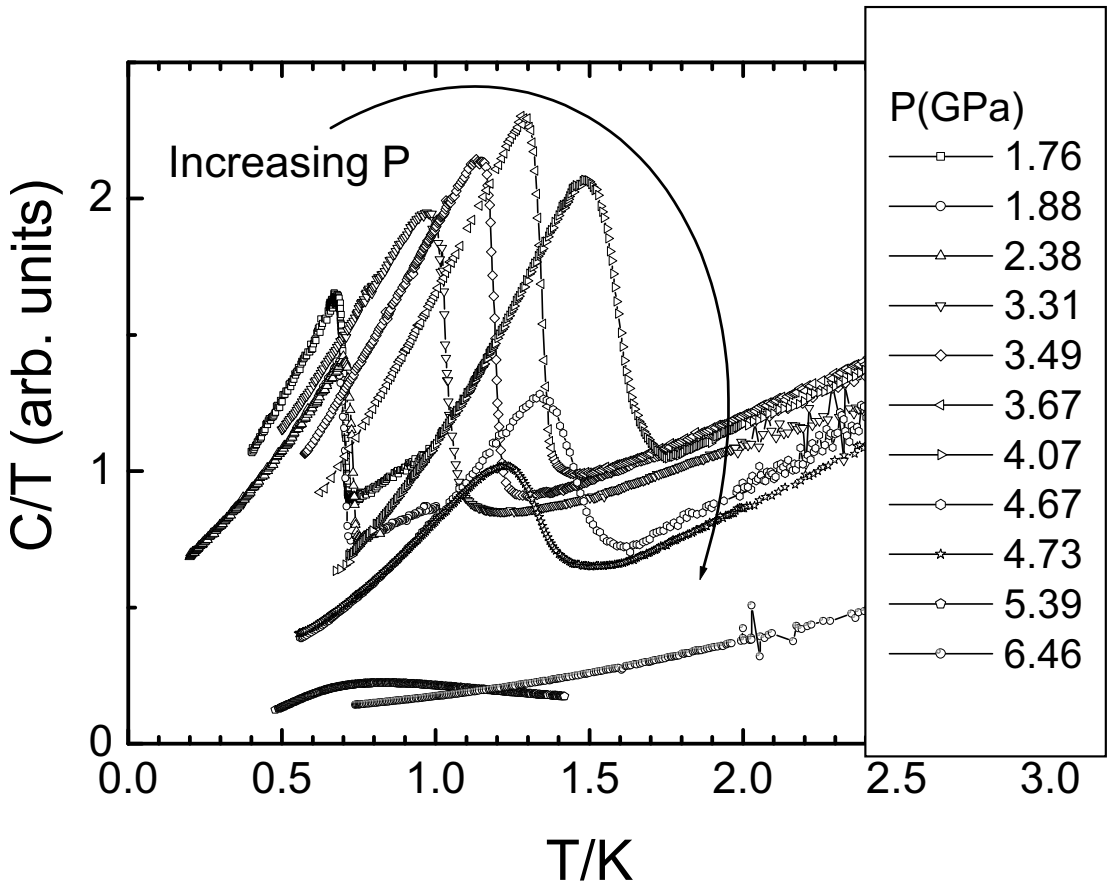

Figure 5.8: Superconducting specific heat jump at different pressures, extracted from the ac calorimetry signal. Note that it remains sharp up to 3.7 GPa, but starts to broaden and collapse even before T_c reaches a maximum. The amplitude of the jump seems to be much larger closer to $P_v \simeq 4.5$ GPa than at low pressure near P_c, however there remains the possibility that this is an experimental artefact.

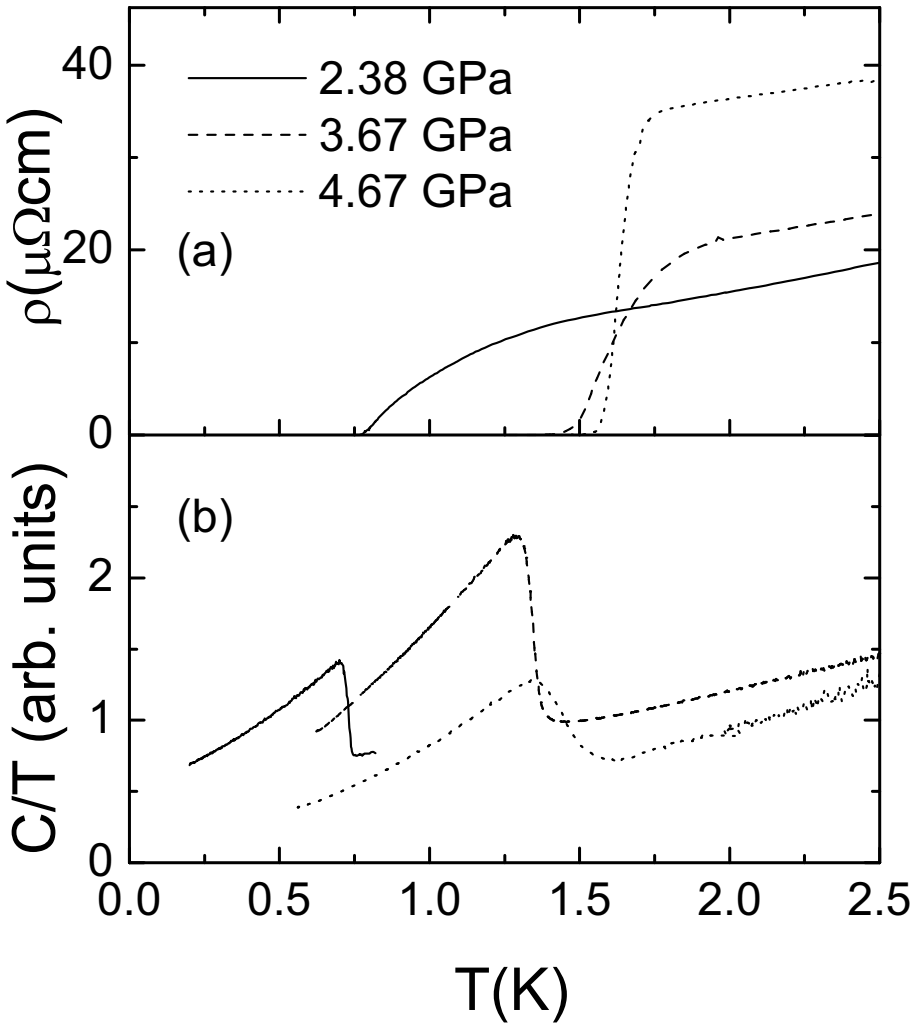

Figure 5.9: Superconducting transition at three pressures in (a) resistivity and (b) specific heat. Note the width of the resistive transitions, and the fact that the start of the jump in specific heat coincides with the completion of the resistive transition.

resistive transition is at its narrowest since ambient pressure. As T_c is driven to zero at high pressure, the superconducting C_P jump becomes smaller and broader (as shown at 4.67 GPa) until it is no longer visible. When the pressure was reduced, the C_P peak recovered its shape, indicating the reversibility of the bulk pressure-induced behavior.

The dramatic increase in the apparent size of the superconducting jump is intriguing, and might suggest the presence of strong coupling (see for example Tsuneto [1998]) or other qualitative change in the SC state. Although the apparent value of $(\Delta C_P/\gamma T)_{T_c}$ is clearly less than the BCS ratio of 1.43, similar ac measurements on $CeCoIn_5$ in an argon pressure medium indicate that there is a substantial contribution to the measured heat capacity from addenda (Braithwaite [2003]). In helium we would expect this to be even more significant.

The increase in the C_P jump size might itself be an artefact of the uncalibrated ac-calorimetry method; nevertheless $(\Delta C_P/\gamma T)_{T_c}$ does appear to show a maximum at a pressure coinciding with the increase in T_c. Furthermore, the assumption of strong coupling provided the best fit to H_{c2} for measurements of the upper critical field in another sample (Vargoz et al. [1998]).

Electronic specific heat coefficient γ

The electronic specific heat coefficient γ, and hence the effective mass m^*/m, can be estimated by following the calorimetric signal C/T, at a fixed temperature and measurement frequency above the superconducting transition, though this includes constant or slowly varying addenda from the helium, diamonds etc. Figure 5.10 shows the estimate $\tilde{\gamma}(P)$, along with the value deduced from measurements of the upper critical field in Ref. Vargoz et al. [1998]. A single constant scale factor has been introduced, showing that the two curves can be superimposed. There is a clear anomaly in $\tilde{\gamma}$ at 4 GPa (just below the pressure corresponding to $T_c^{\max}$), superimposed on a constant reduction with pressure. The effective mass is also reflected in the initial slope of the upper critical field $H'_{c2}(T_c)$, which in our sample also had a maximum at the same pressure as the peak in $\tilde{\gamma}$ (see Fig 5.11. The exact interpretation of $H'_{c2}(T_c)$ depends on whether the sample is in the clean or dirty limit, i.e. how does the mean free path compare to the superconducting coherence length, but in both cases it reflects the effective mass.

Residual resistivity

The residual resistivity ρ_0, has a huge peak at a pressure slightly higher than the maximum in T_c. The magnitude of this peak varies by a factor of more than ten between samples (Vargoz [1998]; Vargoz et al. [1998]). However, it is possible to scale the residual resistivities from different samples onto the same Lorentzian curve (see

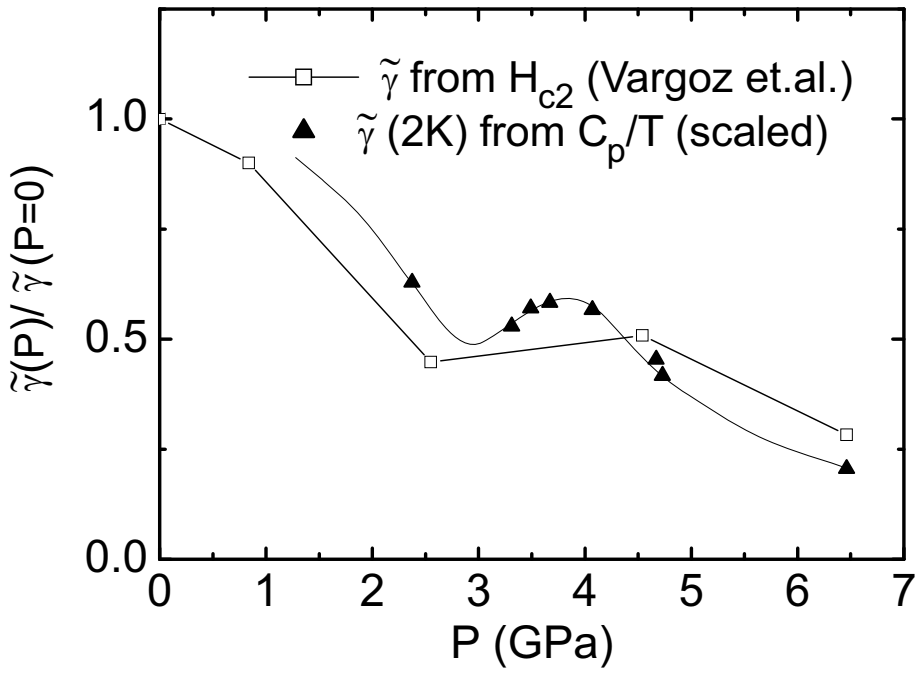

Figure 5.10: Estimate $\tilde{\gamma}(P)$ of the Sommerfeld coefficient from ac-calorimetry signal at 2 K (triangles), scaled for comparison with that deduced from H_{c2} measurements (squares).Vargoz et al. [1998] The noise on the calorimetry signal is smaller than the symbol size, however see text for a discussion of possible systematic errors.

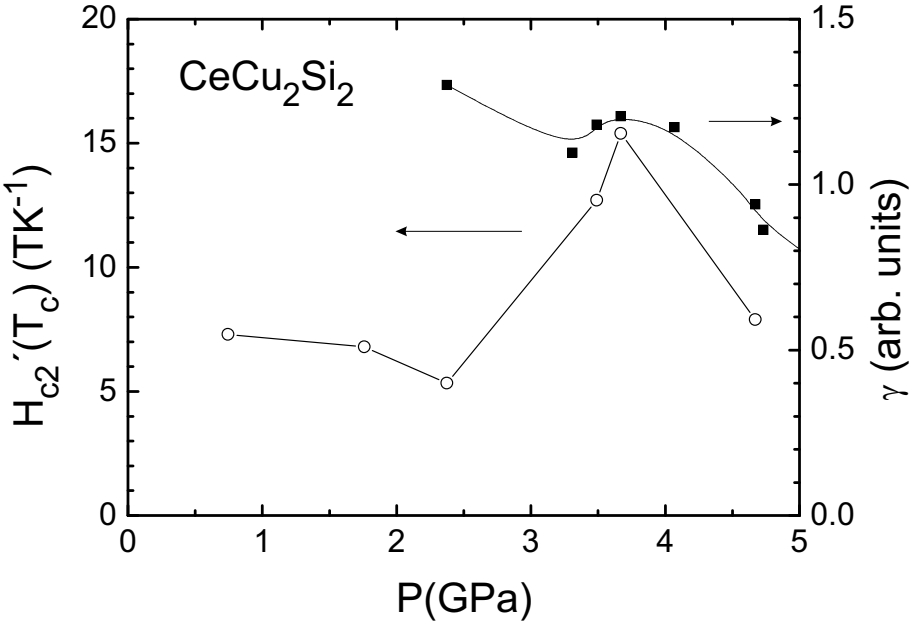

Figure 5.11: The initial slope of the upper critical field reflects the electronic effective mass, and it has a maximum coinciding with that in $\tilde{\gamma}(P)$.

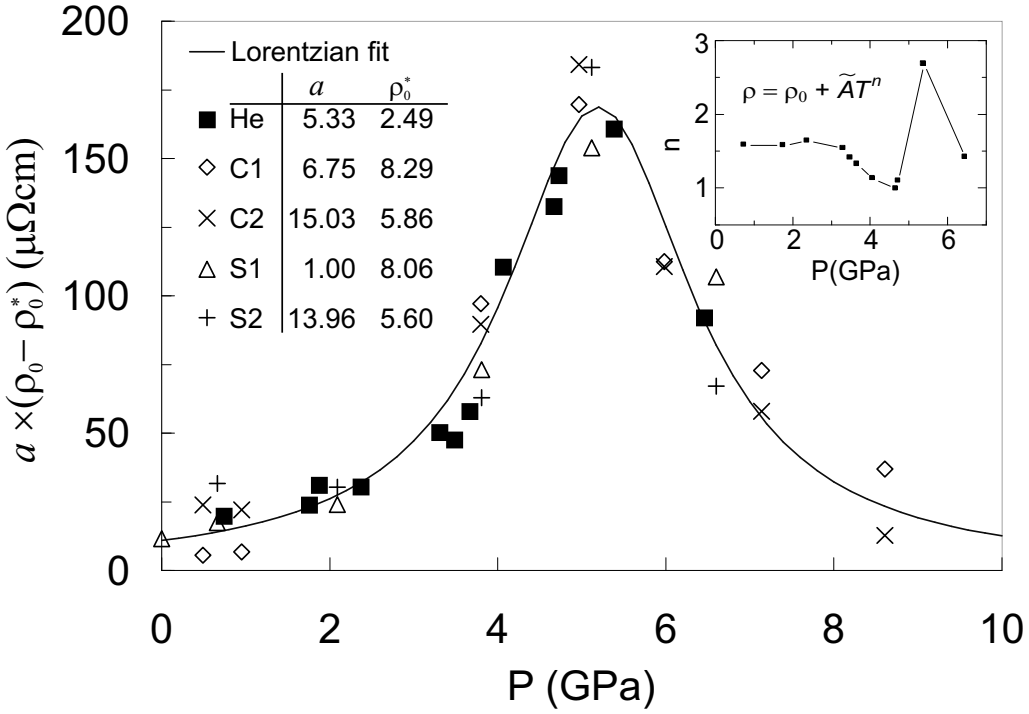

Figure 5.12: Enhancement of residual resistivity in several different $CeCu_2Si_2$ samples, scaled to a universal pressure dependence, with a and ρ_0^* being normalizing factors. The maximum in ρ_0 is at a pressure slightly higher than that corresponding to the maximum in T_c. The inset shows n for a fit of $\rho = \rho_0 + \tilde{A}T^n$. Filled squares indicate results from this work, the rest are reported in Ref. Vargoz [1998] (S and C refer to the original labels and are retained for continuity).

Fig. 5.12). A constant value ρ_0^*, different for each sample, is subtracted from ρ_0 at each pressure, and the result is multiplied by a scale factor, a (i.e. $\rho_0' = a(\rho_0 - \rho_o^*)$), so that all lie on the curve defined by sample S1, which has the highest residual resistivity (i.e. $a_{\mathrm{S1}} = 1$). The raw values of ρ_0 are plotted below in section 5.2.3.

According to the theoretical prediction, the residual resistivity ρ_0 is given in Miyake and Maebashi [2002] as

$$\rho_0 = B n_{\mathrm{imp}} |u(0)|^2 \ln \left| \left(-\frac{\partial n_{\mathrm{f}}}{\partial \epsilon_{\mathrm{f}}} \right)_{\mu} / N_{\mathrm{F}} \right| + \rho_0^{\mathrm{unit}}, \tag{5.3}$$

where the coefficient B depends on the band structure of host metals, n_{imp} is the concentration of impurities with moderate scattering potential $u(q)$ coming from disorder other than Ce ions, N_{F} is the density of states of quasiparticles around the Fermi level, and the last term represents the residual resistivity due to unitary scattering mainly arising from any deficit or defect of the Ce ions. The scaling behavior of ρ_0 shown in Fig. 5.12 would be possible if the universal form is given by $\ln |(-\partial n_{\mathrm{f}}/\partial \epsilon_{\mathrm{f}})_{\mu}/N_{\mathrm{F}}|$. It is an open question whether the observed Lorentzian form is indeed reproduced by Onishi and Miyake [2000b].

There is a striking correlation between the scaling factor a and the behavior of T_c. The sample measured in helium, reported here, and sample C1, pressurized in steatite, both have similar values of a, and both T_c^{onset} and $T_c^{R=0}$ agree over almost the entire pressure range. Sample S1, with the highest ρ_0 at P_{v}, has a lower T_c^{max} ($\simeq 1.2$ K), and the superconductivity disappears at a lower pressure. Samples C2 and S2 have scaling factors a around 14, and show a higher maximum T_c, with superconductivity extended over a greater pressure range than in the samples with larger residual resistivities. These differences between samples, both in ρ_0 and T_c, are vastly amplified from their appearance at ambient pressure. According to Eq. (5.3), the scaling factor a is proportional to the concentration of impurities. Our observations suggest therefore that these have a significant pair-breaking effect.

Non-Fermi liquid resisivity

The inset in Fig. 5.12 shows the result of a fit to $\rho = \rho_0 + \tilde{A}T^n$ between T_c and 4.2 K. There are two important points to note here. Firstly, at the pressure slightly higher than the maximum T_c, $\rho(T)$ is linear in T up to about 25 K. Secondly, the exponent appears surprisingly large ($n \simeq 2.7$) at the slightly higher pressure corresponding to the maximum ρ_0. This is difficult to understand without taking into account the resistivity due to impurity scattering. In sample S1, reported in Jaccard et al. [1998], the residual resistivity reaches $\sim 160\,\mu\Omega$cm at P_{v}, compared to a maximum of $35\,\mu\Omega$cm for the sample reported here. $\rho(T)$ then showed a falloff with temperature very similar to that of a Kondo impurity system (see later in this chapter for more examples of this behaviour). In other samples, this behavior is

hidden by the usual positive temperature dependence of the resistivity. Contrary to the usual situation, where the lowest ρ_0 possible is sought, this example shows how samples whose residual resistivities are large at ambient pressure can reveal interesting physics at high pressure. Even if a negative temperature dependence is not seen, the power-law fit to the resistivity is affected, deviating from the linear relationship predicted in Holmes et al. [2004b] and leading to anomalous values of n. At lower pressure, the $\tilde{A}$ coefficient is an order of magnitude larger, so (for example) almost linear resistivity is observed at the pressure corresponding to $T_c^{\max}$. Note that a quadratic temperature dependence of ρ was recovered at the lowest temperatures when superconductivity was suppressed by a magnetic field greater that H_{c2}.

A versus $T_1^{\max}$ - the crossover from a strongly to weakly correlated system

The normal state resistivity of heavy fermions can usually be understood in terms of the Kondo lattice model (Cox and Grewe [1988]). At high temperature the f-electron moments are localized and disordered, the resistivity is large and dominated by the scattering from spin disorder, with a characteristic $-\ln T$ slope. As the temperature is reduced, Kondo singlets form below a temperature T_K, and coherence effects in a periodic lattice cause the resistivity to drop below a maximum, at $T_1^{\max}$, which can be considered as proportional to T_K. For $T \ll T_K$ away from a critical point, Fermi-liquid-like behavior is recovered, with $\rho \sim AT^2$, where $A \propto T_K^{-2}$ and reflects the hugely enhanced effective mass caused by interactions between the f-electrons. In a real system where T_K is not too large, a second peak in the resistivity occurs at $T_2^{\max} > T_1^{\max}$, due to the crystalline electric field (CEF) effect (Cornut and Coqblin [1972]; Yamada et al. [1984]) (see inset of Fig. 5.13). The low temperature behavior then reflects the characteristics of the lowest CEF-split f-level. When pressure is applied, $T_2^{\max}$ remains fairly constant, while T_K rapidly increases, seen via the rise in $T_1^{\max}$. When $T_K > \Delta_{\rm CEF}$ ($\Delta_{\rm CEF}$ is the CEF splitting between the ground and excited states) the full 6-fold degeneracy of the J=5/2 $4f^1$ multiplet is recovered, even at the lowest temperatures. As a result the resistivity maxima at $T_1^{\max}$ and $T_2^{\max}$ merge into a single peak (Jaccard et al. [1999]). Similar behavior in the magnetic component of the resistivity is found in all Ce compounds studied [such as $CeCu_5Au$ (Wilhelm et al. [2000]), $CePd_2Si_2$ (Demuer et al. [2002]), $CePd_2Ge_2$ (Wilhelm and Jaccard [2002])].

In Fig. 5.13 the A vs $T_1^{\max}$ scaling is explored in both $CeCu_2Si_2$ and $CeCu_2Ge_2$. The value of A was determined from the slope of the normal state resistivity versus T^2, despite the non-Fermi liquid behavior shown in the inset of Fig. 5.12. However, if one allows the exponent n to vary between 1 and 2, the resulting coefficient will not vary more than a factor of two, which is within the scatter of the data. There are two regions where the predicted $A \propto (T_1^{\max})^{-2}$ relationship is followed, separated by an abrupt drop in A of over an order of magnitude. The collapse of A seems closely connected with the enhancement of superconductivity, it is at the start of

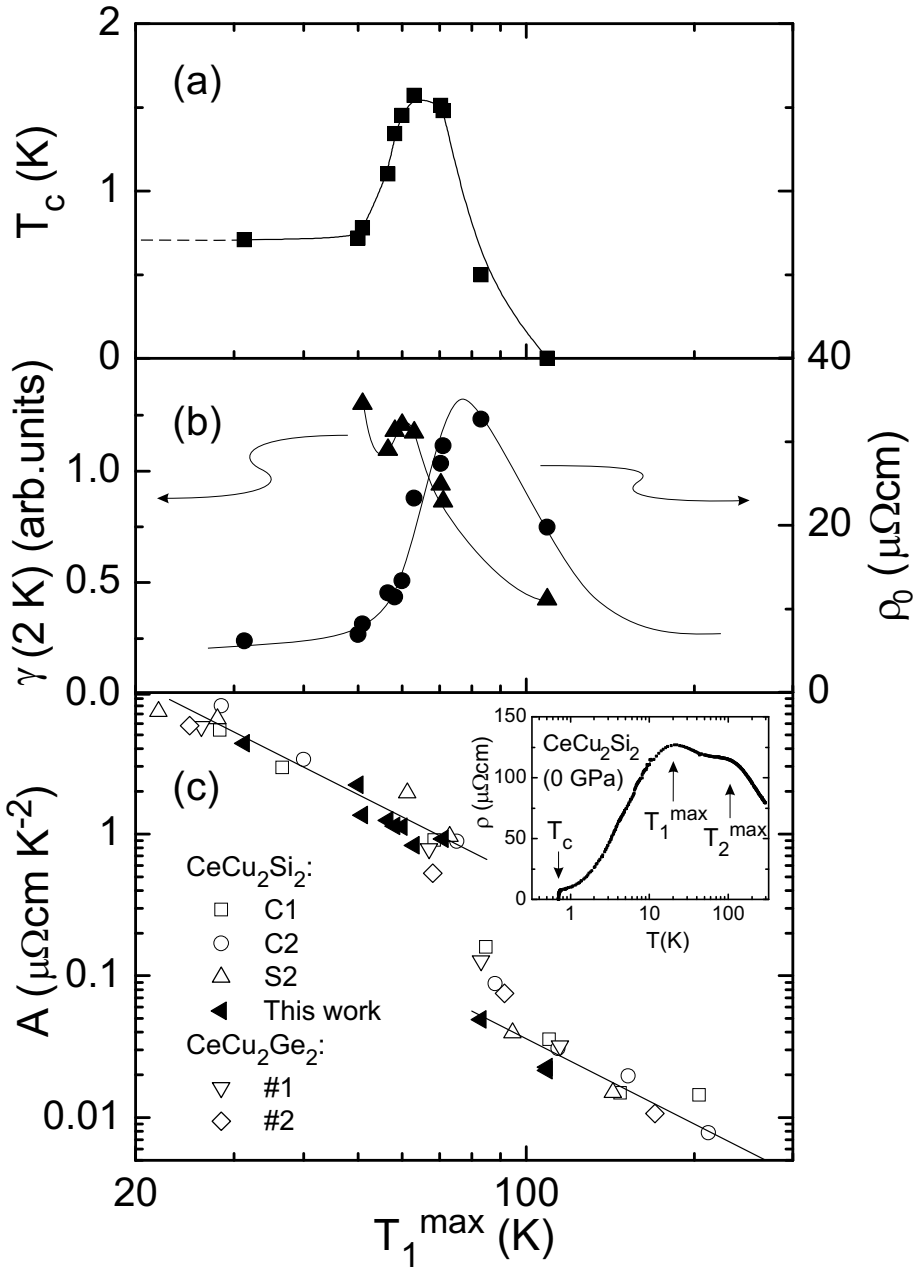

Figure 5.13: Plotted against $T_1^{\max}$ (defined in inset), a measure of the characteristic energy scale of the system, are (a) the bulk superconducting transition temperature, (b) the residual resistivity and estimate $\tilde{\gamma}$ of the Sommerfeld coefficient, and (c) the coefficient A of the $\rho \sim AT^2$ law of resistivity, including data from $CeCu_2Ge_2$. Note the straight lines where the expected $A \propto (T_1^{\max})^{-2}$ scaling is followed. The maximum of T_c coincides with the start of the region where the scaling relation is broken, while the maximum in residual resistivity is situated in the middle of the collapse in A. Pressure increases towards the right-hand side of the scale (high $T_1^{\max}$).

this drop that T_c has maximum, and the superconductivity has disappeared by the point where the $A \propto (T_1^{\max})^{-2}$ scaling is recovered. The residual resistivity however, peaks at around the midpoint of the drop in A, and this is the point where P_v is defined.

Summary of Helium cell results

By careful measurement of the resistivity and semi-quantitative measurement of the specific heat of $CeCu_2Si_2$ in ideal pressure conditions, we have been able to link superconductivity to a variety of other anomalies. These are all found around the pressure corresponding to an abrupt delocalisation of the Ce $4f$ electron. This can be interpreted in terms of a new type of quantum critical point, at a pressure $P_v \simeq 4.5$ GPa, where the fluctuating ground states are based on $4f$ occupation number.

5.2.2 Bridgman cell #1 - four samples

The purpose of the next cell was to investigate Ishikawa's 'high T_c' and 'low T_c' samples, to see whether they were really two different phases of $CeCu_2Si_2$, and if their properties were consistent with our valence fluctuation model with two QCPs.

There is significant anisotropy in the ambient pressure properties of $CeCu_2Si_2$, depending on current direction relative to the c axis. Most notably the size of the resistance maximum at $T_1^{\max}$ compared to that at $T_2^{\max}$ and also, surprisingly, T_c. We therefore also measured two single crystal samples of A/S type $CeCu_2Si_2$, oriented perpendicularly relative to the current direction.

Experimental setup

This cell contained four samples, which will be referred to as Ishikawa #50, Ishikawa #57, A/S ($I \| c$), and A/S ($I \| a$). The first two samples were polycrystals. The A/S samples were monocrystals provided by the Dresden group. Their c-axis was placed perpendicular and parallel(?) to the axis of symmetry of the pressure cell respectively.

At ambient pressure, the values both of ρ_0 and T_c for Ishikawa's samples #50 and #57 agreed with his values.

Unfortunately, there were problems with the contacts, such that only one sample (Ishikawa #50) had true 4-point resistance measurements. The others all contained some contribution from either (a) the connection wires or (b) a small portion of another sample, where voltage contacts were shared.

In three cases, the resulting resistance measured was most probably the sum of the sample and a component typical of the metallic connection wires. It would be possible to subtract a linear term when presenting the results, but in order to do so one must assume quantities such as the residual resistivity, in whose variation with pressure we are interested. In order to avoid introducing more of my own ideas that the data merits, I prefer to present the raw data, multiplied solely by a geometrical factor, unless otherwise indicated.

Anisotropy of the Kondo resistance maxima

The measurements of A/S ($I\|c$), and A/S ($I\|a$) did not have full four-point resistance contacts, and so contained additional contributions from the measurement wires, but it was nevertheless clear that the low temperature resistivity maximum at $T_1^{\max}$ was considerably larger with $I\|a$ than with $I\|c$. The resistance peak at $T_2^{\max}$ was more or less identical, and when the two merged at high pressure, the resulting resistance curve was isotropic. This isotropy at high temperature reflects the the population of the higher crystal field split $4f$ states, and the higher symmetry when the system recovers the 4- or 6-fold degeneracy of the $4f$ multiplet.

T_c versus pressure

Despite the lack of four point resistance measurements in all but one, it was possible to identify T_c^{onset} in all the samples. Figure 5.14 shows this, compared with the results from the helium cell. The most surprising result is that three of the samples have at least partial superconducting transitions up to much higher pressure, while in one [A/S ($I\|c$)], T_c drops to zero in a similar manner to that in the helium cell. This implies that superconducting fluctuations, at the very least, can persist up to much higher pressure than was observed in He.

In Fig. 5.15, all four samples are shown at 7.07 GPa, with the partial transitions clearly visible in all but one.

Residual resistivity

While the resistance measured for each sample may contain an external contribution due to the three-point measurements, it is still possible to identify the enhancement of ρ_0. Fig. 5.16 shows the resistance (multiplied by the geometrical factor of each sample respectively) as a function of pressure. The monotonically decreasing additional term is evident, but it is also possible to see clearly that there is a much larger intrinsic impurity driven resistance peak at P_{v} in the Ishikawa #50 sample. This is also the sample identified as 'Low T_c', and indeed its T_c^{onset} is consistently lower

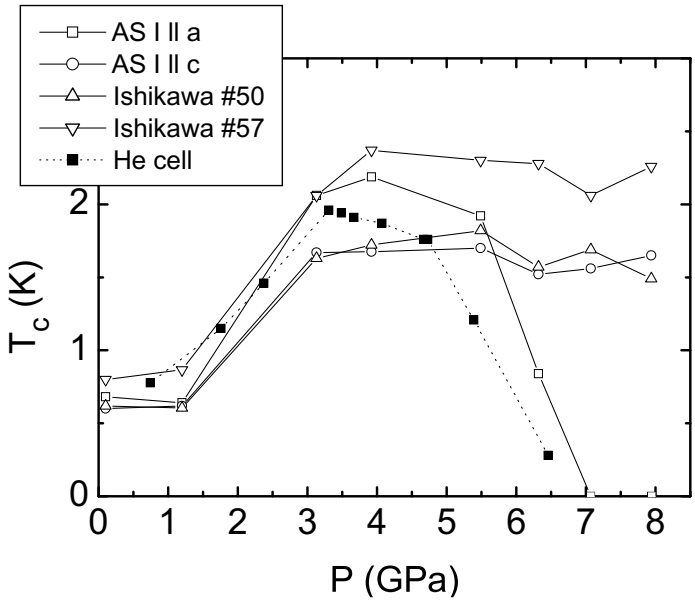

Figure 5.14: T_c^{onset} for the samples in Bridgman cell #1 compared with the result in helium. Samples #50 and #57 do behave as expected at low pressures, with diverging T_c, but both display an enhancement of superconductivity at high pressure. Samples #50 and #57 are unoriented polycrystals, and the current in the helium cell was in the basal plane.

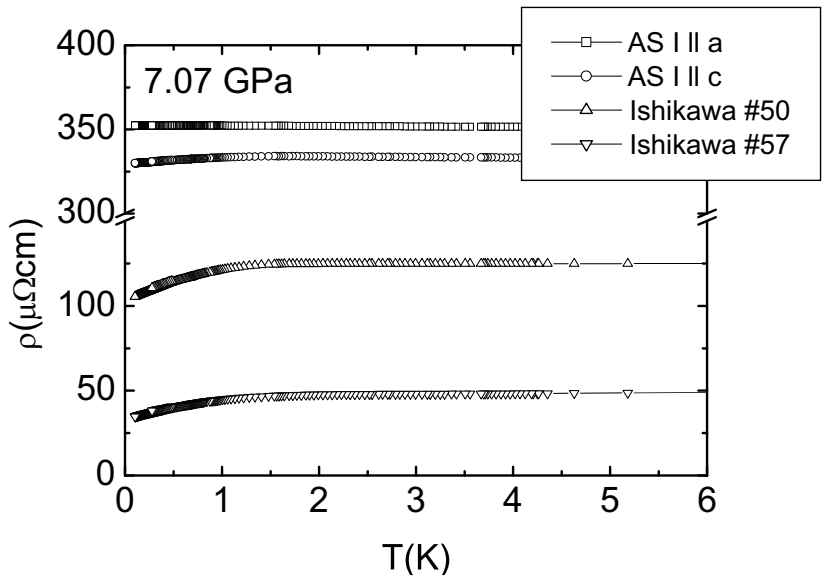

Figure 5.15: At 7GPa, the superconductivity in sample A/S ($I \| a$) has been supressed, but partial resistive transitions persist in the remaining samples. N.b. the resistivity shown contains a external contribution in all samples but #50.

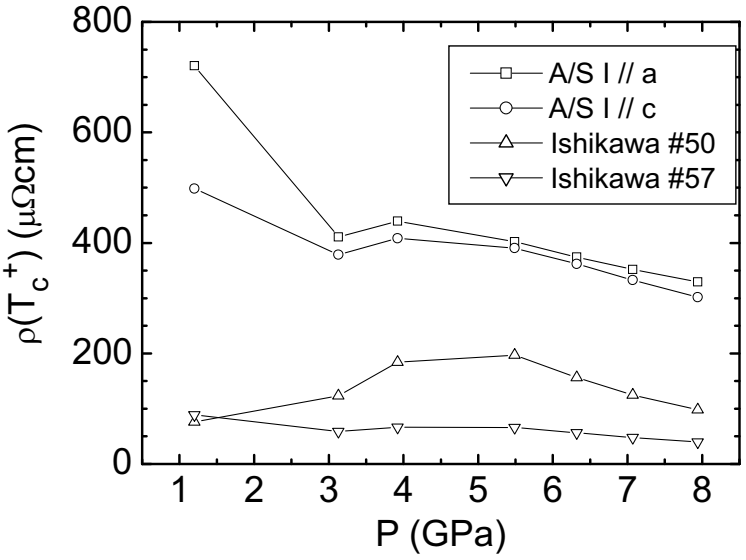

Figure 5.16: The normal state resistivity at T_c is close to the residual resistivity ρ_0. In this figure, one can see the enhancement of ρ_0 around P_v in all samples, superimposed on a monotonically decreasing additional term due to the lack of 4-point contacts in all but sample #50. Taking into account the background, one can still see that the ρ_0 peak in #50 is much larger than in #57, indicating a higher impurity concentration according to Eq. 5.3.

than that of sample #57, and initially decreases with pressure before increasing again around 2 GPa.

Magnetoresistance of enhanced impurity scattering around P_v

The low temperature resistivity of sample #50 at high pressure appears to be dominated by the enhanced impurity resistivity. Vargoz [1998] showed that the low temperature impurity enhanced peak had a negative magnetoresistance, and this is confirmed at 5.49 GPa (Fig. 5.17) where sample #50 has a small but measurable negative magnetoresistance, while the change in resistance with field measured for the other samples is positive. In the framework of valence fluctuation theory, it might be that the Zeeman shift of the f level means that the system moves away from P_v, and the enhancement of impurity scattering is reduced.

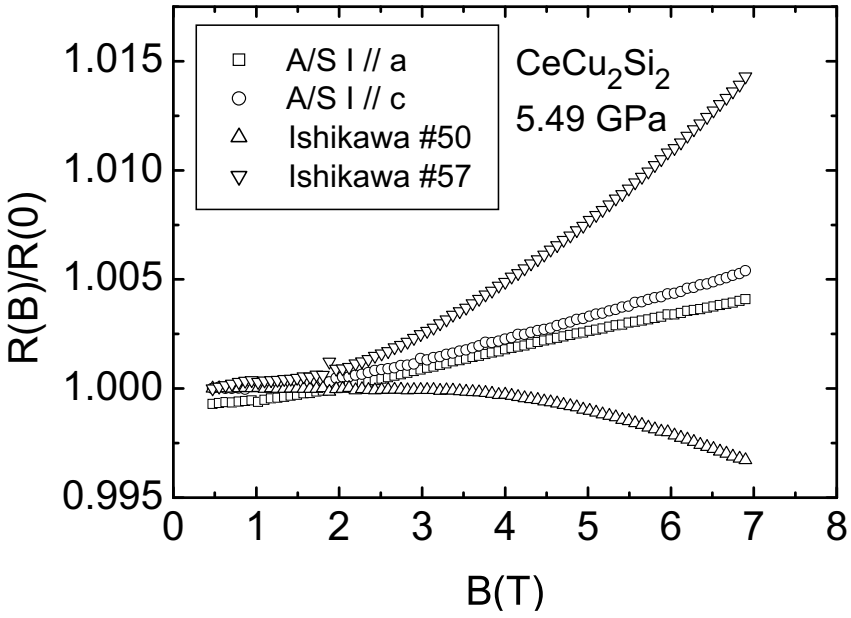

Figure 5.17: Magnetoresistance close to the maximum of ρ_0. In sample #50, the measured signal is due only to the sample. It has the largest enhanced impurity contribution to ρ_0 and has a negative magnetoresistance at 5.49 GPa.

Summary

In the second series of experiments, we examined the 'high-T_c' and 'low-T_c' types of $CeCu_2Si_2$, and also investigated the effect of current orientation relative to the crystal axes.

Thanks to the huge enhancement of impurity scattering around the valence transition, we can conclude that the 'high-T_c' and 'low-T_c' samples have very different impurity concentrations. Yuan et al. [2003b] showed that the superconducting region can be split into two pockets surrounding P_c and P_v if the impurity concentration is large enough, so the initially decreasing T_c in the latter sample may reflect the beginning of that process. Other than a small but significant difference in T_c the two samples behaved similarly over a large pressure range.

The principle difference between resistance measured with the current parallel and perpendicular to the c-axis is that the lower Kondo peak at T_1^{max} is considerably larger for $I \| a$ than $I \| c$. above P_v, where a single maximum is observed, the resistivity is isotropic.

There also appears to be a systematic difference in T_c for different current directions, a rather surprising result. The Ishikawa samples were unoriented, so the value of T_c^{onset} measured will reflect the largest critical temperature present in an inhomogeneous state.

5.2.3 Bridgman cell #2 - the role of uniaxial strain

Current direction is not the only symmetry-breaking condition in the cell. We know from experiments on $CePd_2Si_2$ (Demuer et al. [2002]) that there is a non-negligible uniaxial strain in a steatite pressure medium, which can have a significant effect on the superconducting properties.

Under pressure, it is difficult to know whether the differences in behaviour result from the relative orientations of the crystal axes with respect to (a) current, or (b) any uniaxial stresses present in the cell. The following section addresses this question, at least in part.

Experimental setup

Fig. 5.18 shows the cell used to investigate the effect of uniaxial stresses on two samples of A/S type $CeCu_2Si_2$, both cut from the same monocrystalline sample from the Dresden group. The solid pressure medium in Bridgman anvil cells leads to small deviations from true hydrostaticity. Previous experiments on $CePd_2Si_2$, Demuer et al. [2002], have shown that this can have a dramatic effect on the superconducting and normal state properties of heavy fermions. In that compound, it was found that

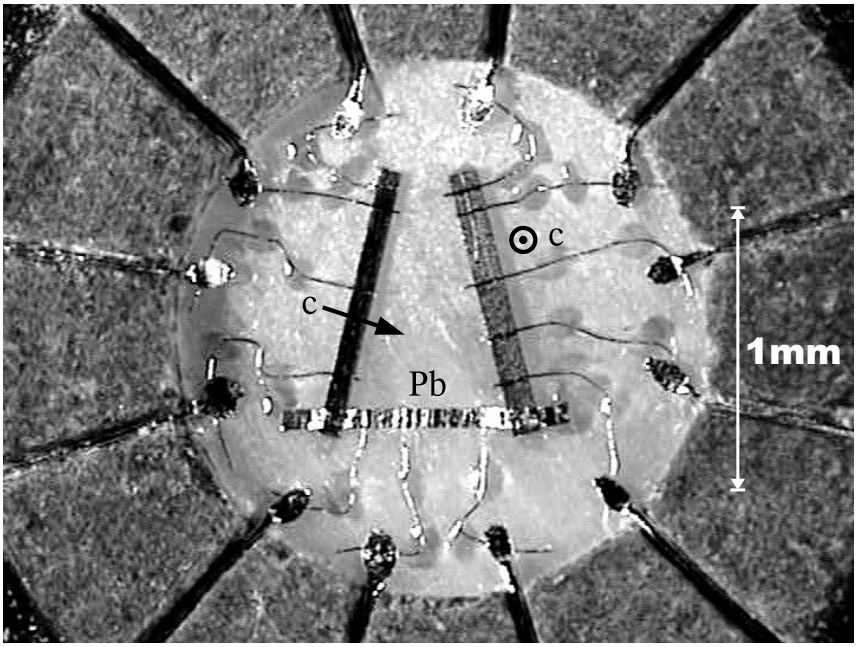

Figure 5.18: Bridgman cell #2. The two A/S type $CeCu_2Si_2$ samples are oriented with their c axis parallel and perpendicular respectively to the cell axis. The measurement current passes through the samples and the lead manometer in series, and its direction is in the basal plane in both samples. Multiple contacts enabled two or three independent voltage measurements to be made on each sample.

the critical pressure P_c was shifted relative to the hydrostatic case, the pressure domain of superconductivity was extended considerably, and the superconducting transition temperature T_c was raised by 40%.

In this experiment, the samples were cut from neighbouring positions in the same A/S sample used in the previous cell. The extension of T_c^{onset} to much higher pressures in three of the four samples prompted us to investigate this systematically. The samples and cell were prepared by D. Jaccard. The samples were oriented such that the current was always in the basal plane, but the c-axis was oriented parallel and perpendicular to the axis of the cell. We shall label these ($\sigma \| c$)and ($\sigma \perp c$)respectively. They had dimensions ($988 \times 109 \times 25 \mu\text{m}^3$) and ($988 \times 73 \times 23 \mu\text{m}^3$) respectively, with the smallest dimension parallel to the cell axis.

After the cell was pressurised, there appeared to be no problems with the contacts. The resistance for each sample was a full four point measurement, and the resistivity was obtained using a form factor derived from the sample geometry, with no further normalisation. The absolute values of ρ are therefore correct to within 10%, and indeed at the lowest pressure we found excellent agreement with a preliminary run at ambient pressure.

Resistivity at high temperature

Figure 5.19 shows the resistivity measured in the two samples over the entire temperature range. Note the three main differences: $\rho(\sigma \perp c)$ is larger that $\rho(\sigma \| c)$, though this may possibly be explained by an error in the form factor; the low temperature peak $T_1^{\max}$ merges with the second peak at $T_2^{\max}$ faster in sample ($\sigma \| c$)than ($\sigma \perp c$); finally the shape of the superconducting transitions are very different.

Superconducting transitions

Fig. 5.20 shows the resistive transitions in the two samples as the pressure is increased. It is rather difficult to draw general conclusions, however there are a few significant features which differ considerably between the two samples at the same pressure: the width of the transition, i.e. $T_c^{\text{onset}} - T_c^{R=0}$; the 'kinkiness' of the transition, i.e. discontinuities in the slope of the resistance curve; and precursor signs well above the main resistance drop (this could perhaps be parameterised by e.g. $T_c^{\text{onset}} - T_c^{10\%}$).

As we had several voltage contacts, it was possible to follow the resistive transitions in different parts of the same sample. There were some small differences, mostly in the low-temperature tail of the transition, but in general, the shape of the transition within a given sample was constant.

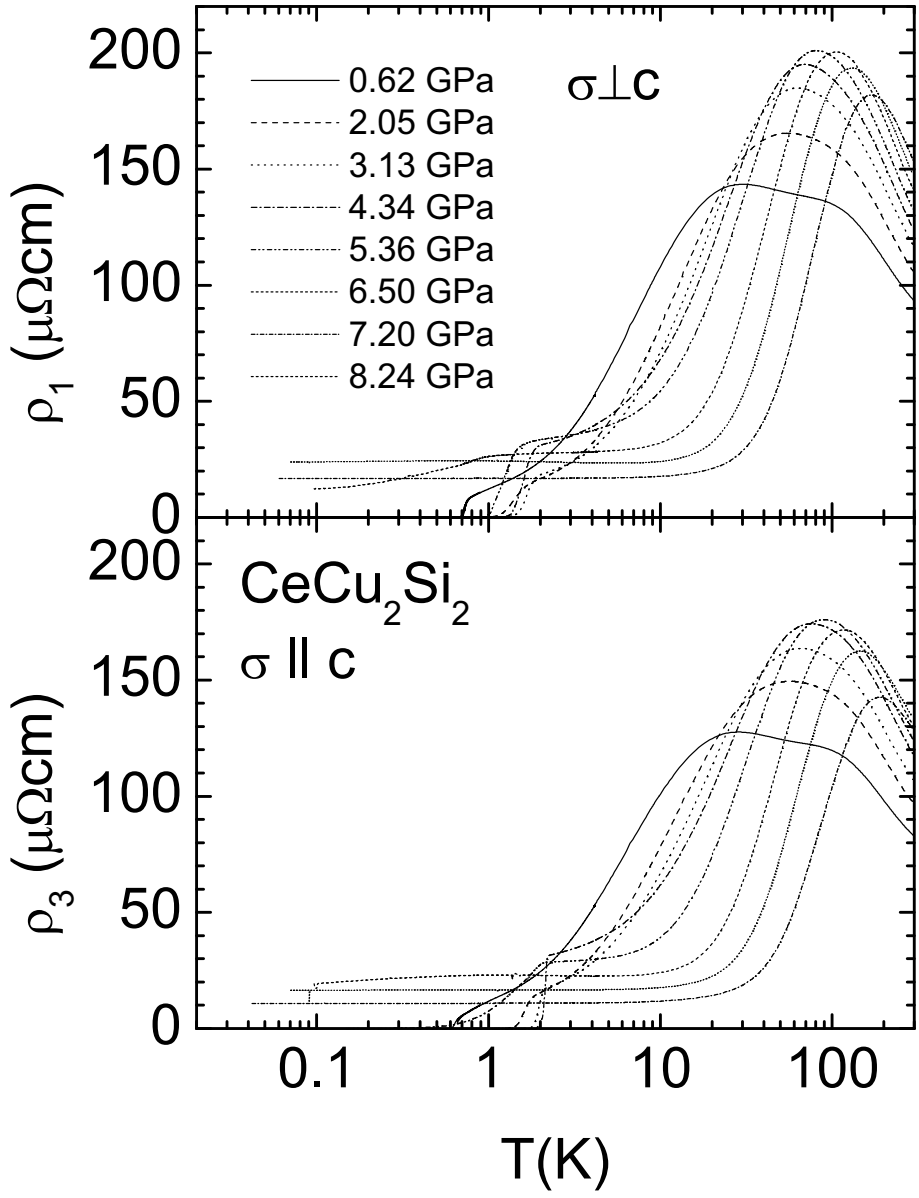

Figure 5.19: Resistivity of $CeCu_2Si_2$ single crystals pressurised in a steatite medium with the c axis oriented perpendicular ($(\sigma \perp c)$, top) and parallel ($(\sigma \| c)$, bottom) to the cell axis. The normal state shows two main differences. $\rho(\sigma \perp c)$ is larger that $\rho(\sigma \| c)$, and the low temperature peak at $T_1^{\max}$ disappears faster in sample $(\sigma \| c)$ than $(\sigma \perp c)$.

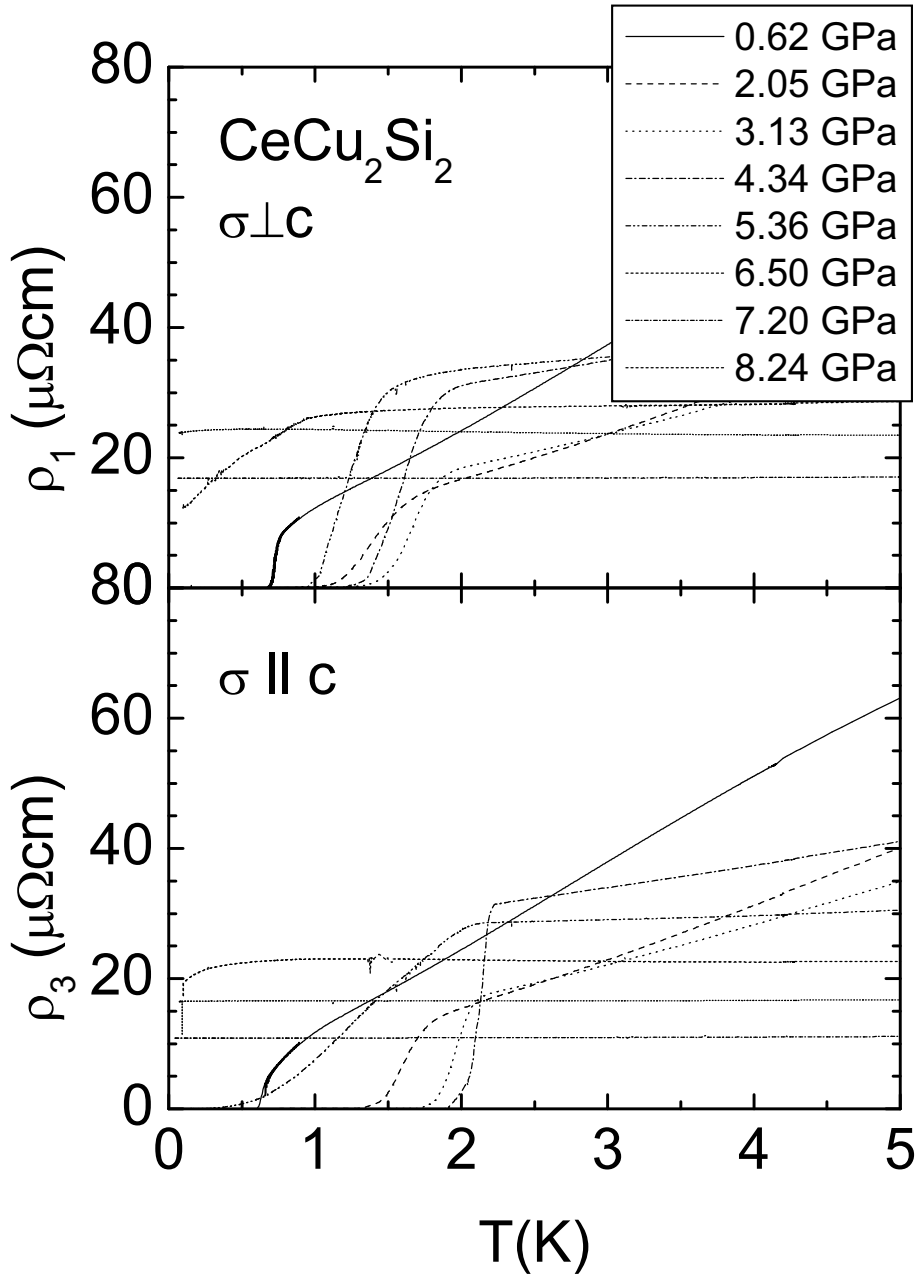

Figure 5.20: Superconducting transitions in the orthogonally oriented $CeCu_2Si_2$ samples. There are significant differences in the both the shape and the transition temperature of the two samples.

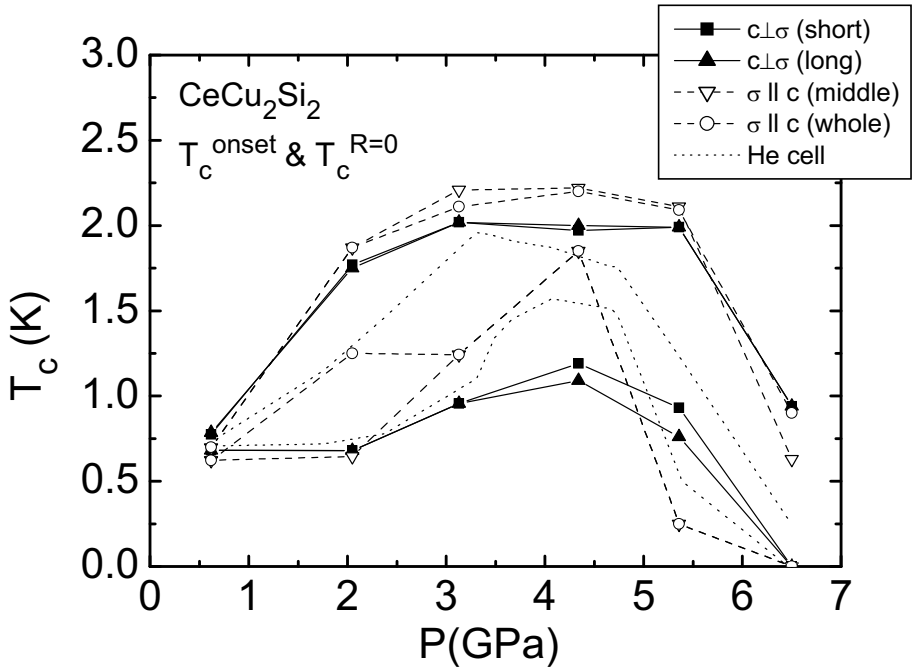

Figure 5.21: Onset T_c^{onset} and completion $T_c^{R=0}$ temperatures of the superconducting transition in $CeCu_2Si_2$ samples ($\sigma \| c$) (empty), ($\sigma \perp c$) (filled) and that measured in the helium cell (no symbol). The two sets of data for the former samples represent T_c extracted from the measurements of the entire sample length, and of a subset of that length.

T_c versus pressure

The evolution of T_c^{onset} and $T_c^{R=0}$ in the two samples is plotted in Fig. 5.21. We had two sets of voltage contacts on each sample, so T_c values extracted from both are shown, allowing the intra- and inter-sample differences to be clearly identified. Results from the helium cell are also plotted for comparison.

While it is difficult again to draw general conclusions, it is clear that in sample ($\sigma \| c$), the maximum T_c obtained is noticeably larger than in the ($\sigma \perp c$) sample, and the differences are largest around this maximum.

Comparing T_c^{onset} with the previous results, the extension of the superconducting domain to much higher pressures is not reproduced in this experiment, indeed both samples appear to closely follow the values of T_c^{onset} found in the sample A/S($I \| a$). This could be due to two reasons, one more heretical than the other. First, the uniaxial strain may have been much larger in the previous cell, due to differences in the cell construction (more care was taken to ensure a proper filling with steatite in the latter experiment). If this is indeed the sole cause of the enhanced T_c then that may explain the difference between the two experiments. The other possibility would be that T_c^{onset} depends on the current direction! This is not entirely inconceivable given

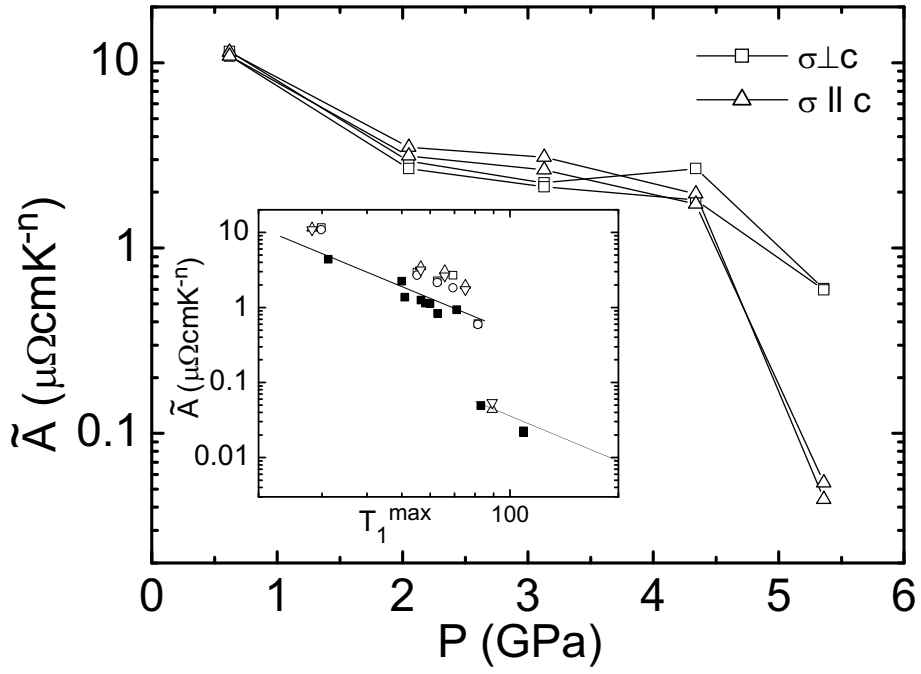

Figure 5.22: The temperature coefficient $\tilde{A}$ drops sooner in sample ($\sigma \| c$), going from a strongly correlated to a weakly correlated regime at a lower pressure. The inset shows $\tilde{A}$ vs. $T_1^{\max}$, with the filled symbols being the quadratic A coefficient from the helium cell results.

the highly local, and perhaps directional nature of the proposed pairing mechanism.

Shift of P_v with uniaxial strain

While the T_c results are rather difficult to interpret, the normal state properties show more clearly the principal conclusion of this experiment. The main effect of uniaxial stress appears to be a shift of P_v, with the valence instability found at a higher pressure in ($\sigma \perp c$) than in ($\sigma \| c$).

In section 5.1.4, it was noted that the A coefficient of the T^2 resistivity law depends strongly on n_f. We can identify a sudden drop in A, and indeed $\tilde{A}$ (where the resistivity exponent is less than two) with a departure from a $4f^1$ regime.

In Fig. 5.22 it is clear that the abrupt change in the $\tilde{A}$ coefficient occurs at a lower pressure in ($\sigma \| c$) than ($\sigma \perp c$), with the latter being an order of magnitude larger at 5.4 GPa than the former. Sample ($\sigma \| c$) is therefore further along the path to a weakly correlated system for a given pressure than ($\sigma \perp c$). Following the same analysis of the results from the helium cell (though with $\tilde{A}T^n$ rather than AT^2), plotting $\tilde{A}$ against $T_1^{\max}$ (inset of Fig. 5.22) shows that the two samples are indeed in keeping with the general scheme shown in Fig. 5.13.

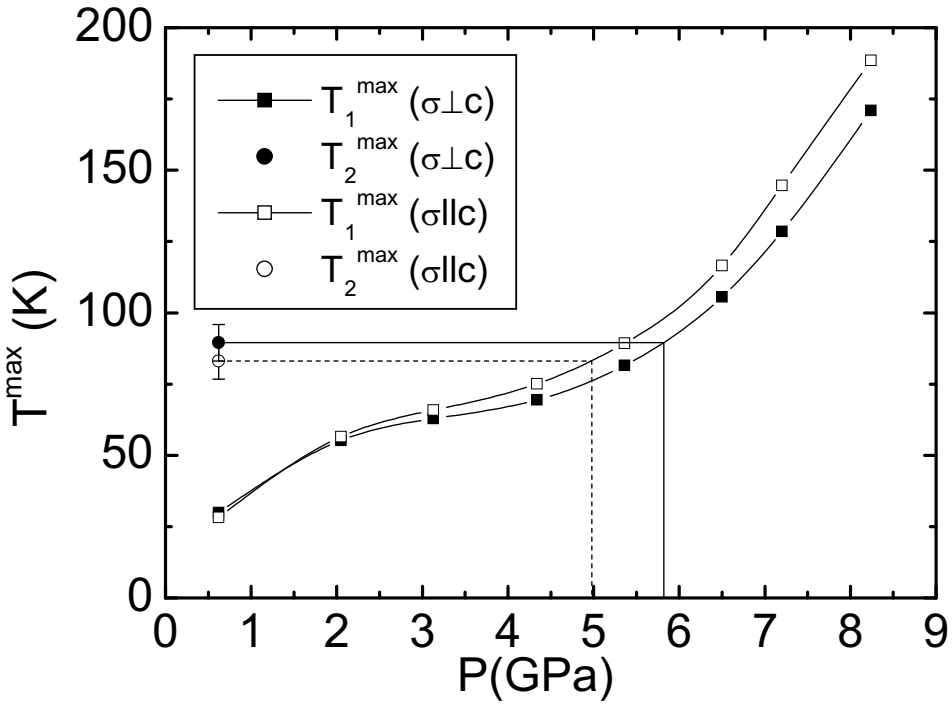

Figure 5.23: The lower Kondo resistance maximum evolves rapidly with pressure, and merges at P_v with the second peak corresponding to excited the crystal-field split f-states. The pressure at which this occurs reflects the same shift of P_v seen in other properties.

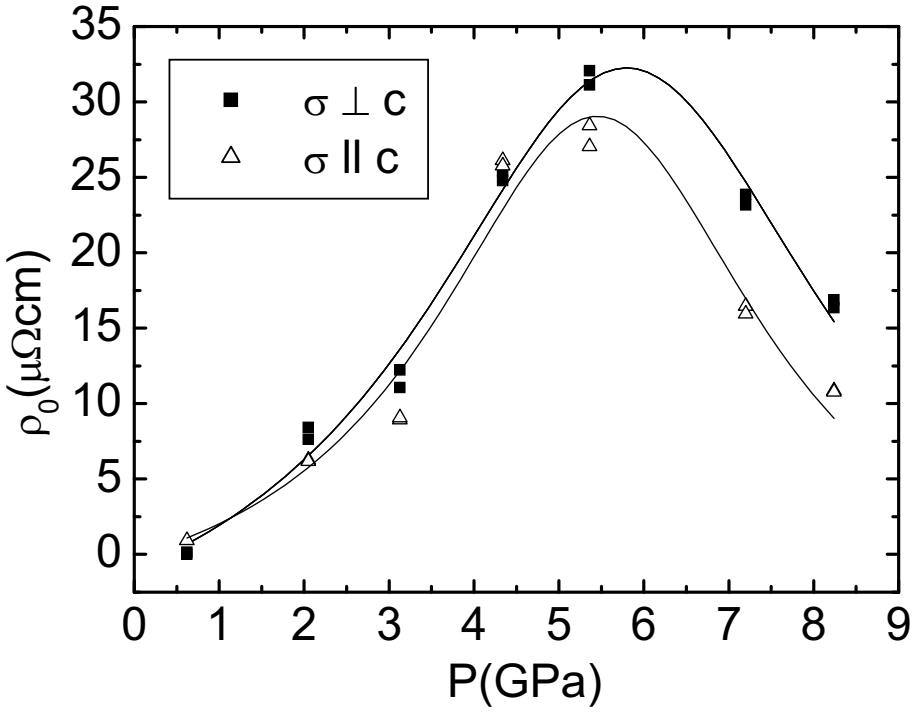

Figure 5.24: Residual resistivity versus pressure in samples ($\sigma \| c$) and ($\sigma \perp c$). The maximum in the enhanced residual resitivity is shifted to a higher pressure in ($\sigma \perp c$), indicating that the valence instability occurs at a higher pressure.

We can empirically identify P_v with the merger of T_1^{max} and T_2^{max}. At this point the Kondo broadening of the ground state f-level becomes larger than the crystal field splitting, and the full 6-fold degeneracy is recovered.

The pressure evolution of T_1^{max} is show in Fig. 5.23, where we see T_1^{max} in the two samples diverging slowly with pressure, and merging with T_2^{max} at a pressure corresponding to the respective P_v's, with slightly less than a 1 GPa separation. The merging points are found at 4.98 and 5.82 GPa for the two samples, with an uncertainty of around 0.5 GPa on both.

In section 6 we identified P_v by the maximum of ρ_0, and this is perhaps the most direct way to track the effect of uniaxial stress. In Fig. 5.24, the shift of P_v is clearest if we fit a Lorentzian to the two sets of data, following the universal form identified above. There is a difference of 0.3 ± 0.1 GPa in the position of their maxima, with that of ($\sigma \perp c$) at the higher pressure, concurring with the inference from Figs. 5.22 and 5.23.

Below P_v, the resistivity increases rapidly with temperature, and any temperature dependence in the enhanced impurity scattering is obscured. However after the steep drop in A across P_v, a negative temperature dependence is revealed in certain

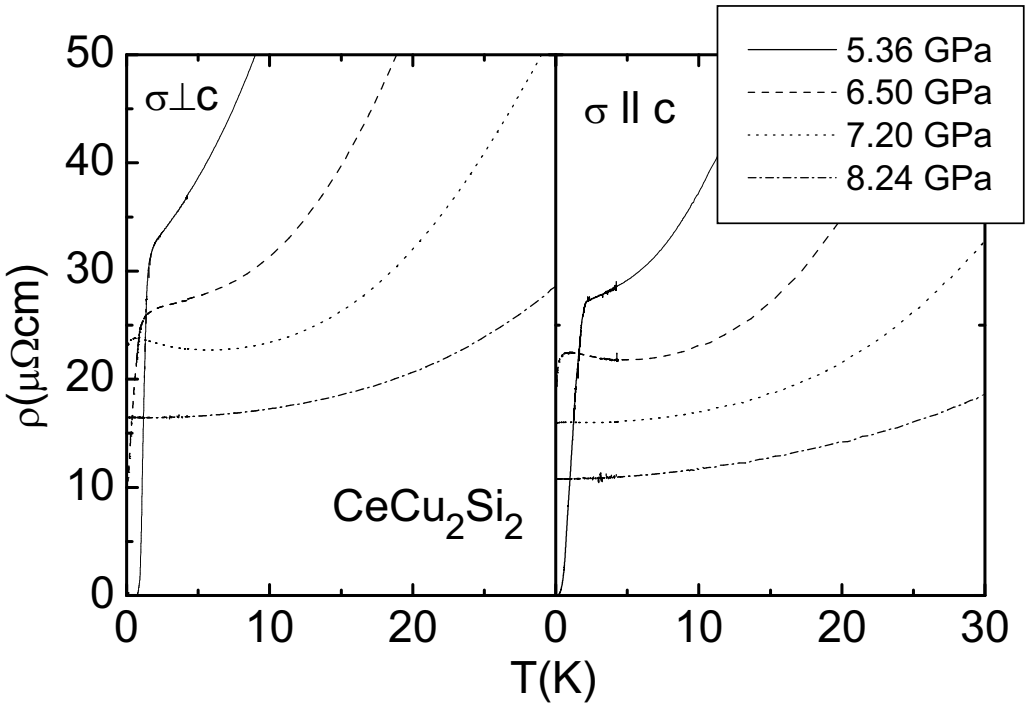

Figure 5.25: At pressures above P_v, the quasiparticle-quasiparticle scattering term becomes small enough to observe a negative temperature dependence at low temperature, associated with the enhanced impurity scattering. This also means that power-law fits cannot be accurately determined in these conditions.

samples. Vargoz [1998] fitted this to a Kondo impurity term at low temperature, and it may be that clusters of Ce^{3+} ions remain in a largely Ce^{4+} lattice, and these are responsible for Kondo-like scattering.

Fig. 5.25 shows the low-T maximum which appears in samples with sufficiently high ρ_0 at pressures beyond P_v. This was observed by Vargoz [1998], and Aliev et al. [1982] who attributed it to Kondo impurity-type scattering from remaining Ce^{3+} ions at high pressure. We note that in contrast to a simple Kondo impurity scenario, there can be a further downturn in resistance as $T \to 0$, reminiscent of the onset of coherence in the Kondo lattice system.

5.3 Discussion

In this chapter I have argued that the superconductivity at high pressure in $CeCu_2Si_2$ is mediated by a new mechanism involving the exchange of critical valence fluctuations. The relationship between valence instability and superconductivity was proposed as far back as 1984 (Bellarbi et al. [1984]), and a theoretical model put forward in 1998 (Miyake et al. [1999]). The results presented above tie these together, and show that there exist a variety of experimental signatures, connected with the high pressure superconducting region, which can be understood to be the result of rapid valence change accompanied by critical fluctuations between nearly degenerate $4f^1$ and $4f^0$ ground states.

One should not lightly claim the existence of a new mechanism of superconductivity, and if we are to accept that the high-pressure behaviour in $CeCu_2Si_2$ is genuinely due to a new phenomenon, we must first be exceptionally sure of our experimental evidence, and secondly that a valence fluctuation scenario really does offer the best possible explanation.

The success of a relatively simple theoretical model in predicting a wide variety of observations is persuasive. The addition of an f-c Coulomb repulsion term to the periodic Anderson Hamiltonian is physically reasonable, and as I explain in section 2.3.5, it can lead to an intuitive understanding of the microscopic mechanism.

There are a number of observations which fall outside the direct scope of the model proposed by Miyake, and I will discuss how they qualitatively fit into a valence-fluctuation scenario, with reference to a complementary phenomenological theory proposed by Monthoux and Lonzarich.

If we do accept the existence of valence-fluctuation mediated superconductivity, its properties are highly unusual and intimately linked with the weakly first order nature of the valence transition, and also with the local environment of the Ce atoms. The results from the Bridgman experiments will be discussed in the light of this.

Interpretation of ac calorimetry results

The helium pressure medium used in the DAC provided ideal hydrostatic pressure conditions. However, the ac calorimetry technique had not previously been used with He under pressure down to such a low temperature. Our calorimetric results in such extreme conditions therefore deserve some discussion.

In particular there appears to be a considerable increase in the specific heat jump at the superconducting transition when P_v is approached. A very large specific heat peak at T_c would be strongly reminiscent of the huge jump found in $CeCoIn_5$, where $\left.\frac{\Delta C_P}{\gamma T}\right|_{T_c} \sim 5$ at ambient pressure (Petrovic et al. [2001]). It is therefore a legitimate question to ask how much the results of the uncalibrated ac calorimetry technique under pressure can be relied on to give an accurate measurement of the specific heat.

The superconducting transition observed corresponds to $\sim 100\%$ of the signal amplitude, and two different methods of extracting C_P from the calorimetry signal give essentially the same result. It therefore seems reasonable to accept our results as a good first approximation to C_P, to within a constant scaling factor, and with an unknown but relatively small component due to addenda.

Furthermore, the apparent anomaly in the normal state specific heat shown in Fig. 5.10 was measured at a fixed temperature and frequency above the superconducting transition, with pressure the only independent variable. The small peak in γ is consistent with the maximum in the initial slope of the upper critical field observed at the same pressure, though the interpretation of the latter depends on whether the sample can be considered to be in the clean or dirty limit, or somewhere in between.

The merging of $T_1^{\max}$ and $T_2^{\max}$ and T_K vs. Δ_{CEF}

Miyake's theoretical model does not consider more than a single f-level, while the crystal field splitting is an inherently multi-channel phenomenon. The merging of the two Kondo resistance maxima seems however to be a general feature at P_v in compounds where a critical valence transition is thought to exist. It can be understood as follows:[2]

The so-called Kondo temperature T_K, related to $T_i^{\max}$ $(i = 1, 2)$, depends crucially on the degeneracy $(2\ell + 1)$ of the local f-state. Above $T_2^{\max}$, the first excited CEF level is partially occupied, and the effective Kondo temperature reflects the degeneracy of both the ground state and first excited state.

The lowest f-level itself is also broadened by the Kondo effect – mixing with the conduction band means that f electrons have a finite lifetime – so the effective

[2]Thanks to K. Miyake for this explanation.

degeneracy can be affected by the higher CEF levels.

$T_K \sim D\exp[-1/(2\ell+1)\rho_F|J|]$, where D is the bandwidth of conduction electrons, ρ_F the density of states of conduction electrons at the Fermi level, and J the c-f exchange coupling constant (Okada and Yosida [1973]). Even though the 6-fold degeneracy of the $4f$-state is lifted by the CEF effect, leaving the Kramers doublet ground state and excited CEF levels with excitation energy Δ_{CEF}, the Kondo temperature T_K is still enhanced considerably by the effect of the excited CEF levels (Yamada et al. [1984]).

The technical degeneracy relevant to the Kondo effect is affected by the broadening ΔE of the lowest CEF level. If $\Delta E \ll \Delta_{CEF}$, the degeneracy relevant to T_K is 2-fold. On the other hand, if $\Delta E > \Delta_{CEF}$, it increases to 4- or 6-fold. The level broadening is given by $\Delta E \simeq z\pi\rho_F|V|^2$ where $|V|$ is the strength of c-f hybridization, and z is the renormalization factor which gives the inverse of mass enhancement in the case of a lattice system. It is crucial that ΔE is very sensitive to the valence of Ce ion because z is essentially given by q [Eq. (5.1)]. In particular, the factor z increases from a tiny value in the Kondo regime, $z \sim (1-n_f) \ll 1$, and approaches unity in the so-called valence fluctuation regime.

Since the factor $\pi\rho_F|V|^2 \gg \Delta_{CEF}$ in general for Ce-based heavy electron systems, the ratio $\Delta E/\Delta_{CEF}$, which is much smaller than 1 in the Kondo regime, greatly exceeds 1 across the valence transformation around $P \sim P_v$, leading to the increase of the technical degeneracy of f-state, *irrespective* of the sharpness of the valence transformation. Therefore, T_1^{max} should merge with T_2^{max}, which corresponds to 4- or 6-fold degeneracy of $4f$-state due to the effect of finite temperature, i.e., $T \sim \Delta_{CEF}$. This may be the reason why T_1^{max} increases and approaches T_2^{max} at pressure where T_c exhibits the maximum, and the KW ratio changes between strongly and weakly correlated classes.

Theory versus experiment

While the experimental picture of $CeCu_2Si_2$ presented here is further advanced than the theoretical, a large number of the features found around P_v, in addition to superconductivity, follow directly from the valence fluctuation approach and the addition of a U_{fc} term to the Hamiltonian. The linear resistivity is explained in chapter two, as is the local maximum in the electronic specific heat, the latter due to the renormalisation of the effective mass by valence fluctuations, superimposed on an overall decrease with pressure. The enhancement of the residual resistivity at low temperature follows from the renormalisation of impurity potentials by valence fluctuations.

The relative positions of the peaks in T_c, γ, and ρ_0 can be compared with Fig. 2.1. If ε_f is considered to be a smooth function of pressure, P_v corresponds to the maximum valence susceptibility $-\partial n_f/\partial\varepsilon_f$. This is where ρ_0 has a maximum, while the peak

in T_c is at slightly lower pressure, and the observed maximum in γ is also shifted below P_v by the background trend towards a weakly correlated system with a low effective mass. For a more precise comparison more detailed calculation would be needed, but our observations are consistent with the valence fluctuation scenario.

The enhanced residual resistivity can be understood as the nucleation of a large number $4f^0$ Ce atoms around a single impurity. Any similar nucleation phenomenon would be associated with a first-order transition, so this observation is difficult to explain in a purely magnetic scenario, where the QCP is usually assumed to be 2^{nd} order. The linear resistivity observed in $CeCu_2Si_2$ around P_v is also difficult to explain in a three dimensional system such as $CeCu_2Si_2$.

Another possible explanation for the enhancement of T_c under pressure in $CeCu_2Si_2$ was put forward in Thomas et al. [1996]. It was suggested that a topological change in the Fermi surface produces a sudden change in the density of states at the Fermi level. While this could explain a sudden change in T_c, it does not account for any other of the anomalies observed.

Other features yet to be fully addressed with the current model are observed to occur in the valence fluctuation region. They are the apparent increase in the specific heat jump at T_c, the temperature dependence of the impurity contribution to the resistivity, and the nature of the superconducting state between the onset and completion of the superconducting transition.

Sample variation and anisotropic properties of $CeCu_2Si_2$

As I noted earlier, one of the characteristic features of $CeCu_2Si_2$ is the variation of its properties between samples. The magnetic properties of $CeCu_2Si_2$ around P_c have been the subject of extensive study, where the exact stoichiometry determines the existence or otherwise of magnetic order and/or superconductivity. The presence of disorder also has a major role to play in the behaviour of the superconducting state.

We have compared different samples under the same pressure conditions, and similar samples differently oriented with respect to the cell axis and current direction. There are several remarks to make about these results.

The difference between the two samples from Ishikawa labelled 'high T_c' and 'low T_c' can most probably be attributed to differing impurity concentrations. The decreasing T_c with pressure is also found in substituted $CeCu_2(Si_{1-x}Ge_x)_2$ (Yuan et al. [2003a]), eventually resulting in a separation of the two pockets of superconductivity. Note however that despite the extraordinary high residual resistivity in sample #50, at nearly 200 $\mu\Omega$cm at its highest, complete resistive transitions were still observed.

While the simplest explanation for such a large residual resistivity would be a high impurity concentration, it is conceivable that there is a qualitative difference with other samples. In Fig. 5.26 one can see that the majority of samples have rather

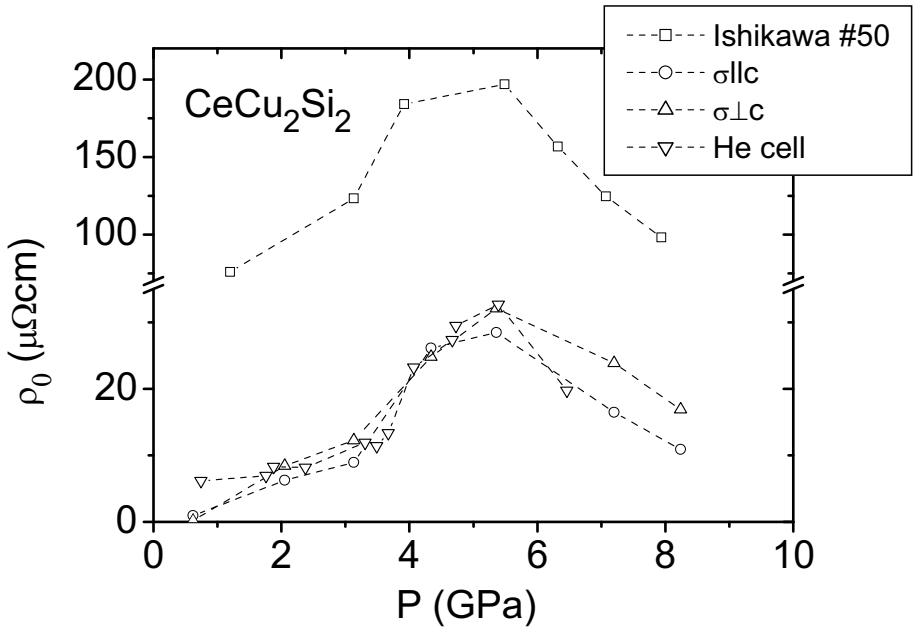

Figure 5.26: The residual resistivity of sample #50 is nearly 200 $\mu\Omega$cm around P_v, and superconductivity is still observed. This huge value for ρ_0 may possibly be qualitatively different from the other samples, if the enhanced scattering depends on the nature of the impurities.

similar residual resistivities, while #50 has scattering an order of magnitude larger. Perhaps this is not a representative collection of results, but it may be that the so-called 'low T_c' samples have impurities which are particularly susceptible to being affected by valence fluctuations, either due to their lattice position or to the nature of the impurity.

The A, A/S, and S type $CeCu_2Si_2$ can be most simply related by a small translation of the pressure axis. While our experiments have not focused on this aspect, we hypothesise that the properties of A type $CeCu_2Si_2$ will come to resemble A/S, then S type with small application of pressure. The justification for this is that the enhancement of T_c at high pressure, around the point believed to be P_v, is seen for all samples of whatever type.

Given these caveats, the simplest categorisation for a given sample of $CeCu_2Si_2$ seems to be based on two criteria: a shift of the pressure axis, and the degree of impurity scattering. The latter may or may not have a more subtle subdivisions.

The effect of uniaxial stress on the superconducting properties of $CeCu_2Si_2$ remains confused, but it is certainly important. The normal state properties provide a slightly clearer picture, with a series of independent observations implying that P_v is at a lower pressure in the the sample ($\sigma \| c$) than ($\sigma \perp c$).

The current direction has a clear effect on the resistivity of $CeCu_2Si_2$. Most remarkable is an apparent difference in T_c, including at ambient pressure. In the normal state properties, the height of the first Kondo peak is strongly dependent on current direction. Unfortunately we have not carried out enough experiments to conclusively separate the effect of current from that of uniaxial stress.

The message to take from these observations is that in order to fully understand this system from a theoretical point of view, it is essential to deal with the fact that it is not an isotropic system. A reason may be that the symmetry of the lowest crystal field split doublet is lower than that when higher states are mixed in by the Kondo broadening of the f-levels.

5.3.1 Two quantum critical points?

Until recently, the physics of heavy fermion superconductors has been assumed to be based on that of a quantum critical magnetic instability. This picture has had some success in explaining the non-Fermi liquid behaviour and superconductivity found in certain HF compounds. However, a solely magnetic picture fails to account for the entire range of behaviour of a material such as $CeCu_2Si_2$.

The presence, and indeed enhancement, of superconductivity so far from the disappearance of magnetic order called into question whether magnetic mediation is really the sole mechanism of superconductivity in $CeCu_2Si_2$. The evidence presented here, along with other anomalous behavior seen at a pressure well separated from the disappearance of magnetism, strongly suggests the presence of a second quantum critical point in $CeCu_2Si_2$, this time related to quantum fluctuations between electronic configurations rather than to collective spin instabilities. While magnetic pairing may be responsible for superconductivity at the magnetic QCP, critical valence fluctuations are responsible for pairing at $P_{\rm v}$. The recent result in $CeCu_2(Si_{0.9}Ge_{0.1})_2$ where two separate pockets of superconductivity are observed when disorder is deliberately introduced, suggests the validity of this point of view (Yuan et al. [2003a]).

Figure 5.27 shows a schematic phase diagram for the $CeCu_2(Si/Ge)_2$ system. The two critical pressures, $P_{\rm c}$ and $P_{\rm v}$, are respectively defined experimentally by the disappearance of magnetic order as T_N tends to zero, and by the region of linear resistivity where ρ_0 has a maximum and $T_1^{\rm max} \simeq T_2^{\rm max}$, accompanied by a maximum in T_c.

In a magnetic phase transition, the relevant order parameter is the average magnitude of the ordered moment. This rises continuously from zero as we pass a second order transition into the magnetically ordered phase. The average f-electron occupation number per Ce atom $\langle n_f \rangle$ can be thought of as the order parameter at the valence transition.

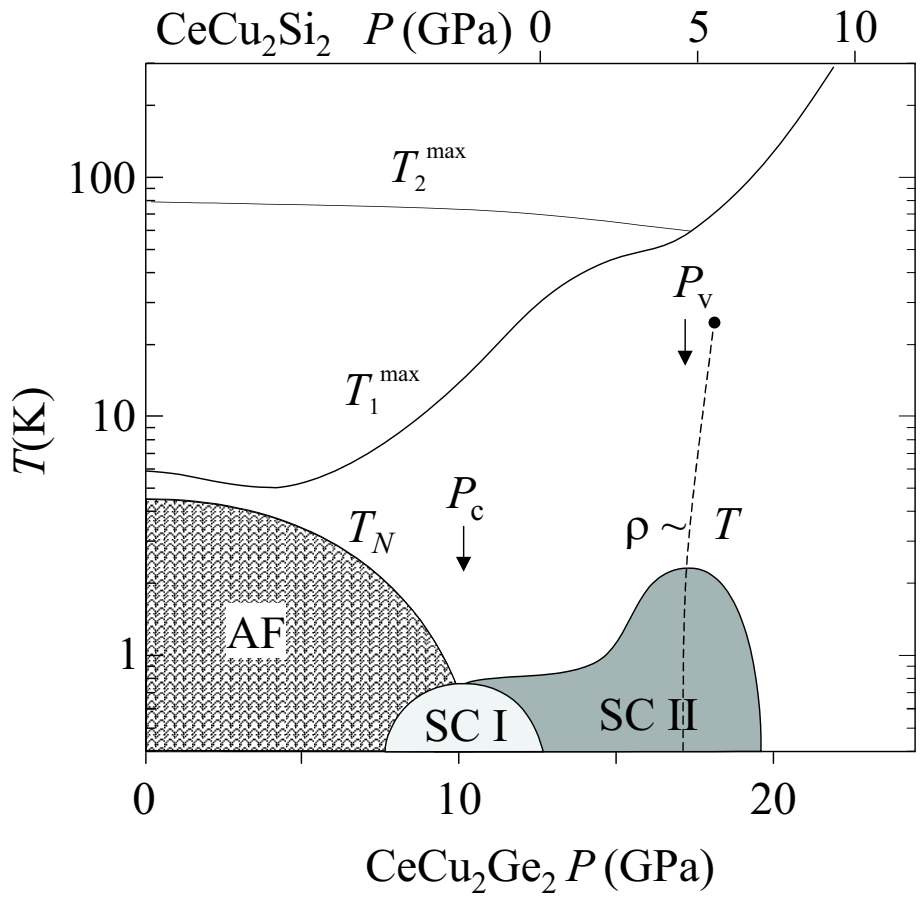

Figure 5.27: Schematic P-T phase diagram for $CeCu_2(Si/Ge)_2$ showing the two critical pressures P_c and P_v. At P_c, where the antiferromagnetic ordering temperature $T_N \to 0$, superconductivity in region $SC\ I$ is mediated by antiferromagnetic spin fluctuations; around P_v, in the region $SC\ II$, valence fluctuations provide the pairing mechanism and the resistivity is linear in temperature. The temperatures T_1^{max}, and T_2^{max}, merge at a pressure coinciding with P_v. The dashed line represents a hypothetical first order valence discontinuity whose critical end point lies somewhere between 10 K and 300 K.

Valence transitions, such as the Ce $\alpha - \gamma$ transition, are typically of first order, characterized by an abrupt change in the volume of a crystalline unit cell while retaining its structure. In the case of $CeCu_2Si_2$, we are proposing that the transition has more of a second order character. This can be understood from the general point of view as the critical end point of a first order transition. If this lies at sufficiently low temperature, the associated low energy fluctuations can mediate superconductivity. More specifically to our theoretical model, Onishi and Miyake [2000b,a] showed that as the Coulomb repulsion parameter U_{fc} is increased, the valence transition becomes increasingly steep, eventually approaching a first order transition.

As $T \to 0$, the valence transition is isentropic, and the phase boundary vertical. The Clausius-Clapeyron relation implies that valence fluctuations will be accompanied by volume, and hence density fluctuations.

Monthoux and Lonzarich [2004] have proposed a phenomenological model of density fluctuation mediated superconductivity, which would include the case of valence fluctuations, along with, for example stripes in high-T_c cuprates. They compared density-fluctuation mediated superconductivity with magnetic mediation, concluding that the while the latter is usually more robust, both mechanisms may coexist. In both mechanisms, T_c is enhanced by a more anisotropic structure, though not necessarily in a strictly 2D system, a result consistent with our observation that the superconducting state is very sensitive to uniaxial strain.

Valence fluctuation mediated superconductivity in other compounds?

The $CeCu_2(Si/Ge)_2$ system proved to be ideal for identifying valence fluctuation mediated superconductivity, as the two critical pressures P_c and P_v are widely separated, giving rise to an unusually large superconducting pressure range with a conspicuous shape. The delocalisation of the Ce $4f$ electron with pressure is a very general phenomenon however, so it is entirely possible that valence fluctuation mediated superconductivity exists in other compounds.

In a compounds such as $CePd_2Si_2$, superconductivity is found in a narrow pocket, seemingly directly connected to the disappearance of magnetism as $T_N \to 0$. However, many of the other anomalies listed in table 5.1 are still observed in this system, for example the rapid change of the A coefficient of the resistivity. These are difficult to explain within a purely spin fluctuation picture. If a valence instability is present in $CePd_2Si_2$, P_v is superimposed on P_c, as identified by the pressure at which $T_1^{max} \simeq T_2^{max}$ (Demuer et al. [2002]).

The physics associated with valence change in $CeCu_2Si_2$ may thus also play an important role in other heavy fermion superconductors. Linear resistivity and an enhancement of ρ_0 have also been seen in the $CeTIn_5$ compounds (Muramatsu et al. [2001]; Petrovic et al. [2001]) where T is Co, Rh or Ir. For this family, supercon-

ductivity extends over a relatively broad pressure range, and it may be that valence fluctuations also play a role, with a critical valence pressure separate from any magnetic instability.

Indeed, the localisation or otherwise of the f-electron can be determined by de Haas-van Alphen measurements in conjunction with band structure calculations. For the $CeTIn_5$ series, it has been determined that the Co and Ir compounds are best described in a delocalised picture, while $CeRhIn_5$ is best fitted assuming a localised $4f$ electron (Elgazzar et al. [2004]).

$CeCoIn_5$ has a maximum T_c of 2.6 K close to 1 GPa, and this may well be the system closest to a valence instability at ambient pressure.

5.4 Conclusions

The enhancement of superconductivity in $CeCu_2Si_2$ under pressure is found to coincide with a number of anomalies in the superconducting and normal state properties that are hard to explain in a purely spin fluctuation scenario. Many of these anomalies are directly related to an abrupt change in valence of the Ce ion, while others can be indirectly connected to such a transition. We propose a second critical pressure P_v at around 4.5 GPa where critical valence fluctuations provide the superconducting pairing mechanism. An extended Anderson lattice model with Coulomb repulsion between the conduction and f-electrons predicts an abrupt change in Ce f-level occupation. The associated fluctuations are sufficient to explain the observed enhancement of T_c, the T-linear normal state resistivity, the enhancement of the residual resistivity, and the peak in the electronic specific heat coefficient γ.

Chapter 6

Conclusions

6.1 Summary of conclusions

Based on the results in chapters two, four and five, we have come to the following conclusions:

- Superconductivity in ε-iron is almost certainly of unconventional origin, mediated by magnetic fluctuations. The experimental evidence suggests that the pairing is of a spin-triplet nature, mediated by ferromagnetic fluctuations. This is in conflict with most theoretical models, which predict an antiferromagnetic ground state.

- $CeCu_2Si_2$ has a new type of quantum critical point, at a pressure P_v around 4.5 GPa, where critical valence fluctuations dominate the electronic properties.

- Superconductivity at high pressure in $CeCu_2Si_2$ is related to the valence transition at P_v, and mediated by valence fluctuations.

- The properties of $CeCu_2Si_2$ around P_v are highly sensitive to anisotropy, and to small variations in sample purity.

- Miyake's model predicts a wide variety of properties found in $CeCu_2Si_2$ at P_v, including superconductivity.

- The mechanism can be understood as highly localised interaction based on the screening of isolated Ce^{4+} ions.

6.2 Original contributions

This work contains several original contributions by the author to the body of scientific knowledge. Their significance is left, however, for the reader to decide.

They can be summarised as follows:

- The helium filled diamond anvil cell technique was advanced to the point where simultaneous resistivity and ac calorimetry measurements could be performed on the same sample under pressures up to 10 GPa.
- The ac calorimetry technique was extended in helium cells to a dilution cryostat environment. It was found that the technique can be used down to at least 100 mK.
- Bayesian statistics were applied to the analysis of non Fermi-liquid power laws in the resistivity.
- A link was established between disorder and superconductivity in ε-Fe, and along with the evolution of the normal state properties observed in this system, this provided strong evidence for spin-triplet magnetically mediated superconductivity.
- Significant new evidence was found, in optimal experimental conditions, linking superconductivity and a valence instability in $CeCu_2Si_2$, and supporting the existence of a new superconducting mechanism based on valence fluctuations. Some of the peculiar characteristics of this exotic phase were explored, including its dependence on anisotropic strain.
- An intuitive physical interpretation of the valence fluctuation mechanism was provided.

6.3 Future prospects

In the case of iron, there are some obvious avenues to explore to further clarify the nature of the superconducting state. Measurements on single crystals in a helium pressure medium should be carried out. In these conditions the α-ε transition is more or less instantaneous, and so the role of the martensitic phase transition could be clarified. Other experimental probes, such as magnetic susceptibility, or inelastic neutron scattering, should be attempted, though the very high pressures needed may rule some of these techniques out.

It may be possible to stabilise non-magnetic phases of pure iron in thin film form on an appropriate substrate. This might help to clarify whether there is a QCP hidden behind the structural phase transition.

An important question following from the work on $CeCu_2Si_2$ is the position of the valence transition line and its critical endpoint. These could be identified directly by cell volume or L_{III} measurements as a function of pressure and temperature.

A general principle is that it is best to have several experimental probes of a single sample. Differences in behaviour between samples can be easily written off as 'sample dependence', when in fact there are subtle systematic effects at work. These are often only made clear by approaching a single sample from several different points of view, and by careful comparison between samples.

Another important problem is whether valence-fluctuation mediated superconductivity is present in any other systems. A good candidate is the $CeTIn_5$ family, where linear resistivity is found to coincide with the maximum in a broad superconducting pocket. These materials, along with $CeCu_2(Ce/Ge)_2$ may prove a useful test-bed for valence fluctuation physics.

There are other systems likely to exhibit similar physics to that of ε-Fe and $CeCu_2Si_2$. Cobalt is the neighbour of iron in the periodic table and superconductivity has been predicted to occur around 50 GPa. The rare earth ytterbium is well known for valence transitions in its compounds. This may also be a good candidate in which to look for valence fluctuations, however in the case of Yb, the competing states are a filled $4f$ level, and that with one hole, and the situation may not be completely symmetrical.

Acknowledgements
Remerciements

Je voudrais sincèrement remercier :

Didier Jaccard, pour son soutien, son expertise, sa patience et son sens de l'humour, des qualités parmi bien d'autres sans lesquelles ce travail n'aurait jamais pu aboutir.

Jean-Marc Triscone, pour son acceuil dans son groupe de recherche et son travail en tant que directeur de thèse, d'autant plus que mon sujet était assez éloigné de son principal domaine d'expertise.

Kazumasa Miyake, pour avoir trouvé une très bonne explication théorique pour notre travail sur le $CeCu_2Si_2$, pour son accueil extrêmement productif à Osaka en 2003, pour avoir eu la patience de lire cette thèse et pour être venu en tant que membre du jury.

Stephen Julian, pour être là au début et à la fin de cette expérience, pour m'avoir envoyé avec ses encouragements faire mon doctorat à Genève, et pour faire parti du jury et juger le résultat.

Jérôme Sierro et Renald Cartoni, pour leur soutien moral et pratique et pour m'avoir fait sentir le bienvenu dans l'ancien groupe Sierro dès mon premier jour.

Albin Demuer et Heribert Wilhelm pour nos discussions animées et instructives sur des sujets scientifiques et autres pendant de nombreuses heures.

Elisabeth Jeantin et ses collègues au secrétariat pour leur compétence incroyable qui permet la tâche quasi-impossible d'assurer le bon fonctionnement d'un groupe de physiciens.

Patrick Magnin pour tout ce qu'il fait pour l'informatique.

Spiros Zanos et son équipe au service d'hélium : le sang qui coule dans les veines de la physique.

Roland Pellet et son équipe de l'atelier mécanique, qui ont construit une bonne partie de ce qui a été utilisé pour produire les résultats présentés dans cette thèse.

Céline Lichtensteiger, pour avoir lu et corrigé les parties en français de cette thèse.

Mes parents Peter et Ann, qui n'ont jamais douté de ce dont je suis capable, pour peu que j'en fasse l'effort. Ma sœur Tammy, qui a très bien réussi à m'encourager et me distraire pendant la fin de la rédaction. Mes grands-parents qui ont fait un grand effort pour venir me soutenir à la défense de ma thèse.

Bostik, les fournisseurs de Blu-Tak (la pâte magique).

Et finalement tous les autres qui devraient, pourraient ou secrètement voudraient être remerciés.

Ce travail a bénéficié en partie du soutien financier du Fonds National Suisse de la recherche scientifique.

List of Publications

Holmes, A. T.; Jaccard, D.; Behr, G.; Inada, Y.; Onuki, Y., *Unconventional superconductivity and non-Fermi liquid behaviour of ε-iron at high pressure*, Journal of Physics: Condensed Matter. **16**(14): S1121-7 (2004).

Holmes, A. T.; Jaccard, D.; Miyake, K., *Signatures of valence fluctuations in $CeCu_2Si_2$ under high pressure*, Physical Review B **69**(2): 024508/1-11 (2004).

Holmes, A. T.; Demuer, A.; Jaccard, D., *Resistivity and AC-calorimetric measurements of the superconducting transition in $CeCu_2Si_2$ under very high hydrostatic pressure in a helium-filled diamond anvil cell*, Acta Physica Polonica B **34**(2): 567-70 (2003).

Demuer, A.; Holmes, A. T.; Jaccard, D., *Effect of anisotropic strain on the electronic properties of the pressure induced superconductor $CePd_2Si_2$*, Acta Physica Polonica B **34**(2): 459-62 (2003).

Demuer, A.; Holmes, A. T.; Jaccard, D., *Strain enhancement of superconductivity in $CePd_2Si_2$ under pressure*, Journal of Physics: Condensed Matter **14**(28): L529-35 (2002).

Holmes, A. T.; Jaccard, D.; Behr, G.; Inada, Y.; Onuki, Y., *Superconductivity of ε-Fe: complete resistive transition*, Physics Letters A **299**(2-3): 282-6 (2002).

References

Aliev, F. G., Brandt, N. B., Moshchalkov, V. V., Sidorov, V. I., and Lutsiv, R. V. The effect of pressure to 140 kbar on the electrical properties of $CeCu_2Si_2$. *Sov. Phys. Solid State*, **24**, 1786, 1982.

Ashcroft, N. W. and Mermin, N. D. *Solid State Physics*, chapter 26, page 523. Saunders College Publishing, 1976.

Bardeen, J., Cooper, L. N., and Schrieffer, J. Microscopic theory of superconductivity. *Phys. Rev.*, **106**, 162–4, 1957.

Bayes, R. An essay toward solving a problem in the doctrine of chances. *Phil. Trans. Roy. Soc.*, **53**, 370–418, 1763.

Bellarbi, B., Benoit, A., Jaccard, D., Mignot, J. M., and Braun, H. F. High-pressure valence instability and T_c maximum in superconducting cerium copper silicide ($CeCu_2Si_2$). *Phys. Rev. B*, **30**(3), 1182–7, 1984.

Bireckoven, B. and Wittig, J. A diamond anvil cell for the investigation of superconductivity under pressures of up to 50 GPa: Pb as a low temperature manometer. *J. Phys. E: Sci. Instrum.*, **21**(9), 841–848, 1988.

Bohnenkamp, U., Sandstrom, R., and Grimvall, G. Electrical resistivity of steels and face-centered-cubic iron. *J. Appl. Phys.*, **92**(8), 4402–7, 1992.

Bose, S. K., Dolgov, O. V., Kortus, J., Jepsen, O., and Andersen, O. K. Pressure dependence of electron-phonon coupling and superconductivity in hcp. Fe: a linear response study. *Phys. Rev. B*, **67**, 214518, 2003.

Bouquet, F. *Étude thermodynamique de l'état mixte dans* $YBa_2Cu_2O_{7-\delta}$. PhD thesis, Université Joseph Fourier, Grenoble I, 1998.

Bouquet, F., Wang, Y., Wilhelm, H., Jaccard, D., and Junod, A. Calorimetric investigation of $CeRu_2Ge_2$ up to 8 GPa. *Solid State Commun.*, **113**(7), 367–371, 2000.

Braithwaite, D., 2003. (private communication).

Cohen, R. E. Non-collinear magnetism in iron at high pressures. *cond-mat/0301615*, 2003.

Cooper, L. N. Bound Electron Pairs in a Degenerate Fermi Gas. *Phys. Rev.*, **104**(4), 1189, 1956.

Cornut, B. and Coqblin, B. Influence of the crystalline field on the Kondo effect of alloys and compounds with cerium impurities. *Phys. Rev. B*, **5**(11), 4541–61, 1972.

Cox, D. and Grewe, N. Transport properties of the Anderson lattice. *Z. Phys. B: Condens. Matter*, **71**, 321–340, 1988.

Demuer, A. *Etude du point critique magnétique quantique des fermions lourds sous pression hydrosatique*. PhD thesis, Universite Joseph Fourier, Grenoble I, 2000.

Demuer, A., Holmes, A. T., and Jaccard, D. Strain enhancement of superconductivity in $CePd_2Si_2$ under pressure. *J. Phys.: Condens. Matter*, **14**(28), L529–35, 2002.

Doiron-Leyraud, N., Walker, I. R., Taillefer, L., Steiner, M. J., Julian, S. R., and Lonzarich, G. G. Fermi-liquid breakdown in the paramagnetic phase of a pure metal. *Nature*, **425**, 595–599, 2003.

Eichler, A. and Gey, W. Method for the determination of the specific heat of metals at low temperatures and under high pressures. *Rev. Sci. Instrum.*, **50**(11), 1445–1452, 1979.

Elgazzar, S., Opahle, I., Hayn, R., and Oppeneer, P. M. Calculated de Haas-van Alphen quantities of $CeMIn_5$ (M = Co, Rh, and Ir) compounds. *cond-mat/0403338*, 2004.

Eremets, M. I. *High pressure experimental methods*. Oxford University Press, 1996.

Fuseya, Y., Kohno, H., and Miyake, K. Realization of odd-frequency p-wave spin-singlet superconductivity coexisting with antiferromagnetic order near quantum critical point. *J. Phys. Soc. Jpn.*, **72**(11), 2914–2923, 2003.

Holmes, A. T., Jaccard, D., Behr, G., Inada, Y., and Onuki, Y. Unconventional superconductivity and non-Fermi liquid behaviour of ε-iron at high pressure. *J. Phys.: Condens. Matter*, **16**, S1121–S1127, 2004a.

Holmes, A. T., Jaccard, D., and Miyake, K. Signatures of valence fluctuations in $CeCu_2Si_2$ under high pressure. *Phys. Rev. B*, **69**(2), 024508, 2004b.

Ishikawa, M., Braun, H. F., and Jorda, J. L. Effect of composition on the superconductivity of $CeCu_2Si_2$. *Phys. Rev. B*, **27**(5), 3092–5, 1983.

Ishikawa, M., Takeda, N., Koeda, M., Hedo, M., and Uwatoko, Y. Pairing symmetry in two distinct superconducting states of $CeCu_2Si_2$. *Phys. Rev. B*, **68**(2), 024522, 2003.

Jaccard, D., Holmes, A. T., Behr, G., Inada, Y., and Onuki, Y. Superconductivity of ε-Fe: complete resistive transition. *Phys. Lett. A*, **299**, 282, 2002.

Jaccard, D., Mignot, J. M., Bellarbi, B., Benoit, A., Braun, H. F., and Sierro, J. High-pressure transport coefficients of the heavy-fermion superconductor cerium copper silicide ($CeCu_2Si_2$). *J. Magn. Magn. Mater.*, **47–48**, 23–29, 1985.

Jaccard, D., Vargoz, E., Alami-Yadri, K., and Wilhelm, H. Transport properties of heavy fermion compounds. *Rev. High Pressure Sci. Techno.*, **7**, 412–418, 1998.

Jaccard, D., Wilhelm, H., Alami-Yadri, K., and Vargoz, E. Magnetism and superconductivity in heavy fermion systems at high pressure. *Physica B*, **259–261**, 1–7, 1999.

Jarlborg, T. personal communication, 2002a.

Jarlborg, T. Ferromagnetic and antiferromagnetic spin fluctuations and superconductivity in the hcp-phase of Fe. *Phys. Lett. A*, **300**, 518, 2002b.

Jarlborg, T. Spin fluctuations, electron-phonon coupling and superconductivity in near-magnetic elementary metals–Fe, Co, Ni and Pd. *Physica C*, **385**, 513, 2003.

Jaynes, E. T. *Probability Theory, The Logic of Science*. Cambridge University Press, 2003.

Jephcoat, A. P., Mao, H. K., and Bell, P. M. Static compression of iron to 78 GPa with rare gas solids as pressure transmitting media. *J. Geophys. Res.*, **91**, 4677, 1986.

Kadau, K., Germann, T. C., Lomdahl, P. S., and Holian, B. L. Microscopic View of Structural Phase Transitions Induced by Shock Waves. *Science*, **296**(5573), 1681–1684, 2002.

Kadowaki, K. and Woods, S. Universal relationship of the resistivity and specific heat in heavy-fermion compounds. *Solid State Commun.*, **58**, 507, 1986.

Kawasaki, S., Mito, T., Zheng, G.-q., Thessieu, C., Kawasaki, Y., Ishida, K., Kitaoka, Y., Muramatsu, T., Kobayashi, T. C., Aoki, D., Araki, S., Haga, Y., Settai, R., and Onuki, Y. Pressure-temperature phase diagram of antiferromagnetism and superconductivity in $CeRhIn_5$ and $CeIn_3$: 115In-NQR study under pressure. *Phys. Rev. B*, **65**(2), 020504, 2002.

Kawasaki, Y., Ishida, K., Mito, T., Thessieu, C., Zheng, G.-q., Kitaoka, Y., Geibel, C., and Steglich, F. Exotic superconducting phase in $CeCu_2Si_2$ close to antiferromagnetism: A Cu-NQR study under hydrostatic pressure. *Phys. Rev. B*, **63**(14), 140501, 2001.

Kim, Y. B., Hempstead, C. F., and Strnad, A. R. Flux-Flow Resistance in Type-II Superconductors. *Phys. Rev.*, **139**(4A), A1163–72, 1965.

Laplace, P. S. Mémoire sur la probabilité des causes par les événemens. *Mém. Acad. R. Sci. (Paris)*, **6**, 621–656, 1774.

Link, P., Jaccard, D., and Lejay, P. The thermoelectric power of $CePd_2Si_2$ and $CeCu_2Ge_2$ at very high pressure. *Physica B*, **225**(3–4), 207–13, 1996.

Lonzarich, G. G. *Electron*, chapter 6, page 109. Cambridge University Press, 1997.

Louca, D., Thompson, J. D., Lawrence, J. M., Movshovich, R., Petrovic, C., Sarrao, J. L., and Kwei, G. H. Atomic disorder in the heavy fermion superconductor $CeCu_{2+x}Si_2$. *Phys. Rev. B*, **61**(22), R14940, 2000.

Mackenzie, A. P., Haselwimmer, R. K. W., Tyler, A. W., Lonzarich, G. G., Mori, Y., Nishizaki, S., and Maeno, Y. Extremely strong dependence of superconductivity on disorder in Sr_2RuO_4. *Phys. Rev. Lett.*, **80**(1), 161–164, 1998.

Mackenzie, A. P. and Maeno, Y. Superconductivity of Sr_2RuO_4 and the physics of spin-triplet pairing. *Rev. Mod. Phys.*, **75**(2), 657–712, 2003.

Mathur, N. D., Grosche, F. M., Julian, S. R., Walker, I. R., Freye, D. M., Haselwimmer, R. K. W., and Lonzarich, G. G. Magnetically mediated superconductivity in heavy fermion compounds. *Nature*, **394**, 39–43, 1998.

Mazin, I. I., Papaconstantopoulos, D. A., and Mehl, M. J. Superconductivity in compressed iron: Role of spin fluctuations. *Phys. Rev. B*, **65**, 100511, 2002.

Millis, A. J. Effect of a nonzero temperature on quantum critical points in itinerant fermion systems. *Phys. Rev. B*, **48**, 7183, 1993.

Mills, R. L., Liebenberg, D. H., and Bronson, J. C. Equation of state and melting properties of ^{4}He from measurements to 20 kbar. *Phys. Rev. B*, **21**(11), 5137–5148, 1980.

Miyake, K., Matsuura, T., and Varma, C. M. Relation between resistivity and effective mass in heavy-fermion and A15 compounds. *Solid State Commun.*, **71**, 1149, 1989.

Miyake, K., Narikiyo, O., and Onishi, Y. Superconductivity of Ce-based heavy fermions under pressure: Valence fluctuation mediated pairing associated with valence instability of Ce. *Physica B*, **259–261**, 676–677, 1999.

Miyake, K., Schmitt-Rink, S., and Varma, C. M. Spin-fluctuation-mediated even-parity pairing in heavy-fermion superconductors. *Phys. Rev. B*, **34**, 6554, 1986.

Miyake, K. and Maebashi, H. Huge enhancement of impurity scattering due to critical valence fluctuations in a Ce-based heavy electron system. *J. Phys. Soc. Jpn.*, **71**(4), 1007–1010, 2002.

Modler, R., Lang, M., Geibel, C., Schank, C., Müller-Reisener, R., Hellmann, P., Link, A., Sparn, G., Assmus, W., and Steglich, F. The effect of composition on the occurrence of a second phase transition in the vicinity of T_c in $CeCu_2Si_2$. *Physica B*, **206–207**(1–4), 586–588, 1995.

Monthoux, P. and Lonzarich, G. G. Magnetically mediated superconductivity: crossover from cubic to tetragonal lattice. *Phys. Rev. B*, **66**(22), 224504, 2002.

Monthoux, P. and Lonzarich, G. G. Density-fluctuation-mediated superconductivity. *Phys. Rev. B*, **69**(6), 064517, 2004.

Muramatsu, T., Tateiwa, N., Kobayashi, T. C., Shimizu, K., Amaya, K., Aoki, D., Shishido, H., Haga, Y., and Onuki, Y. Superconductivity of $CeRhIn_5$ under high pressure. *J. Phys. Soc. Jpn.*, **70**(11), 3362–3367, 2001.

Nasu, S., Sasaki, T., Kawakami, T., Tsutsui, T., and Endo, S. Mossbauer study of ε-Fe under an external magnetic field. *J. Phys.: Condens. Matter*, **14**(44), 11167–11171, 2002.

Okada, I. and Yosida, K. Singlet ground state of the localized d-electrons coupled with conduction electrons in metals. *Prog. Theor. Phys.*, **49**, 1483, 1973.

Onishi, Y. and Miyake, K. Sharp Valence Transition Caused by f-c Coulomb Interaction in Periodic Anderson Model. *Physica B*, **281–282**, 191–192, 2000a.

Onishi, Y. and Miyake, K. Enhanced valence fluctuations caused by f-c Coulomb interaction in Ce-based heavy electrons: possible origin of pressure-induced enhancement of superconducting transition temperature in $CeCu_2Ge_2$ and related compounds. *J. Phys. Soc. Jpn.*, **69**(12), 3955–3964, 2000b.

Onodera, A., Tsuduki, S., Ohishi, Y., Watanuki, T., Ishida, K., Kitaoka, Y., and Onuki, Y. Equation of state of $CeCu_2Ge_2$ at cryogenic temperature. *Solid State Commun.*, **123**(3–4), 113–116, 2002.

Perakis, I., Varma, C. M., and Ruckenstein, A. E. Non-Fermi-liquid states of a magnetic ion in a metal. *Phys. Rev. Lett.*, **70**, 3467–3470, 1993.

Petrovic, C., Pagliuso, P. G., Hundley, M. F., Movshovich, R., Sarrao, J. L., Thompson, J. D., Fisk, Z., and Monthoux, P. Heavy-fermion superconductivity in $CeCoIn_5$ at 2.3 K. *J. Phys.: Condens. Matter*, **13**(17), L337–L342, 2001.

Rice, T. M. and Ueda, K. Gutzwiller method for heavy electrons. *Phys. Rev. B*, **34**, 6420, 1986.

Roehler, J., Klug, J., and Keulerz, K. The valence of cerium in cerium copper silicide ($CeCu_2Si_2$) under high pressure. *J. Magn. Magn. Mater.*, **76–77**, 340–2, 1988.

Scalapino, D. J., E. Loh, J., and Hirsch, J. E. d-wave pairing near a spin-density-wave instability. *Phys. Rev. B*, **34**, 8190, 1986.

Schilling, J. S. unpublished, 2003.

Shiba, H. Properties of Strongly Correlated Fermi Liquid in Valence Fluctuation System - a Variational Monte-Carlo Study. *J. Phys. Soc. Jpn.*, **55**, 2765, 1986.

Shimizu, K., Kimura, T., Furomoto, S., Takeda, K., Kontani, K., Onuki, Y., and Amaya, K. Superconductivity in the non-magnetic state of iron under pressure. *Nature*, **412**, 316, 2001.

Sivia, D. S. *Data Analysis: a Bayesian tutorial*. Oxford University Press, 1996.

Steglich, F., Aarts, J., Bredl, C. D., Lieke, W., Meschede, D., Franz, W., and Schaefer, H. Superconductivity in the presence of strong Pauli paramagnetism: cerium copper silicide ($CeCu_2Si_2$). *Phys. Rev. Lett.*, **43**(25), 1892–6, 1979.

Steglich, F., Gegenwart, P., Geibel, C., Helfrich, R., Hellmann, P., Lang, M., Link, A., Modler, R., Sparn, G., Buttgen, N., and Loidl, A. New observations concerning magnetism and superconductivity in heavy-fermion metals. *Physica B*, **223–224**(1–4), 1–8, 1996.

Stockert, O., Deppe, M., Geibel, C., Steglich, F., Hohlwein, D., and Schneider, R. Neutron Diffraction Study of the Magnetism in Single-Crystalline $CeCu_2(Si_{1-x}Ge_x)_2$. *Acta Phys. Pol., B*, **34**(22), 963, 2003.

Sullivan, P. F. and Seidel, G. Steady-State, ac-Temperature Calorimetry. *Phys. Rev.*, **173**(3), 679–685, 1968.

Taylor, G. R., Isin, A., and Coleman, R. V. Resistivity of Iron as a Function of Temperature and Magnetization. *Phys. Rev.*, **165**, 621, 1968.

Taylor, R. D., Pasternak, M. P., and R., J. Hysteresis in the high pressure transformation of bcc- to hcp-iron. *J. Appl. Phys.*, **69**, 6126, 1991.

Thakor, V., Staunton, J. B., Poulter, J., Ostanin, S., Ginatempo, B., and Bruno, E. Ab initio calculations of incommensurate antiferromagnetic spin fluctuations in hcp. iron under pressure. *Phys. Rev. B*, **67**(18), 180405, 2003.

Thomas, F., Ayache, C., Fomine, I. A., Thomasson, J., and Geibel, C. Superconductivity and pressure-induced electronic topological changes in $CeCu_2Si_2$. *J. Phys.: Condens. Matter*, **8**(4), L51–L57, 1996.

Thomasson, J., Okayama, Y., Sheikin, I., Brison, J. P., and Braithwaite, D. Transport measurements of the heavy fermion superconductor CeCu2Si2 under hydrostatic pressure in helium. *Solid State Commun.*, **106**(9), 637–641, 1998.

Tsuneto, . *Superconductivity and Superfluidity*, chapter 4.5.4. Cambridge University Press, 1998.

Vargoz, E. and Jaccard, D. Superconducting and normal properties of $CeCu_2Ge_2$ at high pressure. *J. Magn. Magn. Mater.*, **177–181**, 294–295, 1998.

Vargoz, E., Jaccard, D., Genoud, J. Y., Brison, J. P., and Flouquet, J. Upper critical field of $CeCu_2Si_2$ at very high pressure. *Solid State Commun.*, **106**(9), 631–636, 1998.

Vargoz, E. *Propriétés de transport sous pression de composés à fermions lourds supraconducteurs: $CeCu_2$, $CeCu_2Ge_2$ et $CeCu_2Si_2$*. PhD thesis, University of Geneva, 1998. no. 3003.

Varma, C. M., Littlewood, P. B., Schmitt-Rink, S., Abrahams, E., and Ruckenstein, A. E. Phenomenology of the normal state of Cu-O high-temperature superconductors. *Phys. Rev. Lett.*, **63**, 1996, 1989.

Varma, C. M., Nussinov, Z., and van Saarloos, W. Singular or non-Fermi liquids. *Physics Reports*, **361**, 267, 2002.

Varma, C. M., Schmitt-Rink, S., and Abrahams, E. Charge transfer excitations and superconductivity in "ionic" metals. *Solid State Commun.*, **62**(10), 681–5, 1987.

Wang, F. M. and Ingalls, R. Iron bcc-hcp transition: Local structure from x-ray-absorption fine structure. *Phys. Rev. B*, **57**, 5647, 1998.

Wilhelm, H. and Jaccard, D. Calorimetric and transport investigations of $CePd_{2+x}Ge_{2-x}$ ($x = 0$ and 0.02) up to 22 GPa. *Phys. Rev. B*, **66**(6), 064428, 2002.

Wilhelm, H., Raymond, S., Jaccard, D., Stockert, O., v. Loehneysen, H., and Rosch, A. From an antiferromagnet to a heavy-fermion system: $CeCu_5Au$ under pressure. In Manghnani, M., Nellis, W., and Nicol, M., editors, *Proceedings of AIRAPT-17, Hawaii, 1999*, pages 697–700, Hyderabad, 2000. Universities Press.

Yamada, K., Yosida, K., and Hanzawa, K. Comments on the Dense Kondo State. *Prog. Theor. Phys.*, **71**, 450, 1984.

Yuan, H. Q., Deppe, M., Sparn, G., Geibel, C., and Steglich, F. Pressure Effect on the Magnetism and Superconductivity in Single Crystal $CeCu_2(Si_{0.9}Ge_{0.1})_2$. *Acta Phys. Pol., B*, **34**(2), 533, 2003a.

Yuan, H., Grosche, F. M., Deppe, M., Geibel, C., Sparn, G., and Steglich, F. Observation of Two Distinct Superconducting Phases in $CeCu_2Si_2$. *Science*, **302**, 2104, 2003b.